

Stellingen

- 1 De wijze waarop veelal de opbouw van sodaliet, zeoliet A en faujasiet via sodalietkooien wordt geïllustreerd is niet eenduidig.

M.E.Davis, Ind.Eng.Chem.Res. 30 (1991) 1675

- 2 Het beeld verkregen met AFM van het oppervlak van een silicaliet-1 kristal is vermoedelijk niet het ac-vlak zoals gerapporteerd door P.Rasch en co-auteurs maar het ab-vlak.

P.Rasch, W.M.Heckl, H.W.Deckman en W.Haberle,
Mat.Res.Soc.Symp.Proc. 233 (1991) 287

- 3 De synthese van moleculaire zeven m.b.v. microgolven leidt tot aanzienlijke tijdswinst.

J.C.Jansen, A.Arafat en H. van Bekkum, geaccepteerd voor
publicatie, ACS New York, (1991)

- 4 Het uitwendige oppervlak van zeolietkristallen van het MFI-type is vele malen groter dan verondersteld kan worden uit de oppervlakteberekening van de ideale kristalvlakken.

Dit proefschrift, hoofdstuk 7

- 5 De berekening zoals voorgesteld door Taramasso, Perego en Notari van de celcontractie van het MFI-type zeoliet als gevolg van isomorphe substitutie van borium voor silicium is niet te correleren met experimentele waarnemingen.

M.Taramasso, G.Perego en B.Notari 5th-IZC Napels (1980) 40

- 6 Naast draadmodellen van moleculaire zeven ter grootte van een eenheidscel verdienen ruimtevullende atoommodellen ter grootte van een porie-holte met aperturen aanbeveling.

- 7 Het z.g. steamen van een ZSM-5 zeolietfilm zal tot minder film en meer eilandvorming leiden hetgeen de toepassing als membraan niet ten goede komt.

T.Sano, Y.Kiyozumi, F.Mizukami, H.Takaya, T.Mouri en M.Watanabe
Zeolites 12 (1992) 131

- 8 De zeer kleine verandering in de intensiteit in het röntgenpoeder diffractiepatroon van het MFI-type zeoliet kan niet gekoppeld worden aan epitaxiale groei zoals door Tsikoyiannes en Haag wordt gerapporteerd.

J.G.Tsikoyiannes en W.O.Haag, Zeolites 12 (1992) 127

- 9 Op grond van attractiekrachten en moleculaire vormselectiviteit lijkt decadecasil-3R een zeer geschikte moleculaire zeef om CO₂ uit lucht te couperen.

- 10 De veronderstelling dat in een gereduceerd zwaartekrachtveld grotere zeolietkristallen gevormd kunnen worden dient nog door experimenten bevestigd te worden.

- 11 De bijdrage vanuit Nederland aan mondiaal overleg is eerder een zaak van onze grote persoonlijkheden dan van onze politieke invloed.

Artikel over Jhr. Mr. van Lennep in NRC Handelsblad, 2 mei 1992

getiteld: 'Investeren in milieu is geen liefdadigheid'

auteurs: G.van Es en H.Steketee

- 12 Het gecontroleerd gebruik van branden als vorm van bosonderhoud zoals toegepast in verschillende landen leidt in de USA weliswaar tot reductie van het struweel maar ook tot zwart geblakerde sequoias voor de komende decennia.

- 13 Stoplichten en hun groen/rood indicatie dienen voor het autoverkeer te prevaleren in strafrechtelijk en juridisch opzicht boven de rechtsvoorrang regel.

J.C.Jansen

**ZEOLITE CRYSTAL GROWTH AND THE
STRUCTURE ON AN ATOMIC SCALE**

555226
317275g
TR diss 2073

ZEOLITE CRYSTAL GROWTH AND THE STRUCTURE ON AN ATOMIC SCALE

PROEFSCHRIFT

ter verkrijging van de graad van doctor
aan de Technische Universiteit Delft,
op gezag van de Rector Magnificus, prof. drs. P.A. Schenck
in het openbaar te verdedigen ten overstaan van
een commissie aangewezen door het College van Dekanen
op maandag 15 juni 1992 te 16.00 uur

door

KOOS JANSEN

geboren te Den Haag



Dit proefschrift is goedgekeurd door de promotor

Prof. dr. ir. H. van Bekkum

CONTENTS

Chapter 1.	Introduction	1
Chapter 2.	Some general considerations on silicas, silicates, zeolites and phosphate molecular sieves	5
Chapter 3.	The preparation of zeolites and all silica analogues	29
Chapter 4.	On the location and disorder of the tetrapropylammonium (TPA)-ion in ZSM-5 with improved framework accuracy	89
Chapter 5.	Isomorphous substitution of Si by B, Al, Ga and Be during crystallization of large single crystals of zeolite	99
Chapter 6.	First STM surface characterization of a zeolite	109
Chapter 7.	General growth regulation and morphology of zeolite single crystals of the MFI-type	117
Chapter 8.	Controlled growth of thin films of molecular sieves on various supports	135
Summary		145
Dankwoord		150

CHAPTER 1

INTRODUCTION

This thesis deals with zeolites, microporous crystalline aluminosilicates with major applications in ion exchange, catalysis and adsorption.

Some fifty zeolites are known to exist in nature and some of these, chabazite, clinoptilolite, and mordenite are mined.

Mankind has learned to synthesize zeolites with as a first example the synthesis of mordenite by Barrer [1]. Many natural zeolites have now been obtained by synthesis. Moreover a number of new zeolite structures have been synthesized and elucidated. The first example was zeolite A [2], which nowadays is made on a large scale for use in detergent formulations as an ion exchanger.

Present-day production of zeolites exceeds 1 million tons/annually with a division over natural/ synthetic and over the major application areas as shown in Fig. 1.

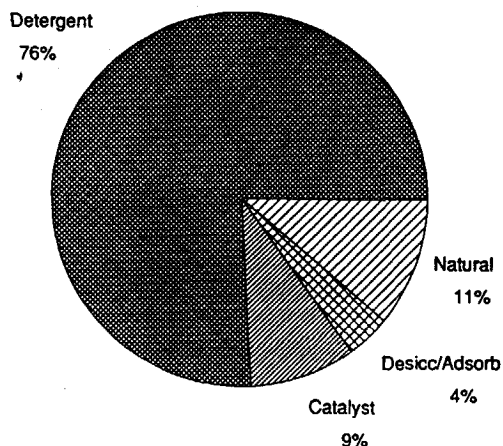


Figure 1. Estimated world zeolite consumption in 1991. [3]

The thesis is focused on different aspects of the zeolite ZSM-5, also known under the structural code name MFI. This zeolite was discovered in 1972 by Argauer and Landolt of the Mobil Corporation [4]. The names ZSM-5 (Zeolite Socony Mobil - 5) and MFI (Mobil Five) reflect this origin. Zeolite ZSM-5 is grown preferably with an organic template, usually tetrapropylammonium ions, which have to be removed in a calcination step to have the pore system available for catalysis or adsorption, see Fig. 2.

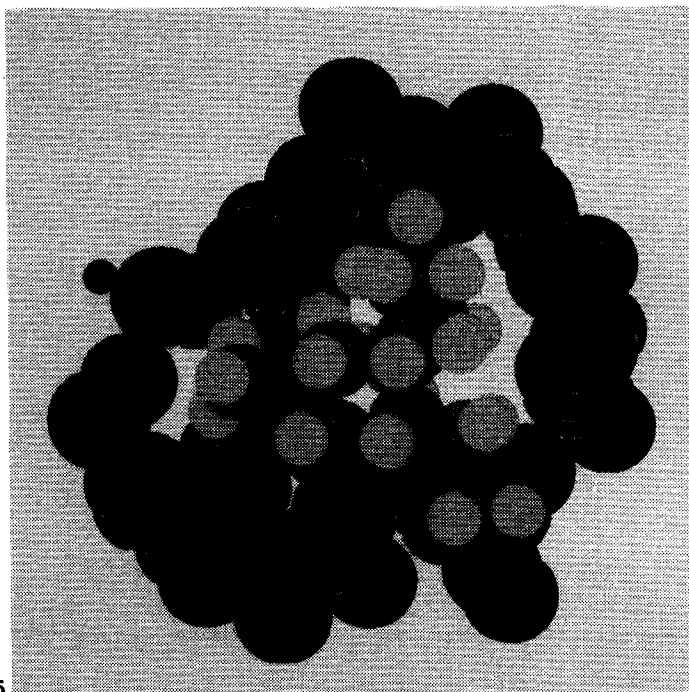


Figure 2, Zeolite TPA-ZSM-5

SCOPE OF THE THESIS

The thesis will be engaged with a number of aspects of zeolite ZSM-5, such as:

- The synthesis of large single crystals of ZSM-5
- The structural X-ray analysis of the as-synthesized zeolite including the template
- The STM imaging of MFI-type crystal surfaces
- The phase transitions that zeolite ZSM-5 can undergo also in connection with:
- the framework flexibility as a function of guest molecules

- The isomorphous substitution of Si in the MFI lattice
- The growth of MFI-type crystals on various surfaces, which seems to open new possibilities for membrane and catalysis purposes.

In chapter 2 general considerations will be given on silicas, silicates, zeolites and molecular sieves of the phosphate type. The latter group is presently expanding towards super-large pore systems.

Chapter 3, will present a literature survey of zeolite syntheses together with many experimental details acquired at the Laboratory of Organic Chemistry and Catalysis.

In order to characterize the structure of the framework and the guest molecule and the guest- guest and guest- framework interaction the zeolite ZSM-5 was prepared in different crystal sizes, 0.2 - 700 μm , whereafter, amongst others, the crystal structure determination of the as-synthesized material, chapter 4, was carried out.

To observe details of the zeolite external crystal surface, scanning tunneling microscopy (STM), supported by SEM, was used to understand better the contribution of the external surface in catalysis performance, chapter 5. For the first time, also a scan was made of the internal surface after cleaving a ZSM-5 single crystal.

The parameters involved in the evolution of different crystal forms of the zeolite ZSM-5 have been found by studying the crystal growth, *in situ*, chapter 6. A special lookthrough autoclave of 3 ml was made for this purpose. Chemical modifications like isomorphous substitution of various T-atoms to obtain different Bronsted acidity have been studied, chapter 7.

In order to develop layers, films and coatings of the zeolite ZSM-5 in different orientations on various supports a study has been carried out, chapter 8, to understand parameters involved for catalysis, membrane and sensor applications.

References

- 1 R. M. Barrer, *J. Chem. Soc.*, 1948, 2158.
- 2 D. W. Breck, *Zeolite Molecular Sieves, Structure, Chemistry and Use*, John Wiley & Sons, Inc. New York, 1974
- 3 Data provided by Dr S. Rock, PQ Corporation
- 4 R. J. Argauer and G. R. Landolt, *U.S. patent* 3.702.886

CHAPTER 2

GENERAL CONSIDERATIONS ON SILICAS, SILICATES, ZEOLITES AND PHOSPHATE MOLECULAR SIEVES

Silicas, Silicates and Zeolites

The last decades a fast developing subgroup of tecto-silicas and -silicates, the microsporous crystalline materials, is of growing interest in research and industrial application [1].

The framework is comprised of four- connected tetrahedral units of either SiO_2 , the pure silicas, or of SiO_2 and TO_2 in which T stands for an equal or lower valency atom partly isomorphously substituting Si, resulting in silicas and silicates, respectively. In the case of $\text{T} = \text{Al}^{3+}$ the product is denoted as a zeolite.

Alumino- and Gallophosphates

Recently an increasing number of microsporous crystalline tecto-phosphates has attracted much attention [2].

In these compounds four connected tetrahedral units of AlO_2^- and PO_2^+ form, in a univariant composition with $\text{Al/P} = 1$, neutral frameworks with a high degree of structural diversity. Various two-, three- or four-valent cations can be, for a fraction, incorporated into the framework leading, depending upon the particular ion, to again neutral frameworks or to the presence of cations counterbalancing the framework charge.

The most modern materials are the gallophosphates, including the so-called Cloverite with a cavity diameter of 30 Å the largest void at present [3].

The frameworks can be in principle formulated as follows:

SILICAS	SiO_2	or TO_2	SiO_2
SILICATES	TO_2^{n-}	SiO_2	$n = 1, 2$
ZEOLITES	AlO_2^-	SiO_2	$\text{Si/Al} \geq 1$
PHOSPHATES	AlO_2^-	PO_2^+	or $\text{GaO}_2^- \text{PO}_2^+$

The microporous cavities in the silica(te)s and phosphates are formed of curved continuous monolayers of interconnected tetrahedral units. Each tetrahedral unit is contributing to a curved layer, or actually, the internal surface. Thus each atom, with the exception of the external surface, is exposed to the microporous system. The tetrahedral units are either in one or in two layers present between neighbouring voids of the porous material, see Fig. 1.

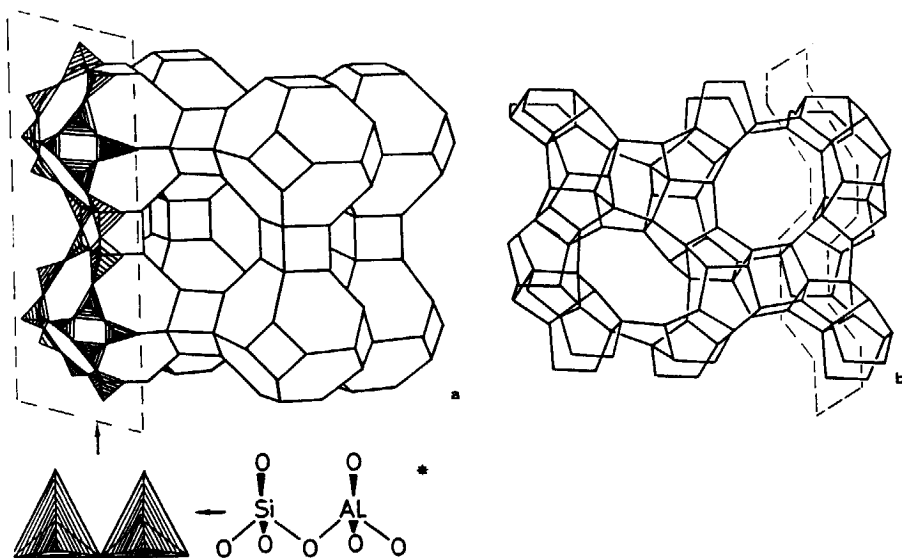
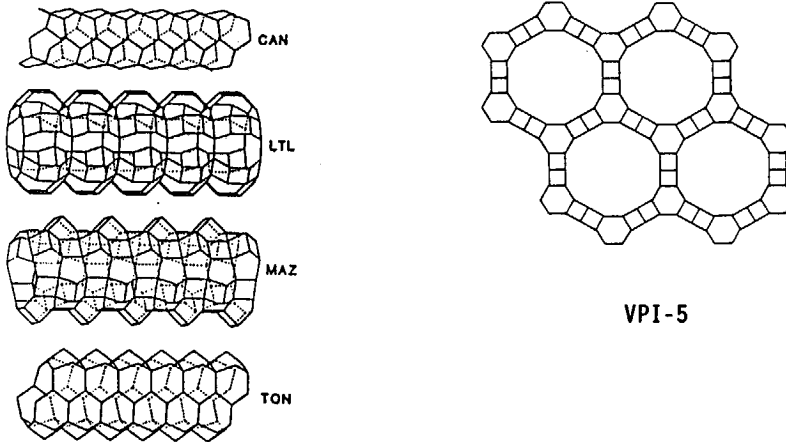


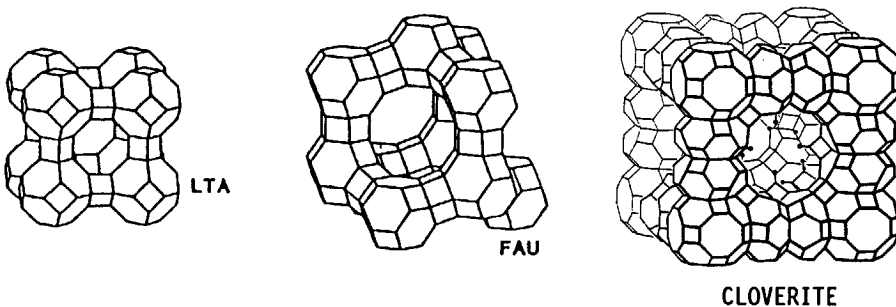
Figure 1, Tetrahedral units [*] cornerlinked forming continuous monolayers [----] in a) zeolite A and b) zeolite ZSM-5. The corners of the models represent the Si- or Al atom positions while the O atoms are located between two corners. All atoms are exposed to the void system.

The configurations of the voids can in principle be divided in the following two forms:

VOID-FORM I channels, crossing or parallel



VOID-FORM II cavities, 2-D and 3-D connected via smaller constrictions



Both forms represent uniformly space-filling pore systems, which have a certain orientation in the typical crystal morphology [1]. The void diameters vary for the crossing and parallel channels and for the smaller constrictions between 3.5 Å and 14 Å and for the cavities between 6 Å and 30 Å.

The above microporous materials are denoted as molecular sieves because the void systems contain dimensions of a molecular scale.

The differences in the molecular sieve types, based on the above mentioned frameworks and void- forms, has led to applications which are given in Table 1 together with the active site of a sieve type for a certain application.

Table 1. Different sieve types, some applications and active sites.

			Active site	
Application			lattice	void
silica	catalysis separation	oxidation	Ti^{4+} , V^{5+}	
		gas, organics from H_2O		
silicate	catalysis	isomerization	B^{3+}	H^+
		aromatization	Ga^{3+}	H^+
		oxidation	Co^{2+}	M^{n+} -complex
	catalysis	cracking		H^+ , (Ln^{3+})
		hydrocracking		H^+ , M^0
		dewaxing		H^+
		paraf. isomerization	Al^{3+}	H^+ , M^0
		arom. isomerization		H^+
		alkylation acid base		H^+ , H^+ , M^0
		butene isomerization	O^{2-}	M^0
		oxidation		H^+ , M^0 , M^{n+} , M^{n+} , M^0 M^{n+} -complex
zeolite	separation	n-, isoparaffin	Al^{3+}	
		o-, m-, p-xylene		
		drying		
		fructose-glucose		
	ion-exchange	amino acids	Al^{3+}	
		Mg^{2+} , Ca^{2+} Cs^{1+} , Sr^{1+}		Na^+
phosphate	new areas	electronics	Al^{3+}	$(CdS)_4$, Zn_4S
		optics		Ag_6
		photochemical		H^+
		electrochemical		earth alk. ions
	catalysis	methanol to olefins	Si^{4+}	H^+
		alkylation of toluene		
		oligomerization		
		oxidation		
phosphate	separation	halobenzenes	Co^{2+}	M^{n+} -complex
		electronics		
		electronics		Se-chain

In general, the most appropriate molecular sieve for a particular application is chosen from:

- 1 the large collection of types, with a broad spectrum of physico-chemical characteristics [5] with
- 2 the proper fine modification [6] applied,
- 3 and also considering the flexible framework behaviour

Ad 1

Variations in the physicochemical characteristics are: *i)* the pore size, pore shape, dimensionality, the presence or absence of tubular- or cage-like constructions, the orientation in the particular crystal morphology, the void volume *ii)* the framework composition in relation to the stability and the acid site strength, location and distribution and *iii)* surface aspects, like defects.

The choice of a zeolite type can depend on the molecular shape selectivity-, the hydrophobic- or hydrophilic- character and the weak or strong acid catalyst performance desired. The physicochemical properties can influence the required catalyst activity. For example, a low Si/Al ratio H-type will result in many acid sites, but low acid site activity, while a high Si/Al ratio type will contain less but stronger acid sites. Moreover, at high Si/Al ratio gradients in Al- distributions often occur with many weak acid sites in the crystal rim and less but relatively strong sites in the crystal interior.

Ad 2

Modifications are based on changing the original preparation procedure or adding a post-synthesis step.

A modification in either the uniformly space filling network of tetrahedral units or the guest species present in the pores will mutually change the properties of the framework as well as the void simultaneously, see Fig. 2.

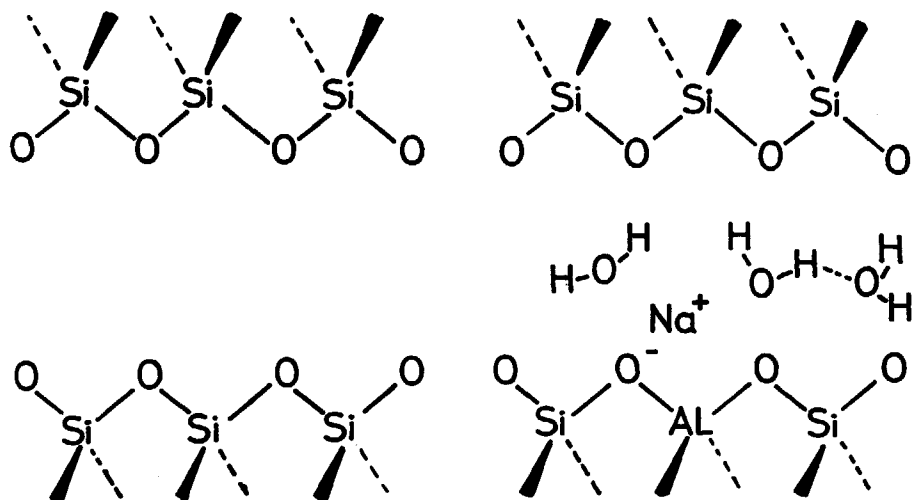
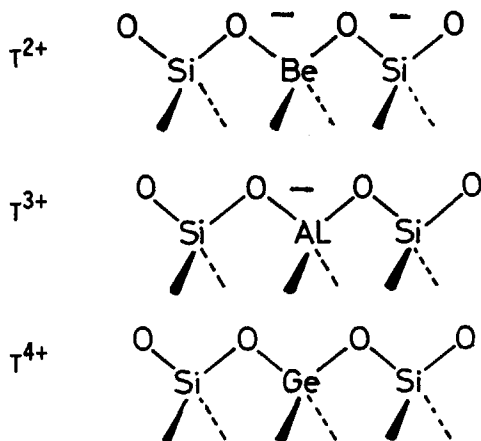


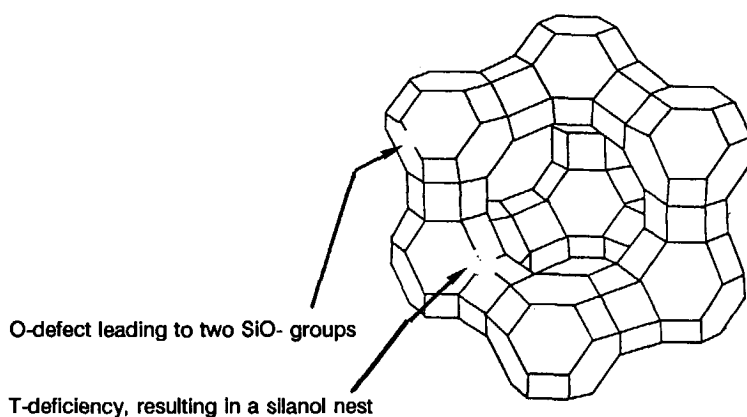
Figure 2, Simultaneous change of the framework- (a) and void- (b) property. Substitution of a Si- atom by an Al- atom leads to occupation of the void by cations and water molecules.

Modifications pertaining to the lattice include:

i) isomorphous substitution, e.g. of Si by T-atoms



ii) T-atom or O-atom deficiencies/defects



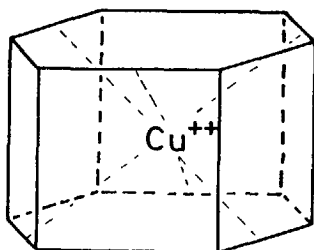
iii) occupation of T-atom- or O-atom deficiencies/ defects

by applying a selected reagent, Ref.[20]

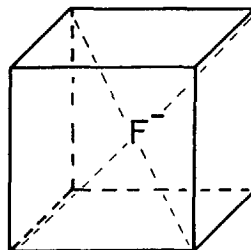
iv) de-alumination of zeolite Y with a so called steaming method to produce an ultra stable Y (US-Y)

v) lattice improvement of the silica Silicalite-1 with a steaming procedure to obtain a hydrophobic lattice without deficiencies and defects

vi) additional cations or anions in small rings or cages



corners are : Si or Al



corners are : alternating Al and P Ref. [7]

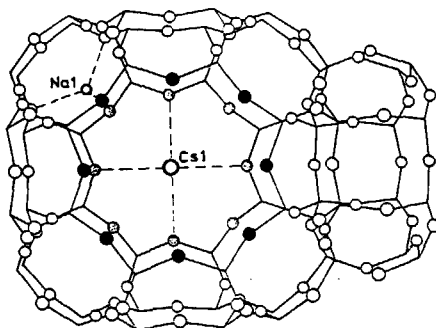
alternating Ga and P

Si

Modifications in the void are:

i) (de)hydration

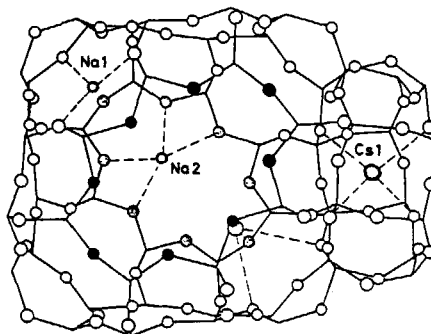
hydrated



silicate zeolite RHO

Ref. [8]

dehydrated



AlPO₄-18

5-coord. Al

4-coord. Al

Ref. [9]

phosphate

VPI-5

6-coord. Al

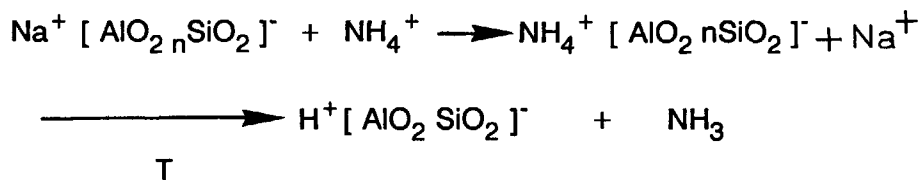
4-coord. Al

Ref. [10]

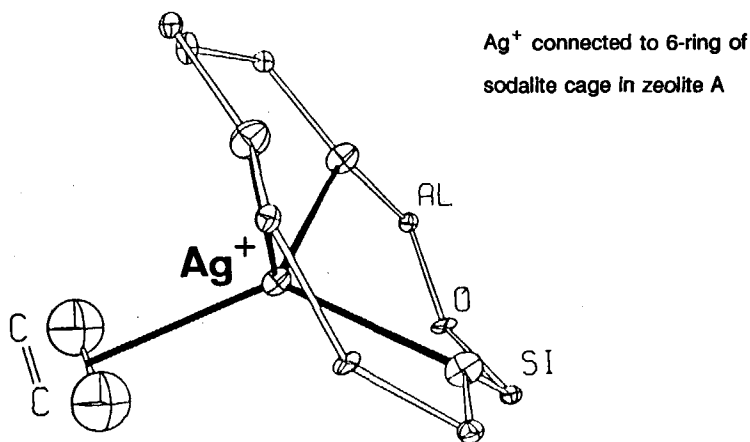
hydrated

dehydrated

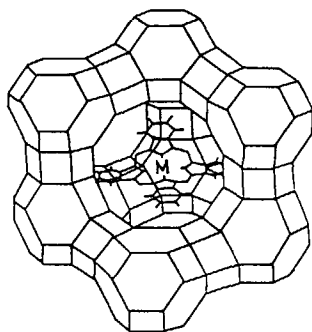
ii) ion-exchange leading to proton- containing zeolites



iii) M^{n+} with or without ligands connected to the pore wall Ref. [11]

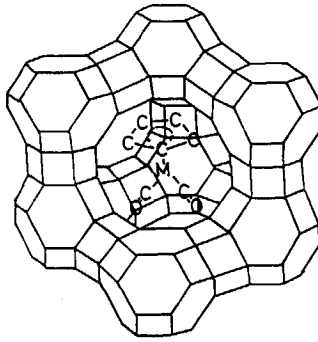


iv) M^{n+} coordination compounds trapped in a void (ship-in-a-bottle-system)



M-phthalocyanine in faujasite

v) organometallics as guest compounds

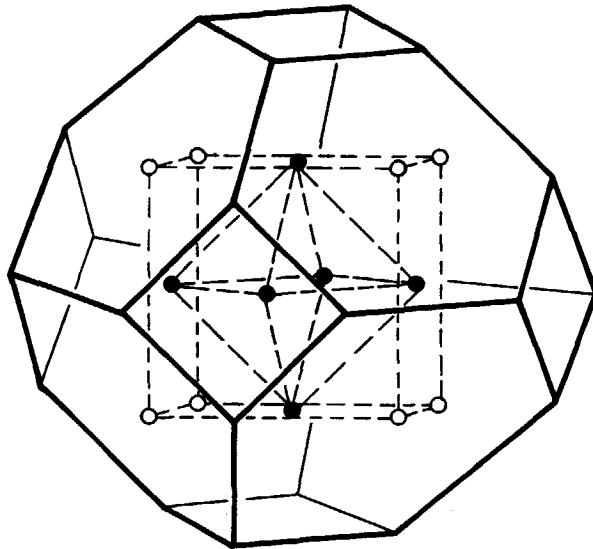


M-dicarbonyl-cyclopentadienyl in faujasite

vi) M^0 clusters trapped in a void

Ref. [11]

a)



Ag_6 -cluster, black, in a frame of $(Ag^+)_6$, white, in a sodalite cage

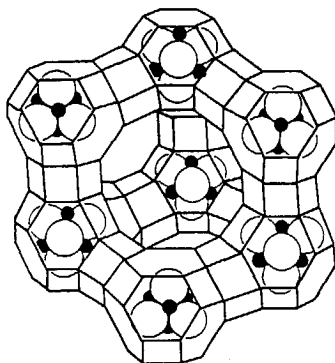
b) Pt, Pd or Rh in zeolite Y or mordenite

vii) non M^0 -clusters accommodated in channels

Ref.[12]

- a) Se-chain in $AlPO_4-5$
- b) Sulfur-cluster in sodalite

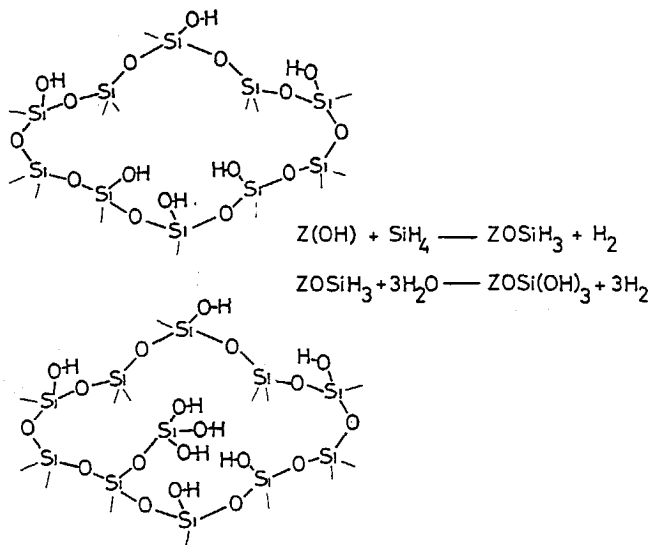
viii) occluded salts



$(CdS)_4$ in sodalite cages. Cd and S, black and white, respectively

Modification of the void entrance includes:

silanation or boronation of SiOH-groups in the void entrance, e.g. Ref. [13]



Chemical vapor deposition of Si- or Ge- alkoxides at the zeolite pore opening, followed by a heat treatment. In this way the pore opening may be narrowed.

The chemical modifications mentioned pertain mainly to the large internal surface of the materials. Each modification of this surface can have a strong influence on the catalytic and adsorptive properties of these molecular shape selective porous materials.

Based on the macroscopic crystal form and the framework topology it is frequently concluded that the external surface of a crystal of a few micrometer is 1% of the internal surface.

Catalysis results and external surface adsorption measurements often indicate, however, that the external surface is much larger.

Thus, recent observations with scanning tunneling microscopy, STM, and scanning electron microscopy, SEM, see Fig.3, indicate a roughness of the external surface which might lead to relatively large undesired surface contributions to the catalyst activity.

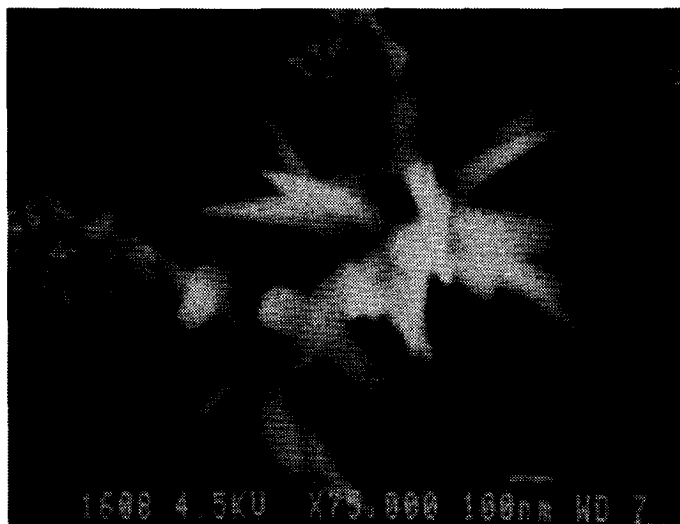


Figure 3a) SEM-picture of the external surface of zeolite ZSM-5. 100 nm particles are indicated by arrows and consistent in size with the particles of the STM-image of the external surface in Figure 3b.

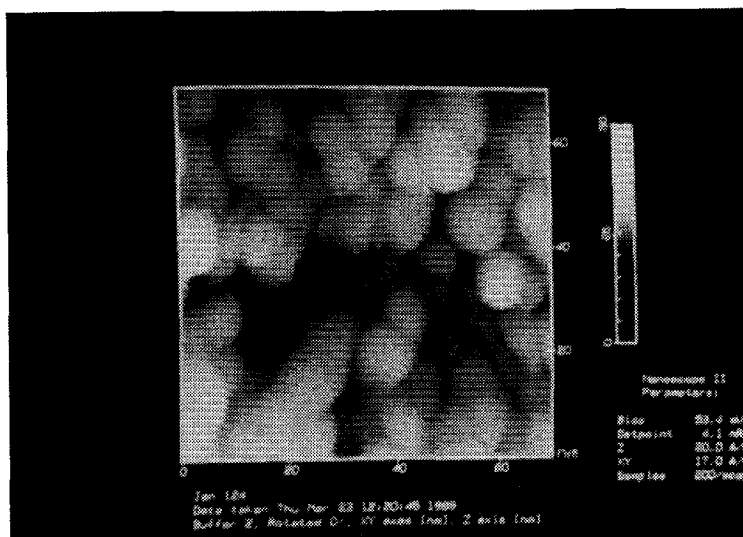


Figure 3b) STM-picture showing details of the external surface of zeolite ZSM-5, proving the rather corrugated character on nanometer scale.

The external/internal surface ratio which must be as small as possible, for reasons of optimal selectivity can be influenced in the following ways:

Inertization of the external surface of the crystals

reaction with bulky silicon-reagents

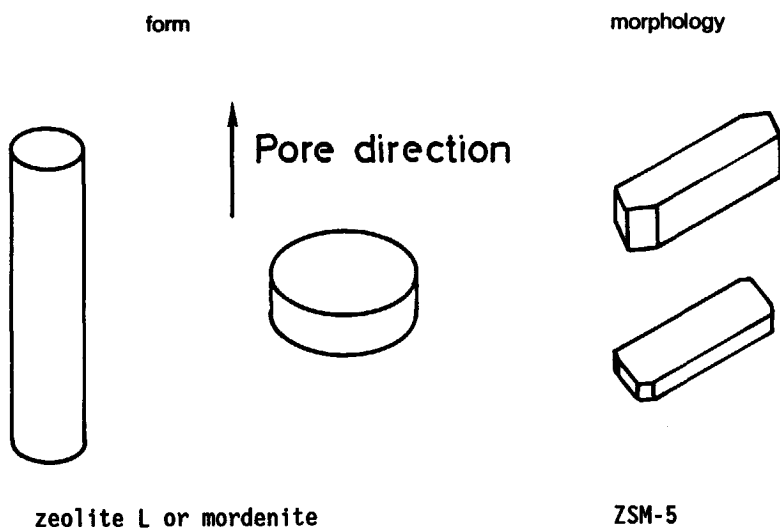
neutralizing acid centers with bulky nitrogen base [14]

de-alumination of external surfaces.

Change in size, form and morphology of the crystals

In the case of zeolite L and mordenite the fastest crystal growth and parallel channel direction coincide. Reducing the length in the needle direction and the extension of the crystal size perpendicular to this direction, *vide infra*, may result in more efficient catalysts.

change



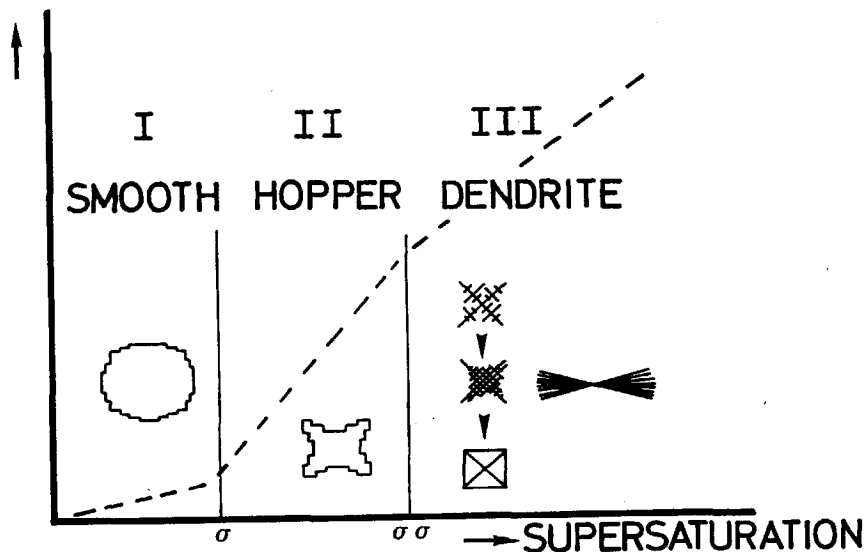
In general the physical modifications such as the size, the form and morphology of the crystals are of influence on the above mentioned surface ratio, the number of pore entrances and the minimization of the pore length. The size of the crystals can be influenced by the number of nuclei formed. The form and morphology are dependant on *i)* the supersaturation of the main tetrahedral units *ii)* the type of cation/template used in the synthesis and *iii)* the presence of inhibiting/promoting crystal growth species.

Many contributions on the size of the crystals are known, however, only a few studies are devoted to the form and morphology of the silica(te) and phosphate microporous crystals which is therefore dealt with in somewhat more detail here.

Ad i)

In general the crystal growth rate and thus the crystal form is a function of the supersaturation [15]. The basic mechanisms resulting in different crystal forms are shown in Scheme 1.

GROWTH RATE



Scheme 1, schematic drawing to illustrate the different crystal forms/morphology as a function of the arbitrary chosen supersaturation region. Three types of growth mechanism are given : (I) dislocation controlled spiral growth (II) 2-D nucleation growth and (III) continuous growth.

In the relatively low supersaturation regime the crystals grow in general via a surface dislocation which can be observed microscopically as a spiral growth on the growing crystal surface, which is macroscopically smooth.

An excellent example of a microsporous silicate crystal face growing this way is shown in Fig.4 for zeolite A. In a relatively high supersaturation the crystals grow via a two-dimensional surface nucleation mechanism. In this case the crystals grow faster at the corners and the rims compared to the faces. An example of this phenomenon, showing 'hopper' crystal faces, is given in Fig.5 for the gallophosphate LTA [7]. In a higher supersaturation regime with apart from the template the same mixture of nutrients dendritic growth must have occurred first as the growth of a highly ordered agglomerate of equally sized gallophosphate crystallites, also denoted as cloverite, is the final product [7]. The high supersaturation in which the crystallization of MFI-type material started to grow dendritically is illustrated in Fig. 6.

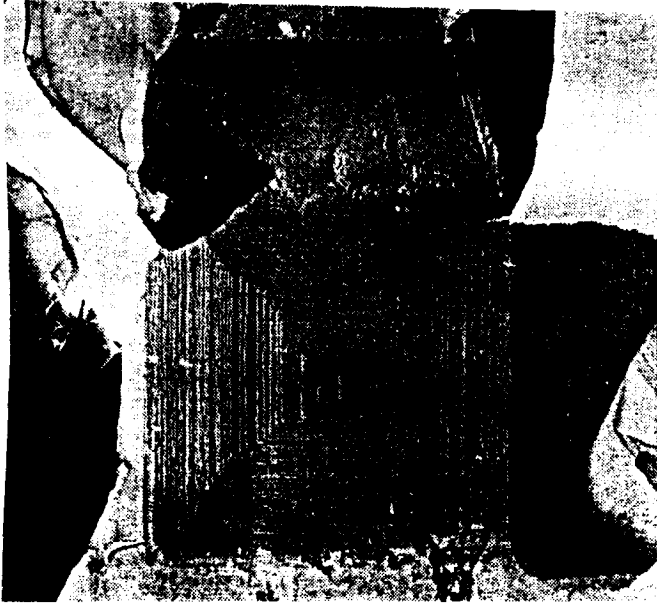


Figure 4. Spiral growth observed on a crystal face of zeolite type A.



Figure 5. Crystals of gallophosphate type LTA showing the 'hopper-like' faces, indicated by arrows, caused by the rather high supersaturation involved [7].

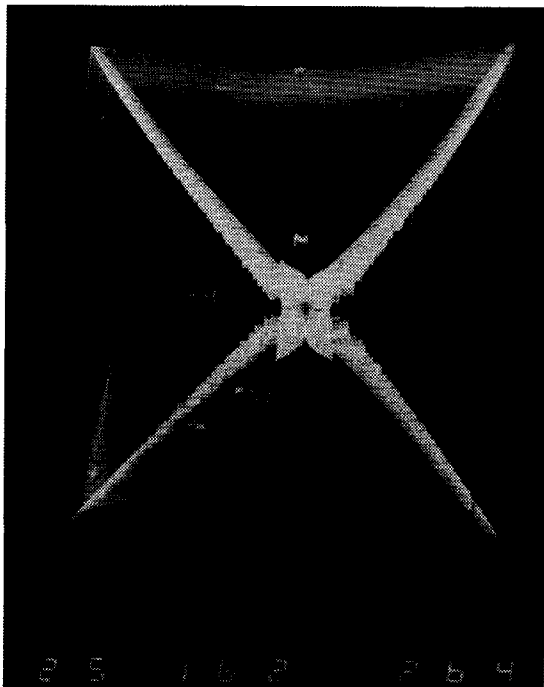


Figure 6 Dendritic form of MFI-type material grown on the external surface of a gelsphere in a highly supersaturated synthesis mixture.

The above described morphologies can be obtained for microporous materials by concentration variations of the main building unit (SiO_2) in the synthesis. Insight in such crystal growth parameters but also the study of the growth history and of the framework interaction with guest or additional molecules are essential to understand the development of crystal size, form and morphology.

Ad ii)

Inorganic and organic cations/templates or molecules necessary in the preparation to stabilize the microporous compound can drastically change, the crystal form/morphology. Factors include ionic-, hydrogen bridge- and C-H...O guest-framework interaction. The variation in guest species can be a difference in symmetry, shape, volume, polarity or chemical composition. For instance we observe that nearly a dimer of a template, see Fig 7a, caused a dramatic change in the crystal form of zeolite ZSM-5, see Fig. 7b.

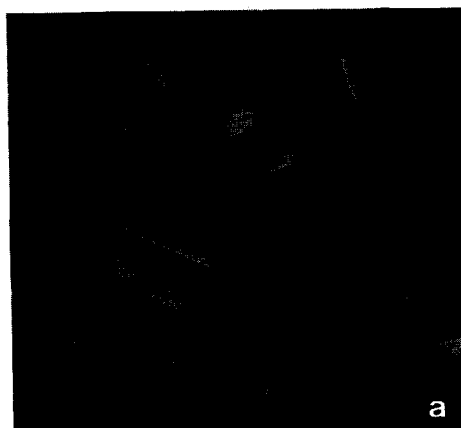
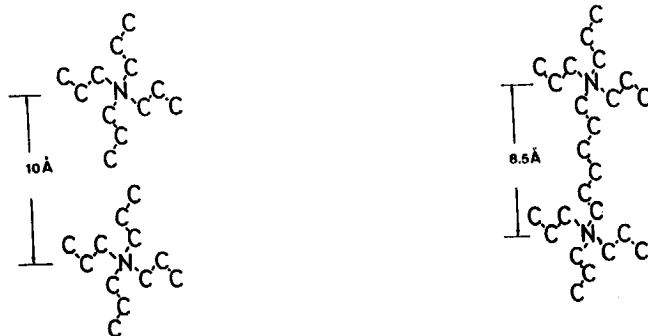


Figure 7, a) two monomers and one "dimer" of tetrapropylammonium. With each template the zeolite ZSM-5 was prepared, however, b) with a completely different morphology.

Ad iii)

Inhibition of crystal growth of certain crystal faces is often caused by additives in the synthesis mixture which are rather similar to the original building units. These species, mainly tetrahedral oxygen-cornered units, are either built in or interact strongly with certain crystal faces [16].

In general a change in crystal form but also an enrichment of crystal faces is then observed.

It is, however, well-known that large molecules like dyes, when present in synthesis formulations, can influence the form/morphology of molecular sieve crystals too [17].

For sensor and membrane applications continuous layers or mono-films of flat crystals are desired. In this case the composite materials are obtained by crystallization onto an added heterogeneous support in the synthesis mixture. The main properties of such a support are the chemical anchoring abilities, the chemical stability under the conditions of the synthesis and the flat surface which is either closed or macroporous.

Ad 3

The final factor tuning the microporous material for a particular application is the framework deformation. The molecular sieve frameworks are flexible as they are built up of tetrahedral units which are only corner-connected forming this way, up to 50 vol.%, porous materials. The variations in bonds and angles are given in Table 2. Furthermore the framework flexibility is illustrated in the case of isomorphous substitution of boron. The possible changes in bonds are given for boron in the framework in Table 2 too.

Table 2, Variation in bonds and angles in microporous materials.

microporous materials	bonds (A) d (T - O)	angles (o) Si - O - Si
SILICATE	1.6 - 1.7	140 - 180
ZEOLITE ZSM-5	1.57- 1.62	145 - 180
ZEOLITE RHO	1.61- 1.75	125 - 145
tetrahedral	1.45	
BORO-SILICATE		
trigonal	1.35	

The parameters influencing the framework deformation, are: (de)hydration, phase transition caused by doping atoms, ion exchange and guest molecule geometries. The framework deformation is generally reversible, as in the case of de(hydration) of many (not all) zeolites, which is actually a characteristic of the zeolites. There are, however, also non-reversible changes such as the transformation of VPI-5 into $AlPO_4$ -8. A frequently, and

most interesting with respect to adsorption properties, observed change in the pore/window geometry is the transition of circular to ellipsoidal. For instance the deformation of the circular- into an ellipsoidal 10-ring geometry of the channels of as-synthesized ZSM-5 after calcination and guest-molecule accommodation can change the cross-section of $5.5 \times 5.5 \text{ \AA}$ into less than $4.5 \times$ more than 6.0 \AA , respectively.

A deformation in the same direction of subsequent 10-rings migration of aromatic guest molecules, see Fig 8, is possible as elucidated in a crystal structure analysis of p-xylene-into-ZSM-5, [18].

The driving force for the deformation is in this case the p-xylene concentration. A larger deformation of the 10-ring membered sinusoidal channel is based on both the monoclinic phase formation, obtained upon cooling after an orthorhombic/ monoclinic phase transformation, and the p-xylene concentration. Although there is an interchange in the ellipsoidal direction of the subsequent 10-rings the p-xylene molecules can migrate into the channel. This is probably due to the accessibility of each ring in the case of the monoclinic or low temperature phase.

The p-xylene-ZSM-5 structure analysis clearly illustrates that the framework deformations can lead to unexpected adsorption and migration of completely differently shaped guest molecules. A less favourable change in the pore/window geometry is the reduction of the channel aperture when the subsequent ellipsoidal pore-forms are rotated 90° , as shown in Fig. 9. The adsorption of n-butane in zeolite RHO, based on adsorption data, was unexpectedly low based on the as-synthesized crystal structure analysis of RHO. For this reason the dehydrated structure of zeolite RHO was elucidated and proved channel aperture reduction, which could, however, not explain the low n-butane loading.

In a rather special case the framework deformation was achieved by external pressure on a pseudo-orthorhombic aggregate of a crystal consisting of monoclinic twin domains to obtain a single crystal of monoclinic ZSM-5, see Fig. 10, [19].

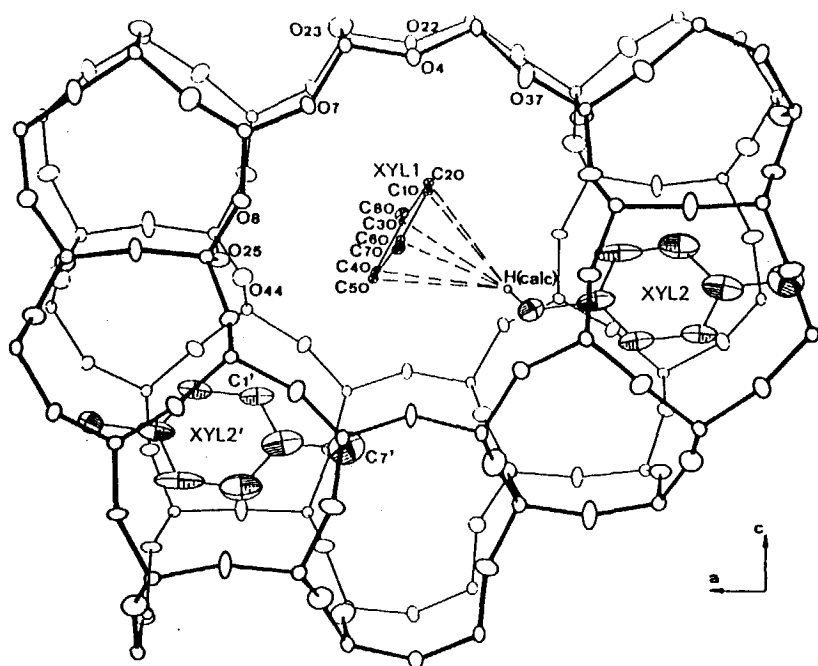


Figure 8, p-xylene molecules in the void of ZSM-5, view along the straight channel.

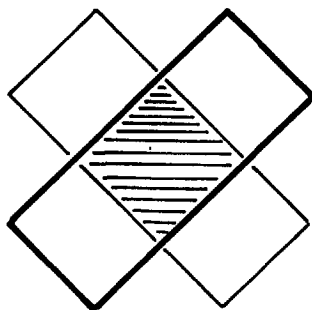


Figure 9 Schematic representation of pore blocking by subsequent rotation of 90° of ellipsoidal windows. Hatched area is the effective pore opening left.

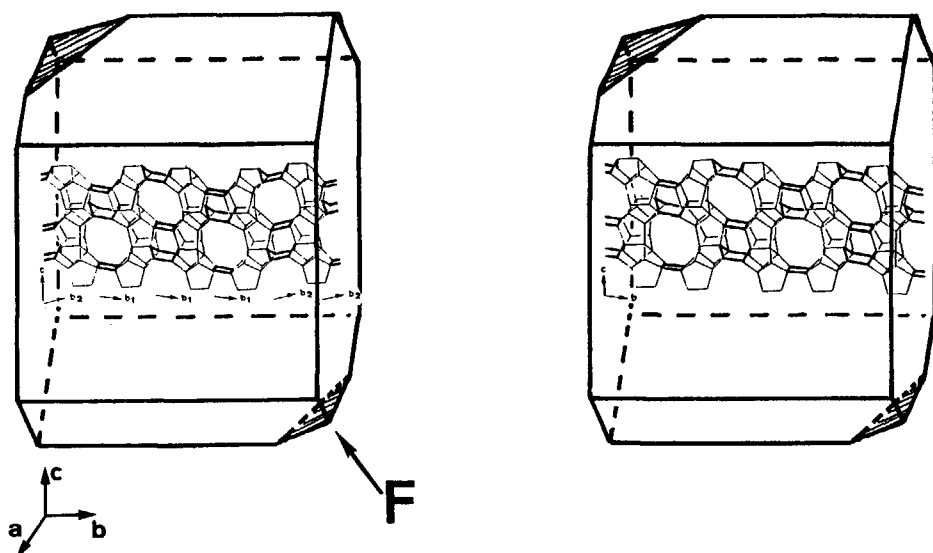


Figure 10, schematic drawing of pressure applied (F) on a monoclinic twinned crystal of the MFI - type to obtain a monoclinic single crystal.

References

- 1 E.M. Flanigen, in *Stud. Surf. Sci. Catal.*, 58, (Eds. H. van Bekkum, E.M. Flanigen and J.C. Jansen), Elsevier, Amsterdam, 1991, chapter 2.
- 2 S.T. Wilson, ref.1, chapter 4b.
- 3 W.M. Meier and D.H. Olson, *Atlas of Zeolite Structure Types*, 2nd. rev. edn., Butterworth, London, 1987.
- 4 M.E. Davis, *Ind. Eng. Chem. Res.*, 30, 1991, 1675-1683.
- 5 W.M. Meier and D.H. Olson, *Atlas of Zeolite Structure Types*, 2nd. edn., Butterworth, London, 1987.
- 6 R. Szostak, *Stud. Surf. Sci. Catal.*, ref.1, chapter 5.
- 7 H. Kessler, *Synthesis/Characterization and Novel Applications of Molecular Sieve Materials*, Mat. Res. Soc., 233, 1991, 47-55.

- 8 L.B. McCusker, and Ch. Baerlocher, *Proc. 6th Int. Zeol. Conf.*, (Eds. D.H. Olson and A. Bisio), Reno, Butterworth, 1984, 812-822
- 9 A. Simmen, L.B. McCusker, Ch. Baerlocher, and W.M. Meier, *Zeolites*, 11, 1991, 654-661.
- 10 L.B. McCusker, Ch. Baerlocher, E. Jahn and M. Bulow, *Zeolites*, 11, 1991, 308-313.
- 11 K. Seff, *Acc. of Chem. Res.* , 9, 1976, 121 - 128.
- 12 G.D. Stucky and J. E. Mac Dougall, *Science*, 247, 1990, 669-678.
- 13 P. de Hulsters, F. Goovaerts, J. Philippaerts, Y. Yan and E.F. Vansant, *Stud. Surf. Sci. and Catal.*, 49A, (Eds. P.A. Jacobs and R.A. van Santen), Elsevier, Amsterdam, 1989, 271-280.
- 14 W.F. Holderich and H. van Bekkum, ref. 1, chapter 16.
- 15 I. Sunagawa, *Bull. Mineral.*, 104, 1981, 81-87.
- 16 J.C. Jansen, E. Biron and H. van Bekkum, *Stud. Surf. Sci. Catal.*, Vol.37, (Eds. P.J.Grobet, W.J. Mortier, E. F. Vansant and G. Schulz-Ekloff), Elsevier, Amsterdam, 1988, 133-142.
- 17 R.M. Barrer, *Hydrothermal Chemistry of Zeolites*, Academic Press, London, 1982.
- 18 H. van Koningsveld, H. van Bekkum and J.C. Jansen, *Acta Cryst.*, B43, 1987, 127-132.
H. van Koningsveld, F. Tuinstra, H. van Bekkum and J.C. Jansen, *Acta Cryst.*, B45, 1989, 423-431.
- 19 H. van Koningsveld, F. Tuinstra, J.C. Jansen and H. van Bekkum, *Zeolites*, 9, 1989, 253-256.
- 20 R. de Ruiter, J. C. Jansen and H. van Bekkum, to be published.

CHAPTER 3

THE PREPARATION OF ZEOLITES AND ALL-SILICA ANALOGUES*

I. INTRODUCTION

a. General

Nature provided mankind with zeolites (ref. 1). Massive zeolite deposits have been discovered at many places in the world (ref. 2). The occurrence of natural zeolites can be assigned to certain geological environments or hydrological systems (refs. 3,4).

Natural zeolites generally form by reaction of mineralizing aqueous solutions with solid aluminosilicates. The main synthesis parameters are: (i) the composition of the host rock and interstitial solutions; pH ~ 10, (ii) the time; thousands of years and (iii) the temperature; often < 100 °C.

The first systematic studies on zeolite synthesis could thus be guided by the geological and mineralogical findings of the natural species (ref. 5). From 1946 on many additional zeolite types without a natural counterpart have been synthesized (ref. 6). The evolution in the preparation of one of the most studied zeolites is illustrated in Figure 1 by the number of papers and patents on the material denoted as ZSM-5 (ref. 7 and Section XII of this chapter).

* J.C. Jansen, The Synthesis of Zeolites, in: H. van Bekkum, E.M. Flanigen and J.C. Jansen (Eds.), Stud. Surf. Sci. Catal. 58, Elsevier, Amsterdam, 1989, pp. 77-130.

NUMBER OF REPORTS

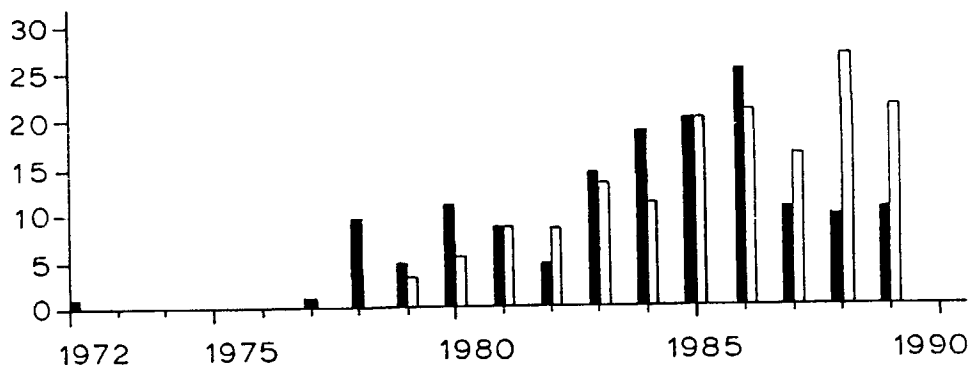
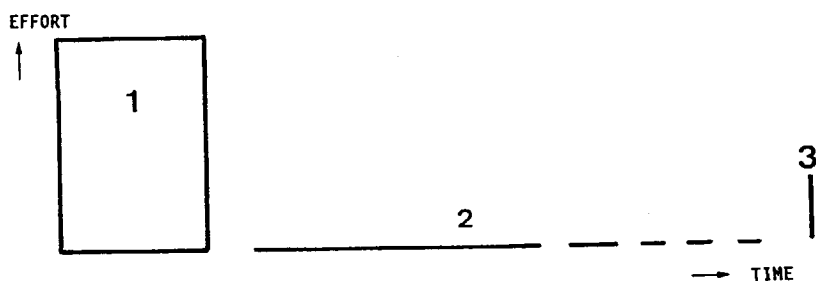


Fig. 1. The annual number of papers (□) and patents (■) on the preparation of zeolite ZSM-5 since the first publication in 1972.

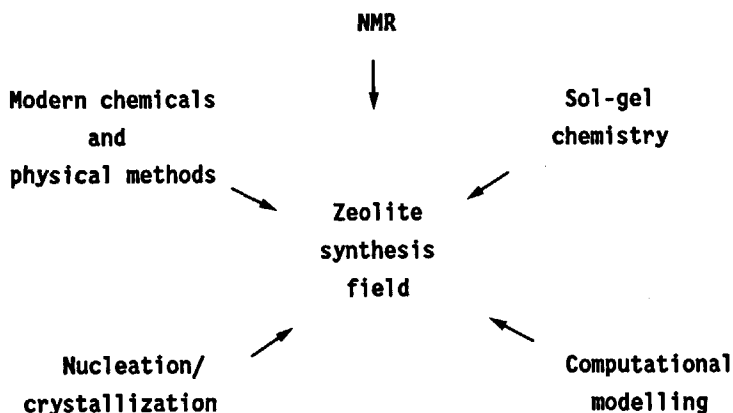
Throughout the last four decades molecular sieves were mainly prepared by precipitation/crystallization of an aqueous mixture of reagents at $6 < \text{pH} < 14$ and temperatures between 100-200 °C. As shown in Scheme 1 a relatively large effort is needed on the optimal preparation procedure of the reactant mixture,



Scheme 1. The effort for the preparatory (1), the reaction (2) and the isolation (3) versus time.

whereafter the hydrothermal reaction process (2) runs autoclaved for a few days or weeks without manual intervention. Isolation (3) of the crystalline material is a simple final step in the synthesis procedure.

The zeolite synthesis field is not only extended and refined by useful data of modern zeolite characterization and application techniques but also by interfacing areas of physical, chemical and mathematical science, see Scheme 2.



Scheme 2. Areas of chemical, physical and mathematical science interfacing the zeolite preparation field.

Studies in the sol-gel chemistry and NMR analysis area have contributed substantially to the knowledge of the hydrothermal reaction process.

Papers and reviews regarding subjects within the different areas which are mentioned in Scheme 2 and which are of interest for zeolite synthesis are given in Table 1.

Besides the annually new zeolite preparations the extensive exploratory efforts of "zeolite scientists" in the last decade has resulted in the synthesis of porous materials like the AlPO_4 -group (ref. 172), the metal-sulfides (ref. 30) and the clathrasils (ref. 31). Accordingly, zeolite synthesis appears to remain a promising area for future research.

The crystallinity of different synthesis products is well illustrated in Plate 1. The morphology and forms of the crystals give a first indication of the type of zeolite present and the purity of the product.

Table 1. Examples of subjects from areas of physical, chemical and mathematical science which delivered contributions to the knowledge of the zeolite synthesis process together with references.

Area	Subject	Reference
Sol-gel chemistry	Hydrolysis and condensation of silicates	8,9
	The sol-gel process	10
NMR	Structure of (alumino)silicate-clusters in solution	11,12
Computational modeling	Lattice energy calculation	13
	Local interactions in lattice	14
Modern chemical and physical methods	Alkoxides as reagents	15
	Fluorides as reagents and mineralizing agents	16
	Gravity - reduced	17
	- elevated	18
	CVD (chemical vapour deposition)	19
	Microwave	20
Nucleation/crystallization theory-practise	Mathematical analyses of zeolite Crystallization. A review	21
	Are the general laws of crystal growth applicable to zeolite synthesis	22
Zeolite		
Characterization	ZSM-5/-11 intergrowth	23
Application	Catalysis	
	- The catalytic site activity	24,25,26
	- The catalytic properties and the crystal size	27

b. This chapter

In this part of the chapter the preparation of two subgroups of the micro-porous tectosilicates (see Chapter 3) i.e. the aluminosilicates and silicates, both including the clathrasils, will be presented. The division between aluminosilicates and silicates is often discussed on Al-poor rather than Al-free level (ref. 30).

The aluminosilicates, starting from Si/Al ratio 1 up to e.g. Si/Al ratio of 10000, do reveal the presence of Al in synthesis, in characterization as well as in application, see Fig. 2 (ref. 31).

The Al-poor zeolites show no, at least no detectible, Al-dependent behaviour and are therefore, together with the Al-free materials, denoted as silicates.

The presence of aluminium, the guest-host interaction and the nucleation and crystallization all contribute to the synthesis events which are chronologically described in Sections II to VII of this chapter.

Section VIII is focussed on the reaction parameters.

In Sections IX and X the silicates and clathrasils are presented.

Examples of research syntheses performed with certain procedures and/or mixture compositions are listed in Section XI.

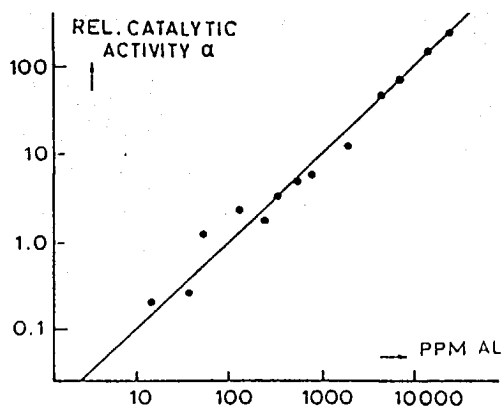


Fig. 2. The relative catalytic activity of H-ZSM-5 versus Al content on ppm scale (ref. 31).

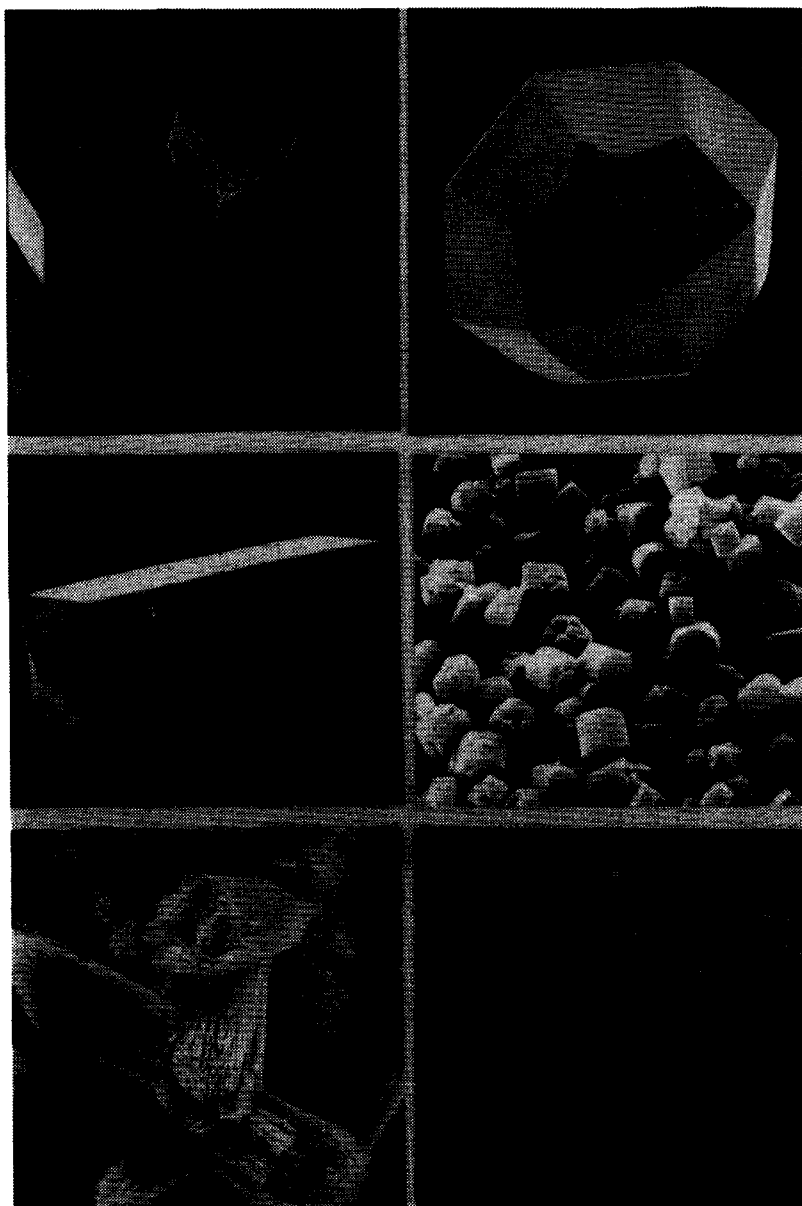


Plate 1. The crystalline nature of zeolites. a) Single crystals of zeolite A and b) and c) of analcime and of natrolite, respectively. d) A batch of zeolite L, e) typical needle aggregates of zeolite mordenite and f) of Nu-10.

II. PREPARATORY

a. Reactants

The chemical sources which are in principle needed for zeolite syntheses are given in Table 2.

Table 2. Chemical sources and their function in zeolite synthesis.

Sources	Function(s)
SiO_2	Primary building unit(s) of the framework
AlO_2^-	Origin of framework charge
OH^-	Mineralizer, guest molecule
Alkali cation, template	Counterion of framework charge, guest molecule
Water	Solvent, guest molecule

Within each type of source a variety of chemicals (ref. 32), has been used as the differences in physical nature and chemical impurities strongly influence the zeolite synthesis kinetics (ref. 34) and sometimes the properties as catalysts (refs. 24-27).

Data on the specifications of regularly used chemical sources are given in the following survey.

- SiO_2 -sources

Recent synthesis papers of the Proceedings of the International Zeolite Conferences (refs. 34-37) and of other zeolite conferences (refs. 38-40) reveal that for laboratory scale particular Si-sources are often used, see Table 3a.

Depending upon the particular synthesis a certain Si-source might favour a specific crystallization. For instance, the Aerosil 200 product can be readily dissolved compared to the Optipur and Gold label material because of the difference in particle size, see Figure 3. As the rate of dissolution can influence the rate of nucleation and crystallization (ref. 41) the product formation can be affected. At the same time the Al and other potentially Si replacing impurities are more than 10000 times higher in the Aerosil 200 product compared to the Optipur and Gold label materials.

The influence of impurities can change the crystal form (ref. 42) and the chemical properties (refs. 24-26).

Table 3. Specifications and the references of recent, regular used sources, and high-pure, * Si-, and * Al-sources.

Si-source (a) Al-source (b)	Specifications		Reference manufacturer
	Phys.	Chem. impurities (ppm)	
(a)			
<i>Silicon compounds</i>			
Si(OCH ₃) ₄ Tetramethyl orthosilicate (TMOS)	liquid	Na,Ca < .5	Merck
Si(OC ₂ H ₅) ₄ Tetraethyl orthosilicate (TEOS)	liquid	Al,Pt < .2	
Na ₂ SiO ₃ ·9H ₂ O (or Na ₂ H ₂ SiO ₄ ·8H ₂ O) Na ₂ O 11%, SiO ₂ 29% Water glass		Al < 200 Fe < 120 Ti < 60 heavy metals < 50	"N" Philidelphia Quartz Co.
<i>Colloidal silica</i>			
Ludox-AS-40 SiO ₂ 40 wt % NH ₄ ⁺ (counter ion)	sol	Al < 500 Zr Fe < 50	DuPont de Nemours
Ludox-HS-40 SiO ₂ 40 wt % Na ⁺ (counter ion)		Ti B < 10	
<i>Fumed silica</i>			
Aerosil-200 CAB-O-SIL M-5	D _p ~ 12 nm	Al < 10 Fe < .6 Ti < 10	Degussa BDH
<i>* Silica</i>			
Optipur Gold label	D _p ~ 200 μm D _p ~ 800 μm	Al < .001 Fe < 0.01	Merck Aldrich

Table 3, continued

(b)

- NaAlO_2 Na_2O 54% Sodium aluminate		Fe < 4	Riedel de Hahn Carlo Erba BDH Ltd.
- AlOOH Pseudo-boehmite Al_2O_3 70% H_2O 30% Catapal-B	$D_p \sim \text{nm}$	Fe < 4 Ti < 40	Vista
- $\text{Al}(\text{OH})_3$ Gibbsite		Fe < 3	Merck
- $\text{Al}(\text{NO}_3)_3 \cdot 9\text{H}_2\text{O}$			
- Al_2O_3 * Aluminium oxide (Ultrax)	$D_p \sim \text{nm}$	Fe < 0.01	Baker

Therefore, a careful choice of the reactants is needed. The high grade Si-alkoxides of which even double alkoxides like -Si-O-Al- are available (ref. 43) do not have the above discussed disadvantages, except for the rate of hydrolysis of the alkoxide groups.

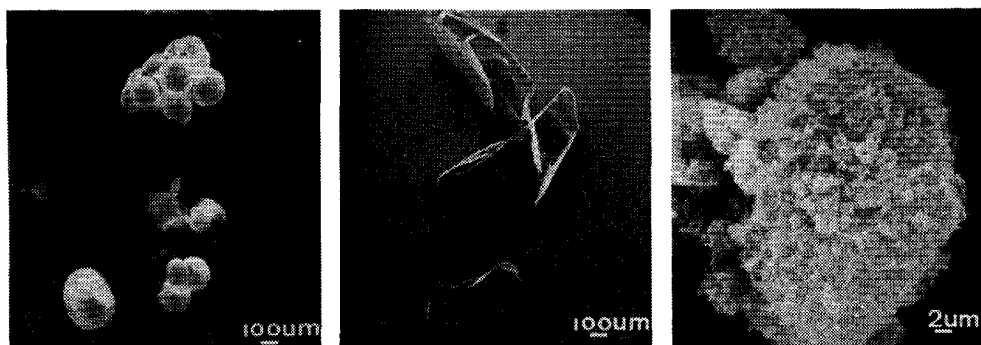
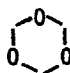
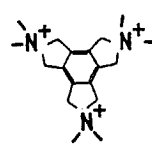
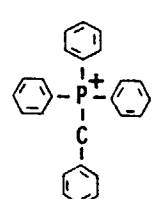


Fig. 3. SEM photographs of (a) Optipur, (b) Gold label, and (c) Aerosil 200.

Table 4. Type of organic templates, functional atoms/groups and references.

Organic template	Functional atom/group aliphatic aromatic	Ref.	Organic template	Functional atom/group aliphatic aromatic	Ref.
amine	$-N<$	49			
	$-N<$ $n=4,5$	50	penta-erythritol	$\begin{array}{c} C-OH \\ \\ HO-C-C-OH \\ \\ C-OH \end{array}$	65
	$N<$	51	amine + alcohol	$>N-(C_n-OH)_x$ $n=2,3$ $x=1-3$	66
di-amine	$>N-C_n-N<$ $3 \leq n \leq 9$	52			
	$N<$	53	ammonium + alcohol	$-N^+-C_n-OH$ $n=2$	67
ammonium	$-N^+-$	54			
	$-N^+$ $n=4,5$	55	acetal		68
	$-N^+$	56			
	$C_n-N^+-C_n$ $n=4,5$	57	amine + ether	$-N<$	69
di-ammonium	$-N^+-C_n-N^+-$ $3 \leq n \leq 9$	58	N-oxide + ammonium	$-O^+-N<N^+-$	70
	$-N^+-N^+-$	59			
tri-ammonium		60	phosphanium	$-P^+-$	71
amine + ammonium	$N<N^+-$	61			72
alcohol	C_n-OH $n=1-6$	62			
di-ol	$HO-C_n-OH$ $n=2-6$	63	bis-phosphanium	$-P^+-C_6-P^+-$	73
tri-ol	$\begin{array}{c} HO \quad OH \\ \quad \\ C-C-C \\ \\ OH \end{array}$	64			

- AlO_2^- source

Often used Al sources, collected from the same references as given for the Si-sources, are listed in Table 3b together with the main chemical impurity. Though the very pure Al_2O_3 product consists of small particles it is not easily dissolved.

- Alkali cation/template

The inorganic cations in the zeolite synthesis are mainly alkaline or ammonium ions. The organic cations/templates used may be divided in charged and neutral molecules containing functional atoms or groups. The large number of organic molecules used in zeolite synthesis is extensively listed in several publications (refs. 44, 45) together with the specific zeolite product formed. To illustrate in general the variation in organic template molecules some of the more common templates are listed in Table 4.

- OH^-

Most zeolite syntheses are performed under basic conditions using OH^- as a mineralizing agent. A second agent is F^- (refs. 16 and 46) of which the different nature compared to OH^- will be discussed in the section on reaction parameters.

Both anions are the counter ion of the inorganic or organic cations used for the syntheses. Depending upon the quality of the mineralizing agent impurities such as Al^{3+} and Fe^{3+} are present at ppm unit scale.

- The overall reactant mixture

In general the chemical behaviour of impurities like Fe^{3+} and Ti^{4+} are of minor importance compared to Al^{3+} in high Si/Al zeolites in the heterogeneous catalysis when based on Brønsted activity. However, in the case of an all silica zeolite, or modified zeolites like B-ZSM-5, Fe-ZSM-5 and Ga-ZSM-5 traces of Al^{3+} from reactants as given in Table 3 may play an unexpected dominant role in the Brønsted activity (refs. 24-26). Extensive information on this point is given in Chapter 5 on the modification of zeolites. Another example of the influence of impurities from reactants is K^+ . The crystallization time can be retarded by factors when K^+ is present in the syntheses of e.g. zeolite Na-A or Na-ZSM-5 (refs. 47, 48).

Impurities like trivalent metal ions sometimes change physical conditions in the reaction mixture indicated by the crystal form or morphology (ref. 42).

b. The reaction vessel and hydrothermal conditions

Depending upon the reaction temperature chosen, mainly between 60 °C and 300 °C, reaction vessels can vary as shown in Table 5. Various Teflon inserted autoclaves, see Fig. 4a, together with relatively low priced (stainless steel) and high priced (reenforced polyetheretherketone) autoclaves are shown in Fig. 4b and 4c.

To follow the course of the events taking place in the synthesis mixture, a lookthrough autoclave, see Fig. 4d, can be used. It was concluded, using such experimental conditions, that nucleation and crystallization of zeolite ZSM-5 occurred *on* and *in*, respectively, gel spheres of about 2 mm (ref. 42).

Another possibility to monitor synthesis events *in situ* is the application of IR internal reflectance using a crystal embedded in an autoclave, as shown in Fig. 5 (refs. 74, 75).

Table 5. Regular used lab-scale reaction vessels, the typical impurities and temperature range.

Reaction vessel	Volume	Impurity	Temperature
Plastic bottle	< 1 l	Zn ²⁺	< 100 °C
Stainless steel autoclave	< 5 l	Fe ³⁺ , Cr ³⁺	>> 200 °C
Stainless steel + teflon lining	< 2 l	nuclei of preceding synthesis	< 200 °C
Quartz autoclave	< 5 ml	Si	< 200 °C

The autoclaves must be filled between 30 and 70 vol % in the case of an aqueous reaction mixture between 100 and 200 °C to maintain a liquid phase (ref. 76).

Cleaning of the reaction vessels can be considered in some cases, e.g. the teflon-lined autoclaves. As memory effects caused by nuclei of preceding synthesis in cavities of the teflon wall can be encountered in subsequent experiments it is important to clean the vessel with either HF and water at room temperature or with NaOH and water at the reaction temperature.

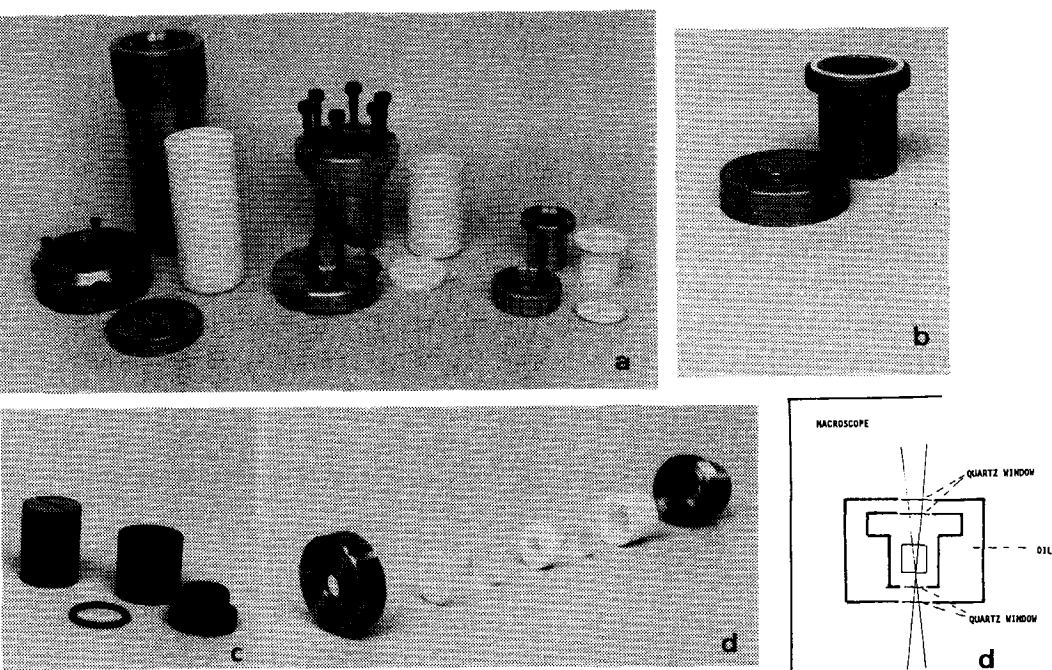


Fig. 4. Different autoclaves for laboratory use. a) Teflon lined autoclaves up to 1000 ml, b) stainless steel autoclave of 25 ml, c) "Arlon" (polyether etherketone) reenforced with carbon fiber or glass fiber) autoclaves and d) stainless steel look through autoclave with quartz windows and Teflon inserts in exploded view together with a schematic drawing of the experimental set up.

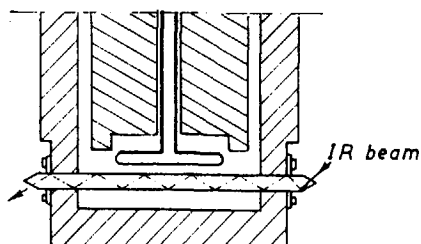
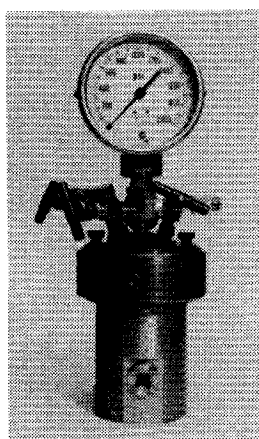


Fig. 5. Parr mini autoclave. IR internal reflection via a crystal embedded in the autoclave makes monitoring of zeolite synthesis events possible (ref. 74).

III. ZEOLITE PRODUCT VERSUS THE SYNTHESIS MIXTURE

a. Two synthesis examples

The fine tuning and differences in the preparation of each zeolite type is too complex to be discussed in this introduction on the synthesis of zeolites. In specific parts of the chapter, however, is chosen for a more detailed presentation of the synthesis of two substantial different zeolite types, i.e. zeolite Na-A and zeolite TPA-ZSM-5. The two zeolites present roughly all the groups in which zeolite types are divided (ref. 77). The synthesis mixtures and chemical and physical properties of both zeolites are given in Table 6.

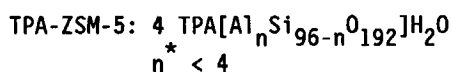
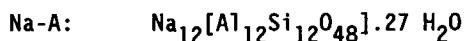
Table 6. The synthesis mixtures, physical and chemical properties of zeolites Na-A and TPA-ZSM-5 (refs. 78-80).

Na-A		TPA-ZSM-5
<i>- An example of synthesis mixtures - (molar oxyde ratio)</i>		
1	SiO ₂	1
.5	Al ₂ O ₃	< .14
1	Na ₂ O	.16
	TPA ₂ O	.3
17	H ₂ O	49
< 100	t (°C)	> 150
<i>- Physical and chemical properties -</i>		
3D, holes connected via windows	pore arrangements	2D, intersecting channels
1.28	density (g/cm ³)	1.77
.37	pore volume (cm ³ /g)	.18
Na ⁺ , H ₂ O	lattice stabilization	TPA ⁺
1	Si/Al	≥ 12
low	Brønsted activity	high
hydrophylic	affinity	hydrophobic

b. Zeolite product versus synthesis mixture

The most simple zeolite product composition can be given by the overall Si/Al ratio and the cation type/content.

More often the unit cell composition of the zeolite crystal is expressed, e.g.



* At higher loadings than 4 Al/uc, TPA^+ is replaced by the smaller cation Na^+ (ref. 81).

The zeolite reaction mixture is often formulated in the molar oxide ratio of the reactants, e.g. $\text{SiO}_2:\text{Al}_2\text{O}_3:\text{Na}_2\text{O}:(\text{TPA}_2\text{O}):\text{H}_2\text{O}$. The ratios of $\text{H}_2\text{O}/\text{SiO}_2$, OH^-/SiO_2 , $\text{SiO}_2/\text{Al}_2\text{O}_3$ and $(\text{Na}_2\text{O}/\text{TPA}_2\text{O})$ then give an impression of the concentration, solubility and the expected zeolite types, respectively (ref. 82). Correlation between the synthesis mixture and the product can be obtained from ternary composition diagrams (see Fig. 6a,b) (refs. 83-86), or from graphs of crystallization fields of zeolite types as a function of reactant ratios, see Fig. 6c and Section XI.b.3.

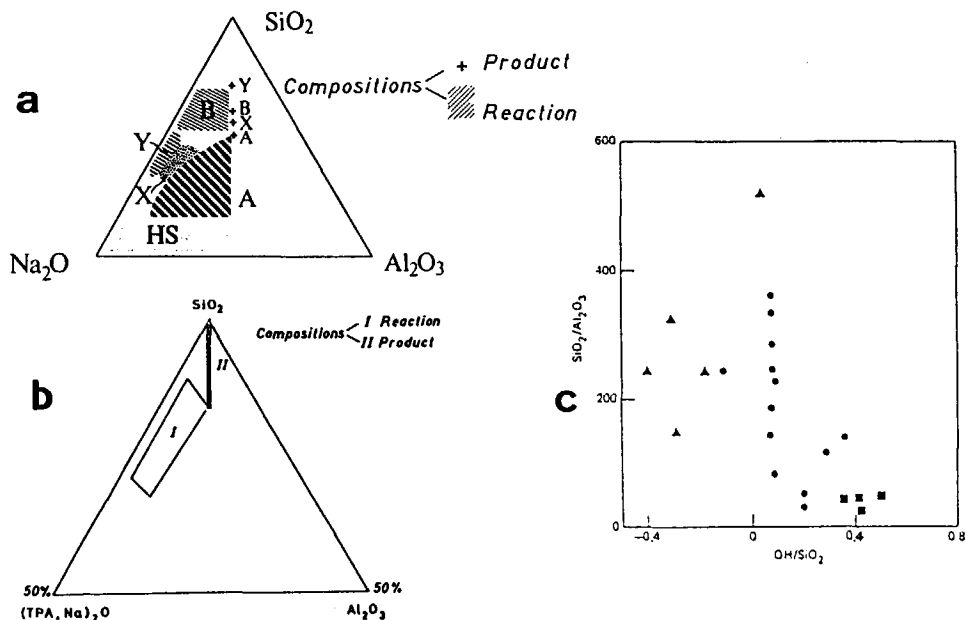


Fig. 6. Zeolite product versus the synthesis mixture. a) and b), ternary composition diagrams with an inorganic and organic cation/template, respectively. c) Crystallization fields, indicating (●) ZSM-5, (■) ZSM-35, and (▲) ZSM-39 (ref. 87).

The product fields at certain P,T, depicted in Fig. 6, are obtained from experimental data which are not always expected from a thermodynamic point of view. As the inevitably heterogeneous synthesis mixture contains micro-domains with different reactant ratios, kinetic parameters might induce other product phases than those derived from the ternary synthesis composition diagram. Because particularly the nucleation is kinetically determined it is thus of interest to understand the different factors, e.g. type of Si-source, cation, Al-source, additives and physical parameters, influencing the kinetic stage of nucleation. The influence of these factors can be recognized in the subsequent events of the zeolite preparation which are given in Table 7 and discussed hereafter in detail.

Table 7. The subsequent events present in the course of the zeolite preparation.

Temperature	Subsequent events
Low (< 60 °C)	Reactant solutions Reactant mixture - gel formation
Low → high (< 60 °C → < 200 °C)	Gel rearrangement Dissolution of gel Dissociation of silicate
High (< 200 °C)	Pre-nucleation phase Nucleation Crystallization
Low (< 60 °C)	Isolation

IV. THE LOW TEMPERATURE REACTION MIXTURE

a. Introduction

The reaction mixture events occurring at low temperature (< 60 °C) will be discussed for two reasons.

- i) Reaction mixtures are prepared at low temperature. Drastic chemical and physical changes take place then.
- ii) Substantial knowledge about the zeolite reaction mixture at low temperature has been obtained using characterization methods such as the molybdate method (ref. 88), the paper chromatography method (ref. 89), the trimethylsilylation method (ref. 90), IR- and laser-Raman spectroscopy (ref. 91), single crystal structure analysis (refs. 92, 93) and the NMR technique (ref. 94).

Mostly, starting reaction mixtures typically consist of a gel phase and a liquid phase which means that nucleation is initiated at high temperature by the presence of a residual gel phase, though there are a few exceptions (refs. 91, 95). The (alumino)silicate gel phase consists of either a homogeneous dispersed phase of branched chains of sol particles, see Fig. 7a, or a more separated solid phase of an ordered aggregate of sol particles (like opals), see Fig. 7b (refs. 96, 97).

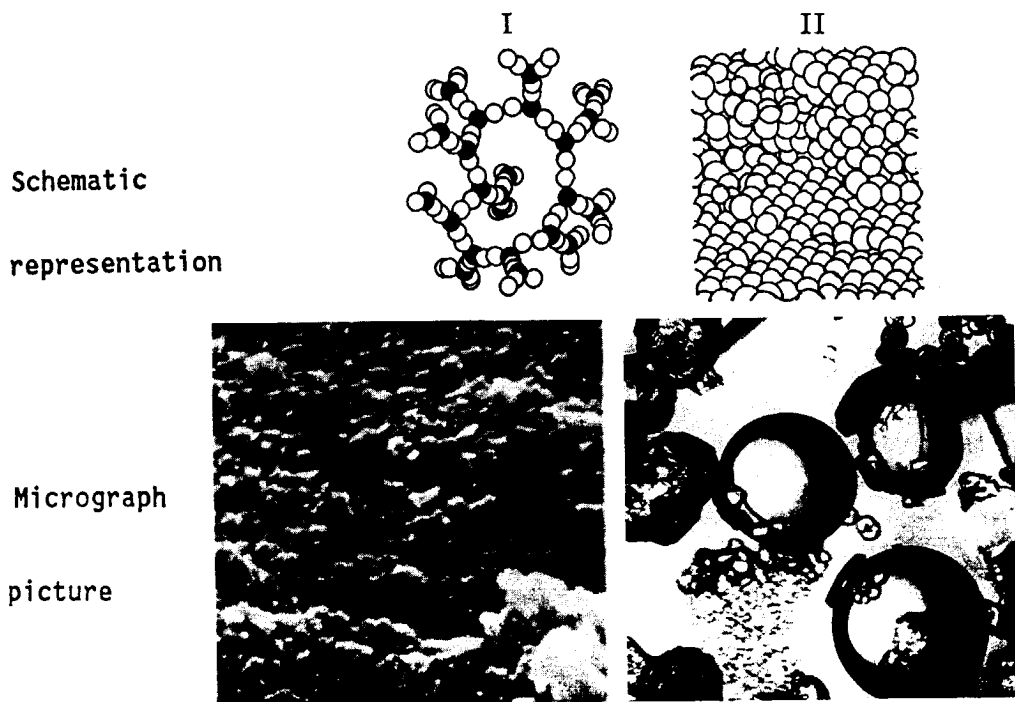


Fig. 7. Alkaline gel forms. Schematic representation and micrograph picture of I) a dispersed low-density gel (ref. 96b) of branched chains of sol particles and II) a separated high-density gel form resulting in spheres consisting of an ordered aggregate of sol particles (like opals).

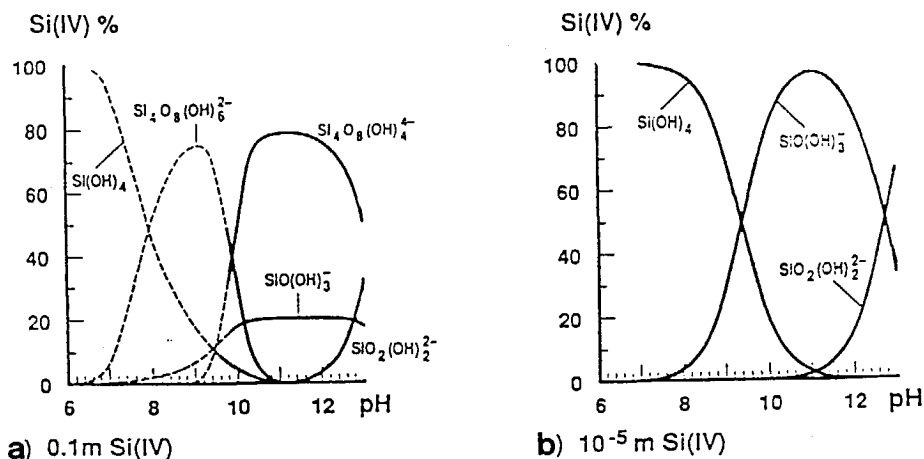
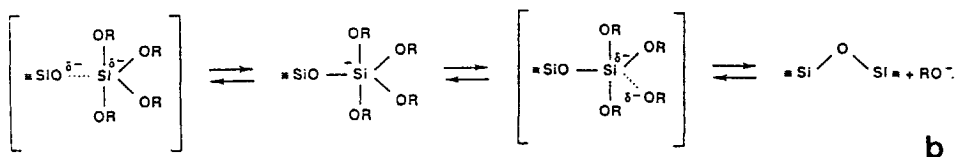


Fig. 8. Silicate distribution versus pH at a) high and b) low silicate concentration (ref. 98).

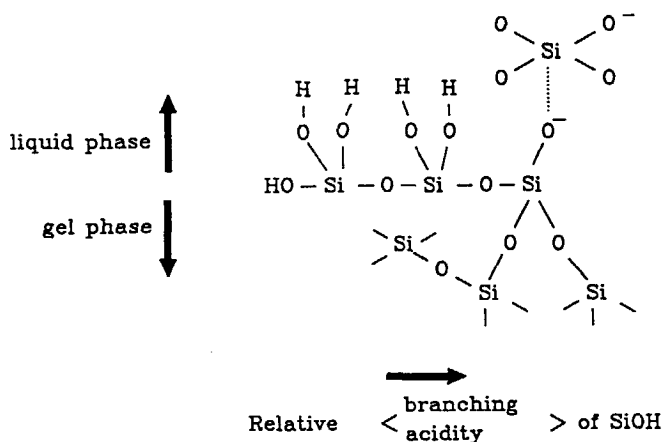
The pH of the liquid phase, in the case of OH^- as the mineralizing agent, lies generally between 8-12. As depicted in Fig. 8 the most abundant form(s) of Si-species at relatively high pH are the monomeric ions, whereas at lower pH value monomeric neutral Si-species can be formed, when the Si-concentration is low. At high concentration, however, cyclic tetramers are most abundant species (ref. 98).

b. Hydrolysis and condensation of silicate

Monomers and oligomers in solution are in equilibrium with the gel phase. At this ambient stage of the reaction mixture monomeric silica species can be released from the gel via hydrolysis reactions and are present in solution as e.g. $\text{Si(OH)}_3\text{O}^-$ and $\text{Si(OH)}_2\text{O}_2^{2-}$. The dissolution of the gel is promoted by the OH^- -coordination of silicon above four, thus weakening the other siloxane bonds to the gel network. This nucleophilic mechanism is presented to occur via a $\text{S}_\text{N}2$ -Si transition state as shown in Scheme 3a (ref. 9).



Scheme 3. a) Hydrolysis and b) condensation mechanism of silicate species at room temperature.



Scheme 3c. Growth site in the gel phase for monomers from solution.

The mechanism of the condensation reactions in aqueous systems at high pH involves the attack of a nucleophilic deprotonated silanol group on a monomeric neutral species as represented in Scheme 3b (ref. 9).

The acidity of the silanol group depends on the number and type of substituents on the silicon atom. The more silicon substituents are present, the more acidic the OH groups of the central silicon atom. As shown in Scheme 3c, at high pH the most favourable polymerization is the reaction between large most highly branched species and the monomer silica species.

At more neutral pH, hydrolysis and condensation of clusters, containing specific bonding configurations, see Fig. 9, indicate that inversion in the pentacoordinate state of Si, illustrated in Scheme 3, is not essential (ref. 99).

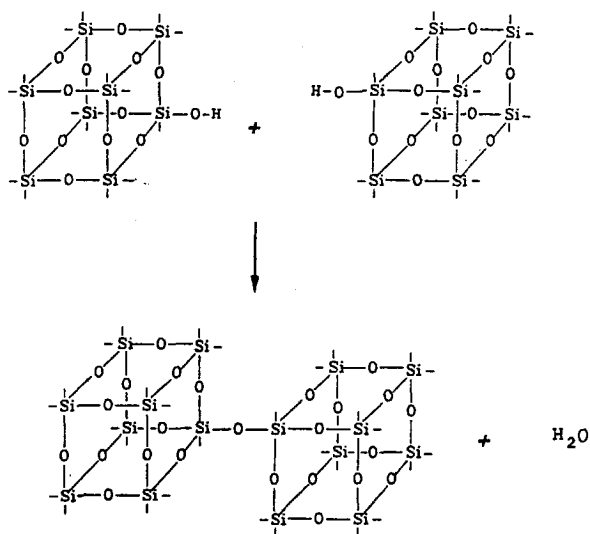


Fig. 9. Condensation of octamers, A) with retention of the configuration.

The pentacoordinate silicon intermediate state is, however, confirmed crystallographically (ref. 100).

Condensation of the monomers lead, as the pH of the zeolite synthesis mixture is above the isoelectric point of silica (ref. 101) to ramified clusters. Such clusters can be reorganized into fewer larger particles with a corresponding reduction in surface energy, according to the Ostwald ripening principle. The structural evolution of a growing cluster is schematically given in Fig. 10.

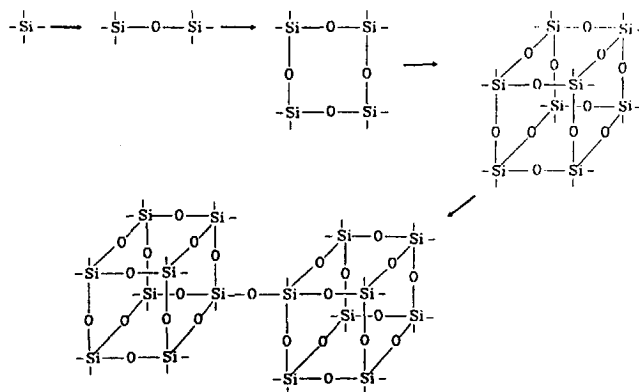


Fig. 10. Structural evolution of silicate clusters.

c. Evidence for silicate clusters

In the course of the gel dissolution the monomers form dimers, according to ^{29}Si -NMR studies (ref. 94), via condensation reactions whereafter trimers and tetramers, cyclic trimers and tetramers and higher order rings are observed as condensation products, see Fig. 11.

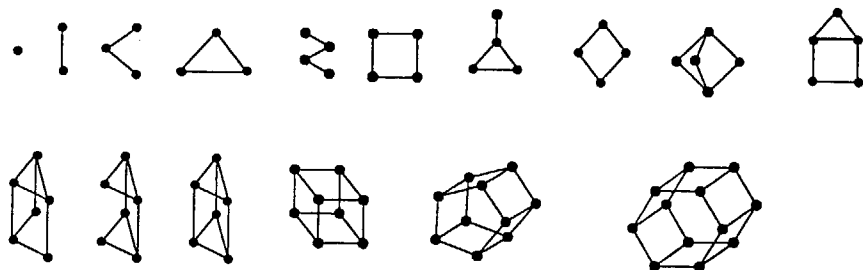


Fig. 11. Numerous oligomers characterized in solution at low temperature by ^{29}Si -NMR (ref. 101).

Evidence for the existence of e.g. double four rings resulted from the single crystal structure analysis of so-called pseudo-A, a material, *not a zeolite*, crystallized at ambient temperature from a mixture of SiO_2 , tetrabutyl ammoniumhydroxide (TBAOH) and H_2O , see Fig. 12 (ref. 93).

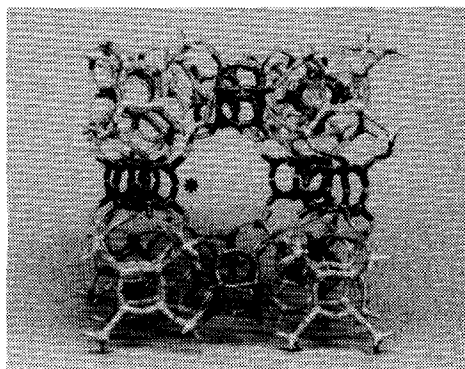


Fig. 12. Model of a part of the framework of pseudo-A; the double four ring units are indicated by asterisks (*).

The silicate species identified in the liquid phase by a.o. NMR, SAXS (ref. 102) and IR, (ref. 103) are products in a simple reaction mixture of SiO_2 , NaOH and H_2O at room temperature.

The interaction of alkali ions in such systems is not clear. It is often suggested (ref. 104) that the ordered hydration sphere of a.o. Na^+ stabilizes silicate species. Recent NMR results indicate that interaction between cations and silicate species (ref. 105) do occur.

An organic cation/template added as ingredient(s) to the simple reaction mixture shows in typical experiments according to NMR measurements interaction with the gel and silicate species, respectively (refs. 106-108). However, the highly complicated set of interactions and fast changing equilibria, due to the increased number of type of species after addition of template and/or Al^{3+} has not been unravelled yet.

V. THE TEMPERATURE RAISE OF THE REACTION MIXTURE

Temperature raise, from $< 60^\circ\text{C}$ up to $< 200^\circ\text{C}$, can be performed in several ways as shown in Fig. 13 for one type of autoclave and reaction mixture. The different heating rates are achieved in static systems.

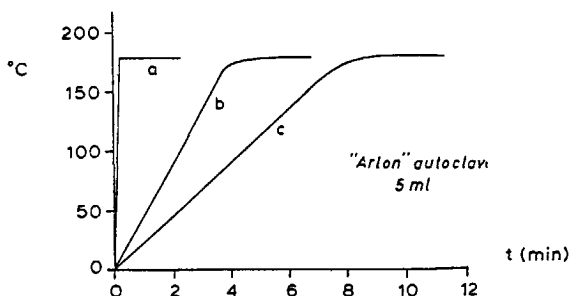


Fig. 13. Different heating rates for one type of autoclave achieved by (a) microwave, (b) hot sand bath and (c) hot air oven.

The size of the autoclave, the viscosity of the reaction mixture and the way of agitating i.e. static, tumbling or turbostirring are factors modulating the temperature raise of the reaction mixture.

During the temperature raise of the reaction mixture from ambient to reaction conditions primary events are:

- Accelerated dissolution of the gel into monomeric silicate species.
- Dissociation of silicate oligomers in solution and increase of monomers as measured by NMR up to $\sim 100^\circ\text{C}$ (refs. 109-112). As shown in Fig. 14 a model study with NMR on trimethylsilylated silicate confirms (ref. 109) a shift of the silicate anion equilibrium from relative high-molecular, mainly double four rings, to low-molecular weight, monomers and dimers.

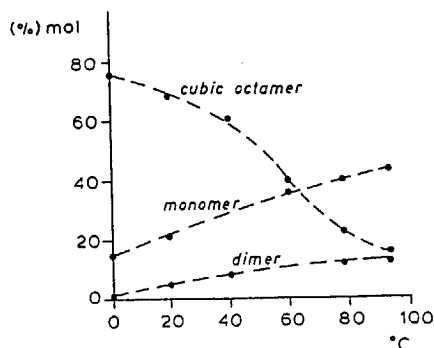


Fig. 14. Main changes in composition (% mol) of trimethylsilylated silicate solution versus temperature.

- Higher concentration and mobility of monomeric silicate- and eventually aluminate species.
- Association of primary building units.
- Possible nucleation and crystallization of unwanted (metastable) phases.

Some secondary events are:

- The start of the degradation of quaternary ammonium ions, which can be substantial in a ZSM-5 synthesis (ref. 42) as depicted in Fig. 15.
- Start of the drop in pH caused by the Hofmann degradation.

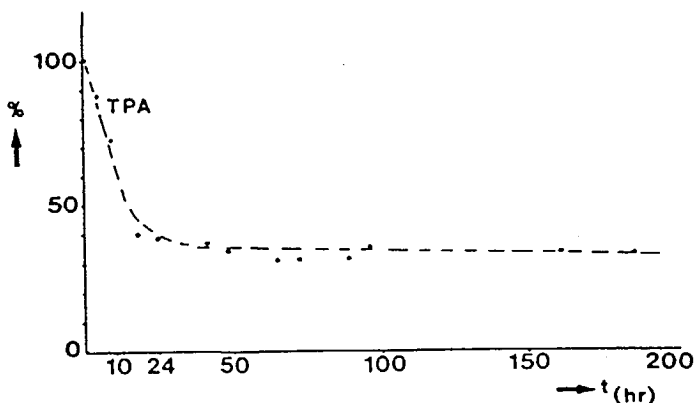


Fig. 15. Degradation of tetrapropylammonium versus time at 180 °C and pH - 13.

VI. THE HIGH TEMPERATURE REACTION PROCESS

a. Introduction

The main event occurring in the synthesis mixture at the reaction temperature is the formation of zeolites from amorphous material. Chemical reaction processes accelerated by the high temperature lead to:

- i) further reorganization of the low temperature synthesis mixture;
- ii) whereafter primary (homogeneous or heterogeneous) and secondary (seed crystals (ref. 113)) nucleation;
- iii) and finally, precipitation (based on reactions) as a form of crystallization.


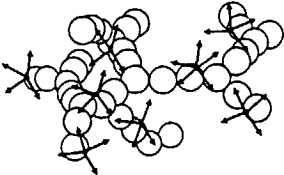
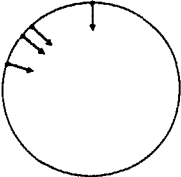
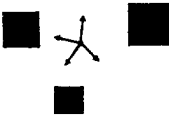
b. Nucleation

At the high temperature of the reaction mixture the zeolite crystallization is expected after an induction period in which the nucleation occurs. During the induction period the gel and species in solution (mentioned above in the low temperature section) rearrange from a continuous changing phase of monomers and clusters, e.g. polysilicates and aluminosilicates. These clusters form and disappear through inhomogeneities in the synthesis mixture via condensation and hydrolysis processes. The continuous dissolution of the gel phase increases, however, the amount of clusters and the possibility of further association of the clusters and cations. In the course of this process particles become stable. Nuclei of certain dimensions, e.g. ~ 10 Å for zeolite Na-A (ref. 114) and ~ 20 Å for zeolite ZSM-5 (ref. 115), are formed and crystallization starts.

c. Crystallization

The lines along which ideas on zeolite crystal formation are developed, either based on bulk and macroscopic observations or on molecular mechanistic scale are described in this paragraph. Four cases of nucleation and crystallization are schematically presented in Table 8. (a) Zeolite crystallizations, which might occur in clear synthesis solutions, or, more often, in heterogeneous reaction mixtures where (b) highly dispersed or (c) dense gel forms are present, see also Fig. 7. In some occasions (d) metastable solid phases undergo transformation during synthesis. Homogeneous nucleation followed by crystallization has been observed in (a) clear solution experiments (refs. 91, 92).

Table 8. Four cases of crystal growth environment and schematic representation of nucleation and crystallization.

Crystal growth environment	Nucleation (•) Crystallization (→)
(a) Clear solution	
(b) Dispersed low density gel	
(c) Separated high density gel	
(d) Solid phase	

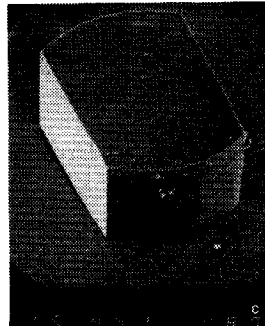
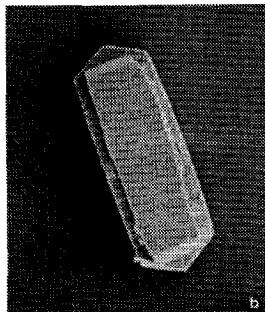
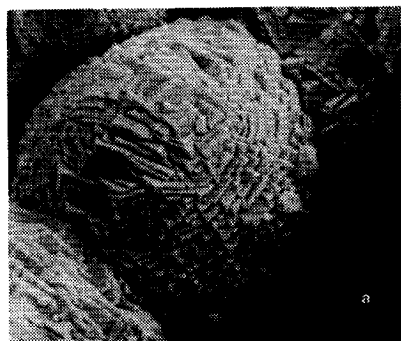


Fig. 16. a) Powder and b) a twinned elongated prismatic crystal of ZSM-5 from a dispersed gel phase and c) a cubic form of ZSM-5 from a dense gel phase.

Nucleation (heterogeneous) occurs at the liquid-gel interface in the dispersed gel-solution mixtures (b) (ref. 108). The forms of the crystallization products in the case of a dispersed gel phase are shown for ZSM-5 in Fig. 16a,b. Similarly to the clear synthesis solutions, the driving force for crystallization is equal in all directions as shown in Table 8a,b. In the case of a dense gel phase present in the synthesis mixture, see Table 8c, crystallization proceeds *into* the gel (ref. 42 and Chapter 8 of this thesis) as shown schematically in Fig. 17. Deviating crystal forms compared to crystal forms from dispersed gel systems are then observed, as shown in Fig. 16c.

Generally, the typical form and morphology of a zeolite crystal reveals not only information on the type of the zeolite formed but also on the crystal growth history, as shown above.

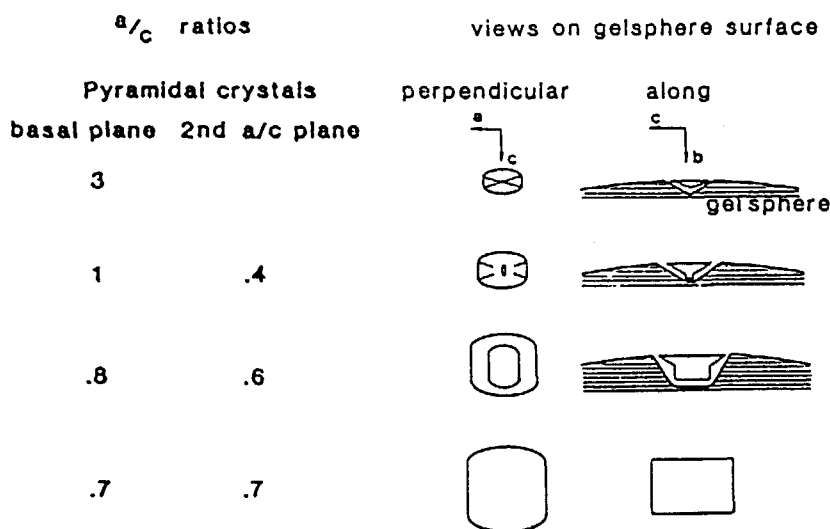


Fig. 17. Average a/c ratios of developing crystals and schematic drawing of growth process in the gel spheres.

As a liquid phase is continuously present between the dissolving dense gel phase and the growing crystal, the crystallization is, however, still solvent mediated.

When a metastable solid phase, e.g. a zeolite, is present in the synthesis mixture, a transformation into a more stable phase is possible, according to the Ostwald rule of successive transformations (ref. 116).

The nucleation and crystallization of the new phase, illustrated in Table 8d, occurs in the supersaturated solution generated by the dissolution of the former phase (ref. 117).

In the last three cases of Table 8 dynamic equilibria between successive steps of dissolution, ion transportation and precipitation, can be recognized (ref. 118). Especially, the precipitation/crystallization step, i.e. the type of crystal building units and the way of crystal growth on molecular level, has been subject of many studies.

d. Crystal-building units

At least three types of crystal-building units have been suggested which are described below.

d.1. The primary building unit

Arguments that primary building units, i.e. tetrahedral monomeric species, can be involved in the crystallization are:

- i) The general view from crystal growth theories that crystals are formed via primary building units (ref. 119);
- ii) The general view in sol/gel chemistry (refs. 8, 10) that the most favoured condensation reaction occurs between a monomeric and polymeric species. In terms of the zeolite crystallization: between a primary building unit and a crystal surface; see Section IVb;
- iii) The observation that upon raising the temperature (up till 100 °C) the concentration of monomers increases (ref. 109) at the expense of clusters. Though in situ measurements (till 200 °C) are not actually performed, the above experimental results might indicate that at reaction temperatures mainly monomers are present;
- iv) The fact that studies on the crystallization of zeolite have shown that the growth of a zeolite occurs by a surface reaction of monomeric anions (ref. 120).

d.2. A typical cluster as building unit

As shown in Chapter 3 of this book secondary building units (SBU's) are relatively low (\leq 16-Si-tetrahedra) polymer units. SBU's were introduced several decades ago (ref. 121) and used since to present structural (ref. 6) and further physical features of the zeolites. At the same time SBU's acting as non-chiral independent units can generate a certain zeolite structure. It is, however, though the SBU's show sometimes a superficial resemblance to silicate

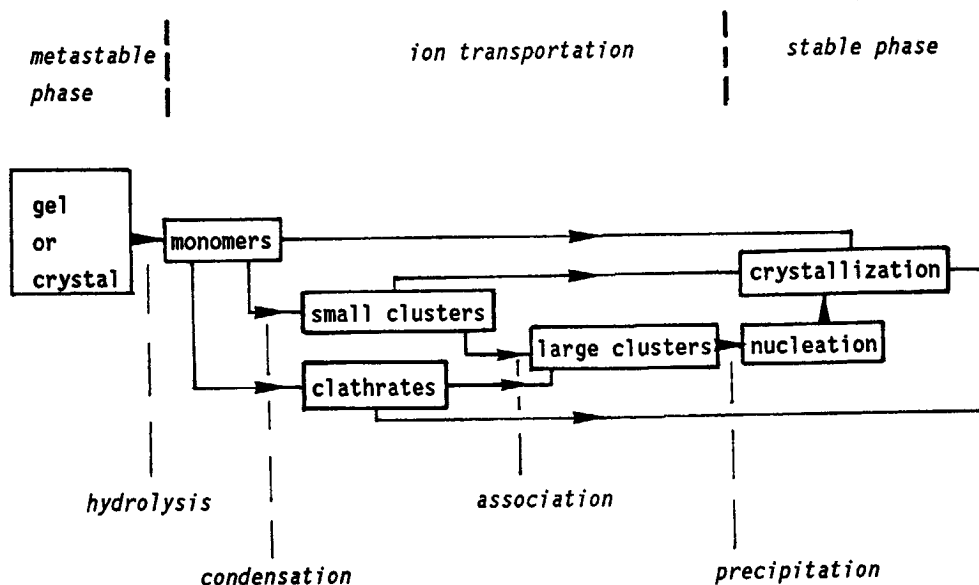
anions, not likely that SBU's are the building blocks of the growing crystal (ref. 122). On the other hand, the building of the porous and different zeolite frameworks with monomers condensating in the right topology seems less favourable compared to a typical cluster-building unit (ref. 123). From this point of view suggestions are raised about a typical or common cluster-building unit for all zeolite structures.

d.3. The cation templating theory

Organic as well as inorganic cations show structure directing, i.e. water-ordering, properties. Typical examples are given in a review of single crystal structure analysis of organic water clathrated cations (ref. 124). The water molecules comprising a tetrahedral network in the first layer around the cation might be partly replaced by silicate and aluminate anionic tetrahedra. The clathrated cations might serve this way as crystal building units.

An example of such a templating/clathrating role is the formation of sodalite with tetramethylammonium (TMA^+) cations (ref. 125).

The high temperature events, discussed above, are summarized in Scheme 4.



Scheme 4. Representation of successive steps in the evolution of zeolite crystallization.

e. Nucleation-crystallization kinetics

Nucleation and crystallization events are generally illustrated on characteristic S-shaped crystallization curves (ref. 126). The yield (wt % of crystalline material), often determined by indirect methods, plotted against time gives an impression of the nucleation and crystallization time and certain reaction temperatures. More accurate information on the crystallization kinetics can be provided when, based on crystal size and size distribution, the linear crystal growth rate and the rate of nucleation can be determined. Of the studies (ref. 127) on zeolite crystallization, one contribution (ref. 128) reporting on a method to collect kinetic data is briefly described here.

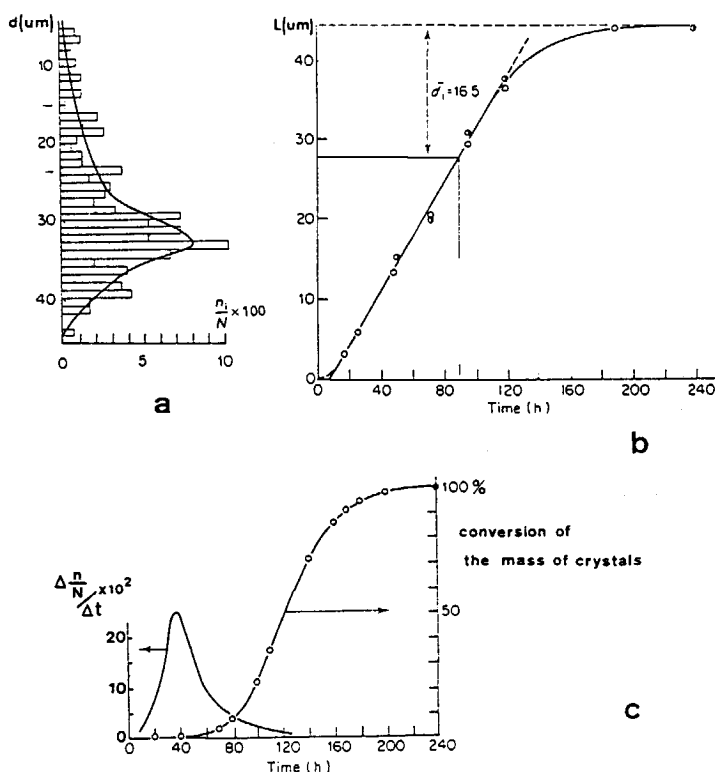


Fig. 19. a) Histogram of the crystal size distribution in the final product, b) diameter of the largest crystals of different unfinished crystallization runs versus time, resulting in the crystal growth rate graph and c) (i) the nucleation rate (number of crystals of each unfinished crystallization run versus time) together with (ii) the yield curve.

A number of identical synthesis experiments, but differing in total synthesis time, were performed. The average diameter of the largest crystals which could be collected from the various products was measured. In the case of zeolite Na-X it was found that in a plot of crystal size versus time the linear crystal growth rate ($.5 \Delta L/\Delta t$) was constant, irrespective of the crystal size, even until near exhaustion of the crystal building units, see Fig. 19b.

The nucleation time can be determined now for any crystal in the final product of this Na-X crystallization, knowing the growth rate. For instance, a crystal of $16.5 \mu\text{m}$ nucleated at $t \sim 90$ h. Together with the particle size distribution curve, Fig. 19a, the rate of nucleation was found, see Fig. 19c.

The nucleation rate curve and the yield curve calculated from both the growth rate and particle size distribution curve, indicate that as soon as the crystallization starts the chemical nutrients are consumed for crystal growth. The formation of fresh nuclei is from then on largely suppressed. In conclusion, it can be said that zeolite synthesis, resulting in a good crystalline product can deliver accurate information on nucleation and crystallization kinetics.

f. Energy of activation

Though zeolitic material can be prepared at low temperature ($20-60^\circ\text{C}$) most nucleation and crystallization processes are performed at temperatures between 60 and 250°C . The choice of the reaction temperature is governed by the energy of activation required for the zeolite crystallization.

Table 9 shows the energy of activation (E_a) as a function of the Si/Al ratio.

Table 9. E_a 's of different zeolite framework types and Si/Al ratios.

Guest molecule	Framework	Si/Al	E_a (kcal/mol)	Ref. 129
Na^+ ; H_2O	Y	1.5	11.8	a
		1.8	12.3	
		2.2	14.1	
		2.5	15.6	
TPA^+	MFI	30	7	b
TPA^+	MFI	∞	11	
Na^+ ; H_2O	MFI	80	18	c

It appears that the E_a 's are not related to diffusion of crystal building units in solution (E_a (diff.) $< 5 \text{ kcal mol}^{-1}$) but to condensation reactions between the crystal surface and crystal building unit. As shown in Table 9 the E_a of Na-X changes as a function of the Si/Al ratio which indicates that the more silicious the zeolite, the larger the E_a . Generally, this trend is also observed between different zeolites, although the contribution to E_a of cations and templates, as shown for ZSM-5, can be substantial.

VII. ISOLATION OF THE ZEOLITE PRODUCT

Products of zeolite preparations can be composed of either one pure zeolitic phase, a mixture of zeolitic phases or a mixture of a zeolitic phase and e.g. quartz, cristobalite or gel phase. Mostly the product is isolated by decantation/centrifugation or filtration.

If the product consists of crystals with a uniform crystal form which is recognized as characteristic for the expected product, the zeolite can be separated by decanting the mother liquor followed by washing with water.

If there is, however, e.g. some gel phase present, this may be either co-precipitated as a separate phase or adsorbed on the crystals. Careful dissolution of the gel phase with e.g. a dilute basic OH^- solution at slightly elevated temperature is strongly advisable prior to the isolation of the zeolite. Especially in the case of adsorbed gel on the crystal surface elemental analysis (AAS, ICP or EMPA) is required to control the Si/Al ratio of the crystals before and after the washing procedure (ref. 130). The final step in the zeolite preparation is the drying or calcination procedure after which the zeolite void volume is free for different modification and/or application.

VIII. REACTION PARAMETERS

a. Introduction

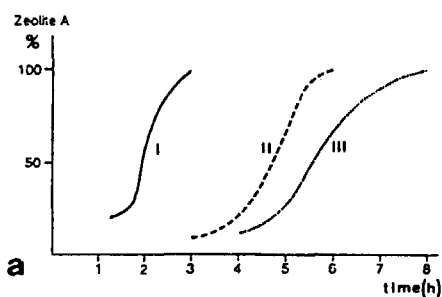
The type of reactants, the way the reactant mixture is made, the pH and the temperature typically affect the crystallization kinetics and product formation.

Furthermore the pre-treatment of the reaction mixture, the addition of crystal growth inhibitors, the reaction mixture temperature trajectory and the use of seeds have an influence on the zeolite preparation.

Some aspects of the type of the above mentioned factors are discussed in the following paragraphs. Illustrations are mainly given on the zeolite A and ZSM-5 formation.

b. The Si-source

As mentioned in Section II of this chapter the different types of the Si-sources contain impurities which may affect zeolite crystallization. Another parameter, the specific surface area of these sources, can result in different nucleation and crystallization times as shown for zeolite A in Fig. 20a (ref. 47). The shorter induction and crystallization times lead to more and smaller crystals, see Fig. 20b.



Silica source	rel. number	Crystals size
I	48	.7
II	30	2.6
III	15	4.8

b

Fig. 20. a) The yield of zeolite A versus time of different silica sources.
b) The specific surface areas of the silica sources (I > II > III) result in different amounts and sizes of crystals.

c. The type of template

Many types of template are regularly used (see e.g. Section II of this chapter). The surprising performance of certain templates on stabilizing the type of zeolite framework formed is illustrated in Table 10. One type of template can be used to crystallize various zeolites whereas the same type of zeolite may be crystallized while using different templates.

Table 10. Single template and mixture of templates/cations in the preparation of different zeolite types.

Single template	Zeolite	Ref.	Mixture of template/cation	Zeolite	Ref.
TMA ⁺	Sodalite	131	TMA ⁺ , Na ⁺	A, X, Y	135
	Gismondine	132		L (+ K ⁺)	136
				Sodalite, P, S and R	136
				ZSM-6 and ZSM-47	137
				Omega	138
TPA ⁺	ZSM-5	133	TEA		
			EDA		
Na ⁺	ZSM-5	134	Ethanolamine		
			3-Hydroxypropyl amine		
				, Na ⁺ ZSM-5	139
			Ethanol		
			Glycerol		
			Morpholine		
			1,6-Hexanediol		
			TPA		

The role of the single template/cation in stabilizing subunits of different zeolite types is not unravelled yet.

A common factor, however, appears to be the size of a certain free void diameter in the structures of sodalite and gismondine, 6.8 Å and 7.0 Å, respectively, and the diameter of ~ 6.7 Å of the template TMA⁺, see Fig. 21.

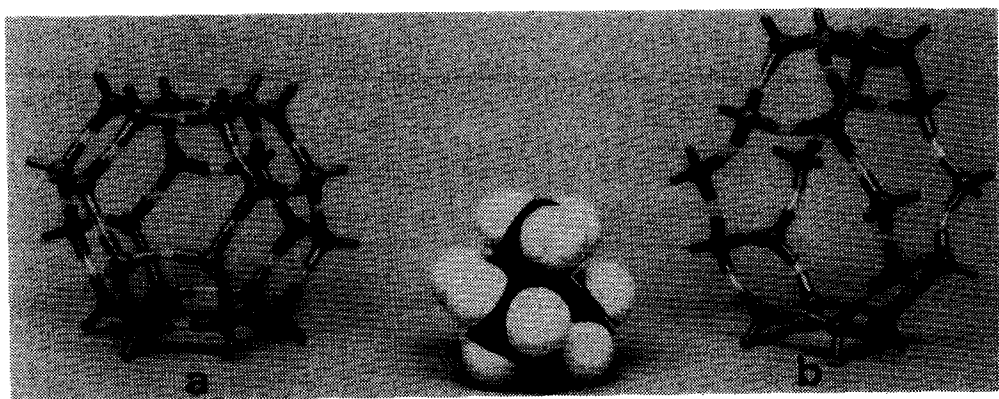


Fig. 21. Models of a) the sodalite and b) the gismondine void and the void filler/template/cation TMA^+ .

Although TPA^+ and Na^+ are rather different templates/cations a common factor might be the stabilization of voids (either intersection of channels or channel windows), see Fig. 22.

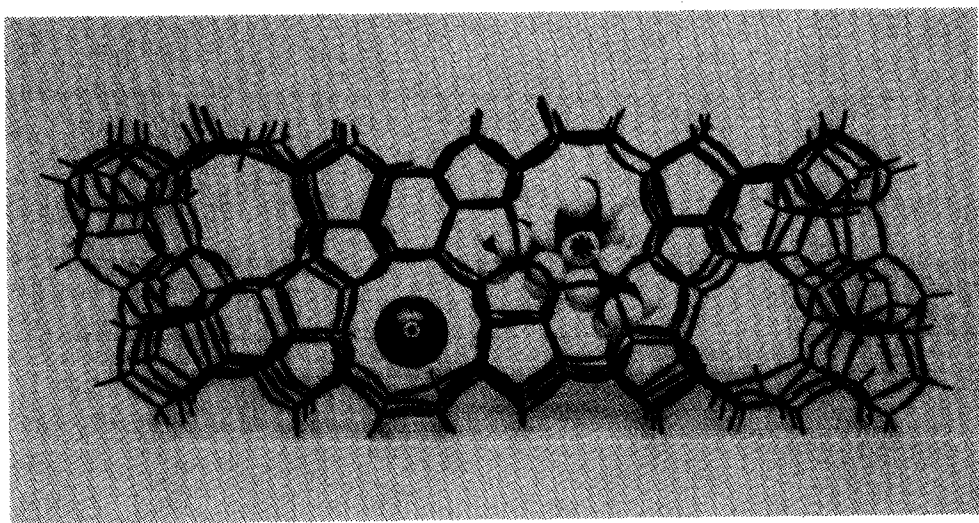


Fig. 22. View along straight channels of wire model of ZSM-5 with either TPA^+ (*) or hydrated Na^+ (O) on intersections of channels and channel windows, respectively.

Charged templates compensate negative framework charges, due to isomorphous substitution of Si^{4+} by Al^{3+} . A range of Si/Al ratios is possible, see Scheme 5. If, however, the number of charged templates required for charge compensation cannot be accommodated for dimensional reasons the zeolite

combines charged templates with e.g. Na^+ . This way, still various Si/Al ratios for one zeolite type are possible as shown in Scheme 5 for zeolite ZSM-5. Sodalite can be prepared with two different Si/Al ratios.

ZSM-5	Si/Al	Sodalite	Si/Al
TPA^+	23 - <10000	TMA^+	5
TPA^+/Na^+	23 - 11		
Na^+	11	Na^+	1

Scheme 5. Different Si/Al ratios for ZSM-5 and sodalite.

d. The reactant mixture

The way reactant mixtures are made, e.g. the addition sequence of the reactants, the stirring and gel aging can result in method-dependent factors influencing nucleation. As shown in Fig. 23 crystals of zeolite A started growing in a zeolite X synthesis mixture whereafter zeolite X crystals started growing on and over the zeolite A crystal (refs. 140, 141).

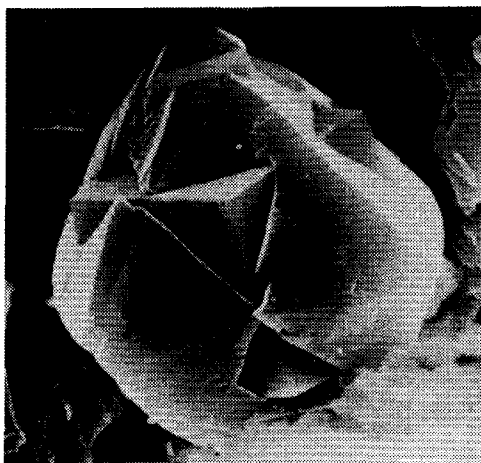


Fig. 23. Overgrowth of zeolite X onto zeolite A.

Though the thermodynamic variables were correctly chosen to prepare zeolite X, synthesis mixtures of zeolite A and X, given below, do have comparable elements and apparently local kinetic factors initiated the synthesis of zeolite A.

	$\text{Na}_2\text{SiO}_3 \cdot 9\text{H}_2\text{O}$	NaAlO_2	Triethanolamine	H_2O	Ref. (142)
zeolite A:	.4	.1	.7	28	} (molar)
zeolite X:	.4	.05	.7	28	

e. The pH

e.1. Introduction

The pH and the solubility of reactants in the synthesis mixture are governed by the presence of OH^- or F^- .

An advantage of F^- compared to OH^- is the higher solubility of e.g. Fe^{III} and Ti^{IV} and the condensation capability for e.g. Ge^{IV} . A too high concentration of F^- , however, prevents the polycondensation mechanisms. A compromise between solubility of certain elements and inhibition of zeolite framework formation leads to F^- synthesis mixtures which are less supersaturated than OH^- media. Hence, only a few zeolite types have been obtained, until now (ref. 16).

e.2. OH^-

Raising the pH of synthesis mixtures using OH^- , mainly influences the crystallization of a certain zeolite in a positive way within the synthesis field. As depicted in Fig. 24a and b for zeolite A and zeolite ZSM-5, respectively, increasing the pH shows an increase in the crystallization rate. The OH^- is a strong mineralizing agent for bringing reactants into solution. The higher the pH and thus the concentration of dissolved reactants the more the rate of crystal growth of zeolites is enhanced (refs. 47, 143).

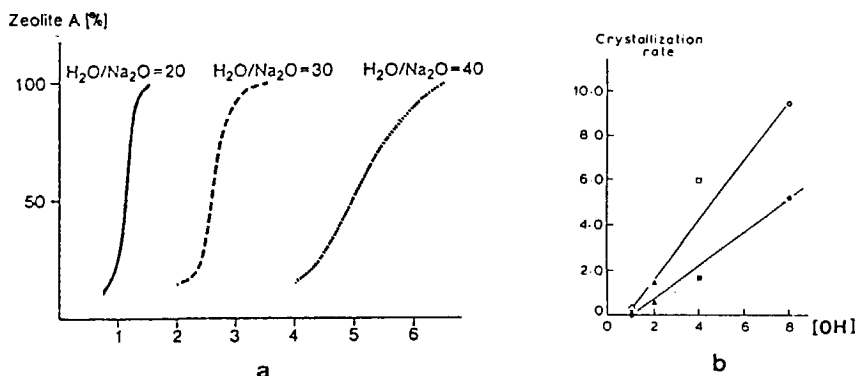


Fig. 24. The influence of alkalinity on a) zeolite A and b) ZSM-5 crystallization.

e.3. F^-

After the first publications on synthesis with F^- (ref. 46) extensive studies have been undertaken to investigate the effect of F^- and possibilities in zeolite synthesis (refs. 16, 46). Replacing OH^- by F^- with e.g. HF, NH_4F and BF_3 the pH values of the synthesis mixture lies generally between 3 and 10. A typical synthesis formulation is given in Section XII of this chapter. The zeolites obtained so far by this route are silica-rich materials of which the structure types are:

ZSM-5
Ferrierite
Theta-1
and ZSM-23

f. The temperature

It has been shown for many zeolites that raising synthesis temperatures within a certain zeolite synthesis field increases the crystal growth rate (refs. 47, 144, 145). As shown in Fig. 25a and b for zeolite A and zeolite ZSM-5, increasing temperature influences the crystal growth rate whereas in the case of zeolite A the crystal size does not change significantly compared to substantial variations in the ZSM-5 product.

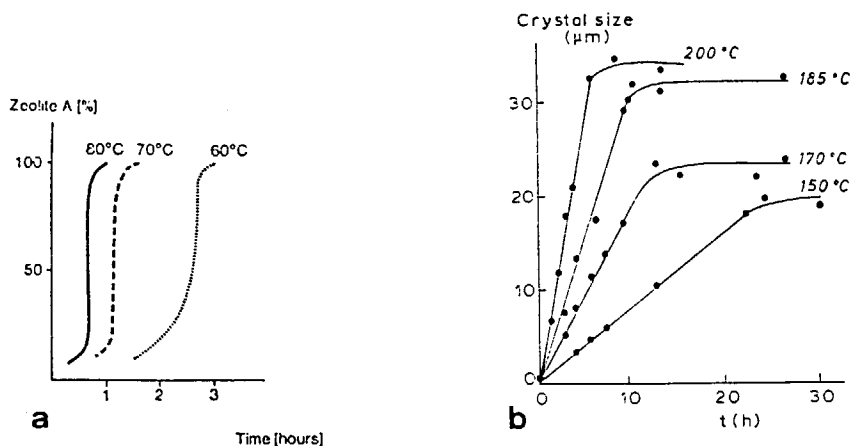


Fig. 25. Influence of temperature on the crystallization of a) zeolite A and b) zeolite ZSM-5.

IX. ALL-SILICA MOLECULAR SIEVES

a. Introduction

Two preparation routes can be followed to obtain all silica molecular sieves:

- i) A direct synthesis to crystallize molecular sieves with a SiO_2 composition and well-known zeolite topologies.
- ii) A secondary synthesis. After the direct synthesis of a zeolite a dealumination procedure, e.g. steaming (ref. 146), ammonium hexafluoro-silicate (ref. 147) or silicon tetrachloride (ref. 148) can lead to an all silica molecular sieve.

b. Synthesis

Though the neutral all-silica molecular sieves do formally not need to be stabilized with cations the silica structures usually contains the cations used in the synthesis. For example, tetrapropylammonium for silicalite-1, tetrabutylammonium for silicalite-2, and tetraethylammonium for silica-ZSM-12. Recently, amines, di-amines (ref. 149) and poly-amines (ref. 150) have been used as templates.

Table 11 contains a list of all-silica molecular sieves with two examples of synthesis recipes and references.

Table 11. All-silica zeolites, recipes and references.

Product	Ref.
Silica-ZSM-48	150
Recipe: 14.6 g of triethylenetetramine is dissolved in 18 ml H_2O whereafter the solution is stirred into dry 1.2 g SiO_2 . The smooth dispersion is then autoclaved between 120-180 $^{\circ}C$ for 28-105 days, respectively.	
Silica-ferrierite	151
Recipe: 0.75 g $Si(OC_3)_4$ is added to a solution of 1.2 g ethylenediamine (EDA) in 10 ml H_2O . After adding 2 ml 1 M aqueous boric acid the solution is sealed in a silica tube and heated at $\sim 170^{\circ}C$ for 56 days.	
Silicalite-1 (Silica-ZSM-5)	152
Silicalite-2 (Silica-ZSM-11)	153
Silica-ZSM-22	149

c. Remark

The main property of the silica molecular sieves is the strong hydrophobic character of the pores. The preferential uptake of e.g. traces of organic compounds (ref. 152) from water, which is not accommodated (ref. 154), in silicalite-1 testifies of this.

X. CLATHRASILS

a. Introduction

The name "clathrasil" has been introduced for a subclass of porous tectosilicates different from zeolites. The windows of the framework, connecting the cages, are too small to let guest species, stabilized during the synthesis, pass.

This characteristic of a clathrate together with the all silica composition is considered as specific for the members of the clathrasils (ref. 29).

There are, however, exceptions. The recently synthesized decadodecasil-3R (DD-3R) (ref. 155) contains windows of eight-rings of oxygen, indicating that diffusion of small molecules through the porous structure is possible after calcination. This structure can therefore be considered to form an interface between the clathrasils and the silica molecular sieves.

A modified type of DD-3R denoted as Sigma-1 (ref. 156) can, however, be seen as a link between clathrasils and zeolites, because some Si-framework sites are isomorphously substituted by Al. Finally, there is a novel tectosilicate, Sigma-2 (ref. 157). The recently solved structure of which two different polyhedra, see Fig. 26, have not been found before, reveals eight-rings of oxygen and cages with a free diameter of 75 nm. Sigma-2 has been prepared in the silicalite as well as in the zeolite form and can thus be considered as an intermediate between clathrasils, zeolites and silicates.

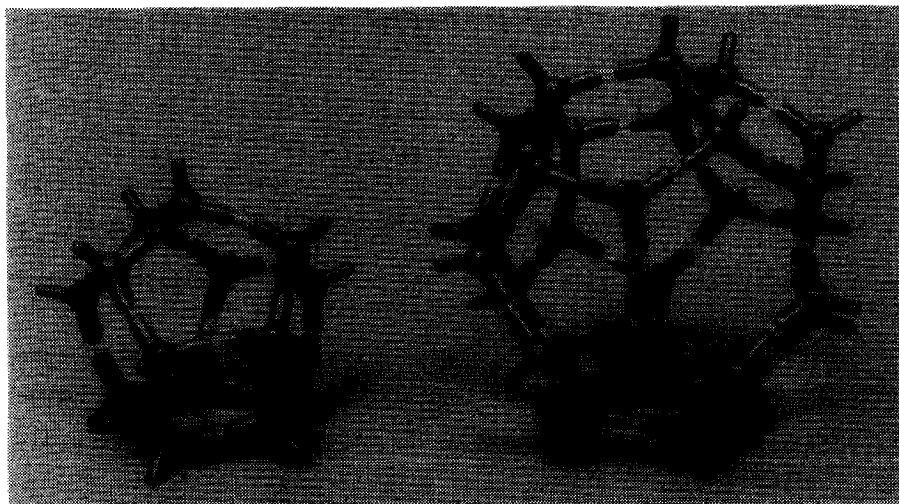


Fig. 26. The nonahedral and eikosahedral cages of Sigma-2.

b. Experimental

The clathrasils can be synthesized generally from .5 M silica, prepared by hydrolyzing an alkoxysilane, e.g. $\text{Si}(\text{OCH}_3)_4$, in solutions containing an amine as guest template molecule. The syntheses are mainly carried out between 160-240 °C. The clathrasils, together with detailed synthesis data and products expected, are given in Table 12.

Table 12. Clathrasils with references to synthesis prescriptions and two examples of synthesis recipes.

Product	Ref.
Melanophlogite	158
Dodecasil 3C	159
Dodecasil 1H	160
Silica-sodalite	161
Sigma-1	156
DD-3R (silica)	155
<p>Recipe: 0.75 g $\text{Si}(\text{OCH}_3)_4$ is added to a solution of 1.2 g ethylenediamine (EDA) in 10 ml H_2O. After adding 350 mg 1-amino-adamantane the solution is sealed in a silica tube and heated at 170 °C for ~ 70 days.</p>	
Sigma-2 (silica and aluminosilicate)	157
<p>Synthesis example: The molar oxyde ratio of the synthesis system is:</p>	
Na_2O	3
AN	20 (1-aminoadamantane)
Al_2O_3	(0.6) (Al-wire)
SiO_2	60 (colloidal silica)
H_2O	2400
<p>The system was crystallized at 180 °C and continuously stirred for a few days.</p>	

c. Remark

The templating role of some of the guest molecules is illustrated in Fig. 26. Polyhedra of different clathrasils are filled with a guest molecule. As only 4-, 5- or 6-ring faces are present in most of the polyhedra it looks like the crystal building units have formed around the guest molecule as this molecule is too large to pass through one of the rings. The clathrate formation might therefore be obtained and based on single building units in solution and/or at the growing crystal surface (ref. 162).

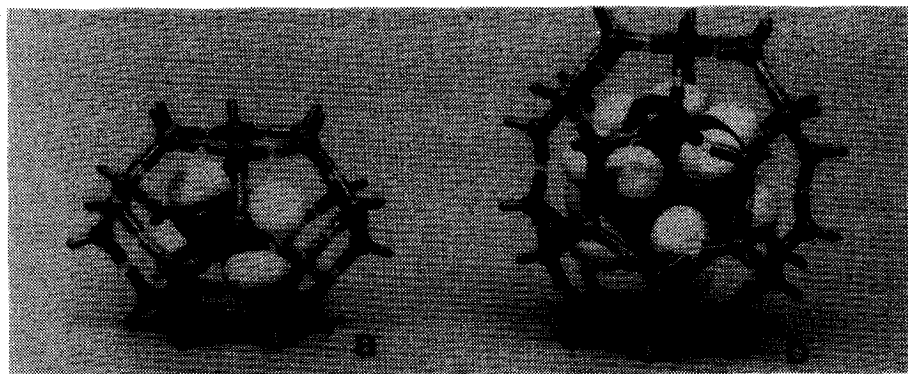


Fig. 27. Orientation of various guest molecules in clathrasils (ref. 163).
a) H_3CNH_2 in $[5^{12}_6{}^2]$ and b) aminoadamantane in $[5^{12}_6{}^8]$ of melanophlogite and dodecasil 1H, respectively.

XI. EXAMPLES OF SYSTEMATIC RESEARCH in the field of molecular sieves preparation to reach various objectives

a. Introduction

A main thrust of research is:

- to synthesize new molecular sieves
- further optimization of recipes
- to gain knowledge on the essential functions of reactants, e.g. structure directing role of cation/template
- to prepare relative large single crystals for fundamental studies

The list can be longer, however, the examples given below illustrate generally the purpose and variety in the research of molecular sieves preparation.

b. Research examples

Objective	Parameter(s)
1) Preparation of zeolites	Non-aqueous solvents
2) Preparation of zeolites	F^- as mineralizing agent
3) Investigation of crystallization fields with pyrrolidine as template	$\text{Na}_2\text{O}-\text{Al}_2\text{O}_3-\text{SiO}_2-\text{H}_2\text{O}$ system was varied

b. Research examples (continued)

Objective	Parameter(s)
4a) Investigation of template-zeolite interaction	Systematic variation of template
4b) Directing role of template in the crystallization	Use of bis-quaternary ammonium compounds
5) Large single crystals	Knowledge on nucleation/crystallization
6) Morphology and form of zeolite products	Change of [SiO ₂], template, cation or additives

b.1. The use of non-aqueous solvents

In contrast to the rich crop of zeolite types synthesized in aqueous systems the results in non-aqueous solvents are poor (refs. 164, 165). Solvents used, of which the choice was a.o. based on boiling point (100-200 °C) and relative permittivity (10-45) (water: 78), are given in Table 13.

Table 13. Zeolite products formed.

Solvents	Na ⁺	K ⁺	Li ⁺	Ca ⁺⁺
Glycol	HS	-	-	-
Glycerol	HS	-	-	-
DMSO	HS	-	-	-
Sulfolane	HS	-	-	-
C ₆ ,C ₇ alcohol	HS	-	-	-
Ethanol	HS	-	-	-

HS: Hydroxysodalite.

Generally mixtures within the following molar oxide ratio were used:

MeO	1-20
Al ₂ O ₃	1
SiO ₂	1-100
Solvent	5-350
and MeO/SiO ₂	0.1-10

As shown in the Table zeolite products could only be obtained in the case of Na⁺. The use of other inorganic and organic cations was not successful.

As the boiling point is a less critical factor than high relative permittivity (reduces the Coulomb force between ions and polar compounds thus enhancing dissolution) other non-aqueous solvents for zeolite crystallization which might be subject to zeolite synthesis tests are given below.

Non-aqueous solvent	E _r
formic acid	57
formamide	84
hydrogen peroxide	93
hydrocyanic acid	95

b.2. The use of F⁻ (ref. 166)

The compositional ratios of the reaction mixtures used were:

	Al or B/Si	F/Si	Temp./Si	H ₂ O/Si
in molar ratio	0-0.5	0.05-6	0.05-6	4-500

with the pH of the mixtures between 1.5-10. The reaction mixtures were heated at 60-250 °C and autoclaved for a few hours to a few months. After isolation the products were washed with water and dried.

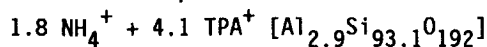
A typical example of a "F⁻" synthesis of ZSM-5 is given below:

- Reaction mixture composition:

36 g	Ammonium aluminumsilicate (Si/Al ~ 7; NH ₄ /Al ~ 1)
18.5 g	NH ₄ F pH = 7
33.2 g	TPABr t = 172 °C
180 g	H ₂ O time = 11 days

- Product

Unit cell composition:



Crystal size

30 x 12 μm

Advantages and differences using F^- instead of OH^- as concluded so far:

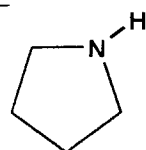
- Low pH compared to OH^-
- Incorporation in the framework of elements sparingly soluble in alkaline medium, e.g. Fe^{III}
- Synthesis without alkaline cations
- New possibility to directly incorporate cations as NH_4^+ and divalent cations such as Co^{2+} as well
- Good stability of usual templates such as TAA^+ in this medium
- Highly crystalline materials

b.3. Pyrrolidine as template (ref. 87)

The crystallization of zeolites in the system $\text{Na}_2\text{O}-\text{Al}_2\text{O}_3-\text{SiO}_2-\text{H}_2\text{O}$ + pyrrolidine as a template was studied. The reaction mixture compositions used are given in Table 14 in molar oxide ratio.

Table 14. Reaction mixture ranges in molar oxide ratios.

Na_2O	0.05-0.5	+ ~ 0.7 pyrrolidine
Al_2O_3	0.002-0.05	
SiO_2	1	
H_2SO_4	0-0.4	
H_2O	20-80	



Two procedures were used:

- I. To a stirred aluminium sulphate solution, calculated amounts of sodium silicate, sulphuric acid and pyrrolidine were added dropwise.
- II. Calculated amounts of aluminium nitrate, colloidal silica and pyrrolidine were added to a stirred sodium hydroxide solution.

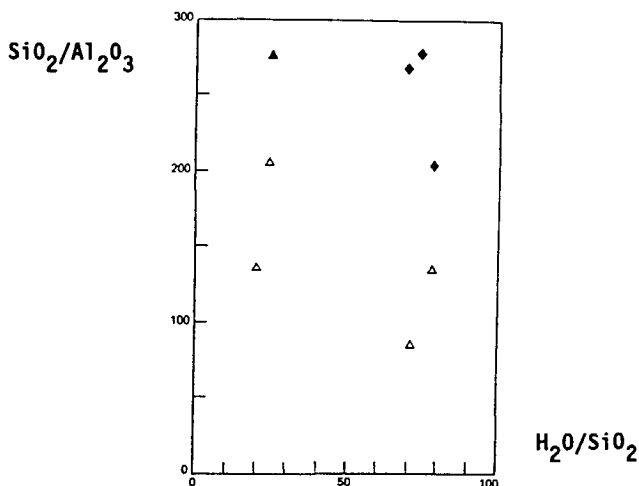


Fig. 28. Crystallization fields of product $\text{SiO}_2/\text{Al}_2\text{O}_3$ versus $\text{H}_2\text{O}/\text{SiO}_2$ of ZSM-39 (△), ZSM-48 (◆) and KZ-1 (△).

The follow-up of both procedures was to autoclave the reaction mixture for 7-40 h at 423-435 K with stirring. After isolation the product was washed with water and dried.

The results of the experiments are given in Fig. 6 for procedure A whereas the results of the experiments with procedure B are given in Fig. 28.

The main conclusion of the study is that pure ZSM-5, ZSM-35, ZSM-39, ZSM-48 and KZ-1 can be crystallized with pyrrolidine in the aforementioned synthesis system. No common factor, based on the use of pyrrolidine, could be recognized in the various zeolite products.

b.4.a. The use of bis-quaternary ammonium compounds in molecular sieves synthesis (ref. 58)

The objective in this study was the systematic variation of template in the synthesis. An example of the synthesis is given below together with the products formed, see Table 15.

The general formula of this bis-quaternary template (T) is:

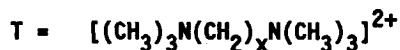


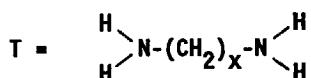
Table 15. Synthesis mixtures and product formation with bis-quat as template.

Synthesis conditions		T	Product formation
molar oxide ratio		x	
SiO ₂	60		
Al ₂ O ₃	1		Zeolite phases
Na ₂ O	10	3	ZSM-39
TBr ₂	10	4	ZSM-12
H ₂ O	3000	5,6	EU-1
		7,8	ZSM-23
			Silica phases
		3	EU-4
(without Al ₂ O ₃)		4,9	EU-2

The reaction conditions were 180 °C, three days and crash-cooling after the synthesis was terminated.

b.4.b. Other biamines (ref. 167)

Systematic variation of the chain length of the template (T) given below in the general formula



resulted in the products, given in Table 16.

Table 16. Zeolites obtained with various α,ω -diamines.

x	Zeolite phase
2-5	Ferrierite
	ZSM-5
5-6	ZSM-5
7-10	ZSM-11

The full synthesis description is given in ref. 167.

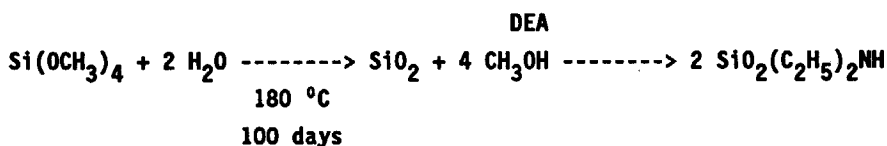
b.5. The synthesis of relatively large single crystals of molecular sieves

b.5.1. Introduction

Pertaining to e.g. the viscosity of the synthesis mixture several systems, clear solution, diluted gel and dense gel phase have been investigated.

b.5.2. Crystallization of ZSM-22 from a clear solution (ref. 149)

In a typical experiment tetramethoxysilane was hydrolyzed in 3 M diethylamine (DEA) according to the following reactions:



Single crystals of silica-ZSM-22 of 45 x 100 x 225 μm were isolated and used for structure determination.

b.5.3. Synthesis of elongated prismatic ZSM-5 crystals

The objective of this study was to obtain large single crystals of ZSM-5. Systems using $\text{Na}^+\text{-TPA}^+$, $\text{Li}^+\text{-TPA}^+$ and $\text{NH}_4^+\text{-TPA}^+$ were investigated applying a reaction mixture given in molar oxide ratio for e.g. $\text{NH}_4^+\text{-TPA}^+$:

TPA ₂ O	4	
(NH ₄) ₂ O	123	T = 453 K
Al ₂ O ₃	1	t = 7 days
SiO ₂	59	
H ₂ O	2280	

Products

Alkaline-free, homogeneous elongated prismatic single crystals of ZSM-5 of 350 μm in length at maximum (ref. 168) were obtained.

b.5.4. Synthesis of cubic shaped single crystals of ZSM-5 (ref. 169)

The synthesis of this type of crystals developed recently (ref. 169) was subject of a study on the crystal growth history (ref. 42) of this type of crystals. The objective was: to pinpoint the driving forces which change the ZSM-5 crystal form from elongated prismatic into cubic. The crystal growth history study revealed that the cubic crystal growth occurred in a dense gel phase.

Perfect single crystals up to 500 μm of zeolite (ZSM-5) and all silica (silicalite-1) molecular sieve type, see Fig. 16c, could be obtained using the following molar oxide ratio:

	ZSM-5	Silicalite-1
SiO_2	12	12
Al_2O_3	1	
Na_2O	44	44
TPA_2O	44	44
H_2O	2000	2000

After 5 days at 180 $^{\circ}\text{C}$ crystals could be isolated and selected from the product.

b.5.5. Synthesis of single crystals of zeolite A and X (ref. 142)

Single crystals of zeolite A and X up to 100-500 μm in size could be obtained using the following procedures.

Procedure for zeolite A:

Solution I: 100 g $\text{Na}_2\text{SiO}_3 \cdot 9\text{H}_2\text{O}$ in 350 ml H_2O + 50 ml TEA

Solution II: 80 g NaAlO_2 in 350 ml H_2O + 50 ml TEA

Both solutions are filtered with milipore filters, whereafter solution II is added to solution I with stirring. The crystallization is performed at 75-85 $^{\circ}\text{C}$ for 2-3 weeks, without stirring.

Procedure for zeolite X:

Identical to the procedure for zeolite A, only 40 g of NaAlO_2 is used in solution II now. The crystallization time is 3-5 weeks.

Careful filtering of the starting solutions substantially reduces the amount of heterogeneous nuclei such as dust and foreign particles in the starting chemicals. The lower the number of nuclei, the larger the crystals.

b.6. Morphology and form of mordenite and ZSM-5

The morphology and/or form of zeolite crystals appear generally to be influenced by:

- $[\text{SiO}_2]$
- Guest molecule type
- Cation (ref. 171)
- Crystal growth inhibitors

A frequently observed crystal form of mordenite is the needle form (with pore channel system parallel to needle direction), see Fig. 29a.

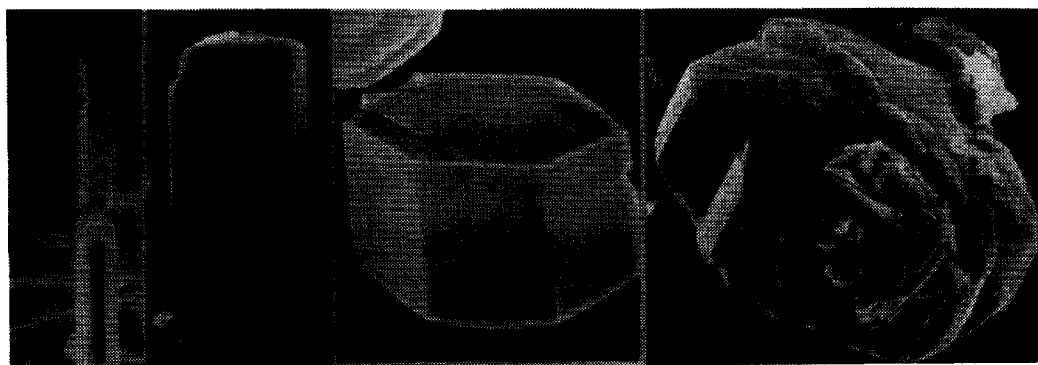


Fig. 29. Different forms of mordenite. The needle form a), the intermediate forms b) and c) and the disk form d). The pore direction is indicated by a bar (ref. 85).

As shown in Fig. 29b, c and d, completely different crystal forms of mordenite can be prepared. According to the synthesis system used (ref. 85) the main influence in the shape of the crystals seems to be the $[\text{SiO}_2]$. The higher the $[\text{SiO}_2]$, i.e. the more the crystallization occurs in a dense gel, the more the elongated form is reduced and changed into a disk form.

The increase in pore entries and decrease in pore length going from needle to disk form is evident and may be of interest in catalysis (ref. 170).

The elongated prismatic form is the most frequently found crystal form of ZSM-5. Changing the $[\text{SiO}_2]$ can change the crystal form as shown in Fig. 30a and b for relatively low and high $[\text{SiO}_2]$ concentrations, respectively.

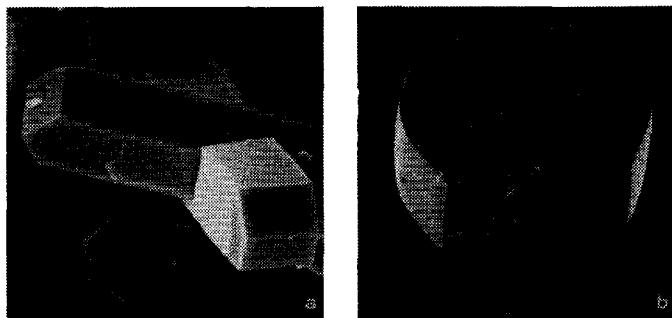


Fig. 30. The elongated prismatic crystal form (a) and the cubic crystal form (b) of zeolite ZSM-5.

Changing the template type, i.e. replacing TPA^+ for the bis-quat ammonium ion, hexapropyl-1,6-hexanediammonium, resulted in different crystal forms for low as high $[\text{SiO}_2]$ as well, see Fig. 31a and b.



Fig. 31. The modification of the crystal form at low (a) and at high (b) $[\text{SiO}_2]$ of zeolite ZSM-5 prepared with biquat as template.

In the case of an additive (inhibitor) like boric acid an enrichment of crystal faces in the c-direction was observed as shown in Fig. 32.



Fig. 32. Additional crystal face {001} compared to regular elongated prismatic form of zeolite ZSM-5.

XII. REVIEWS ON ZEOLITE SYNTHESIS

- *Proceedings of International Zeolite Conferences (IZC)*

1. "Molecular Sieves", Soc. Chem. Ind., London, 1968; Proceedings of the 1st IZC, London, U.K., 1967.
2. "Molecular Sieves I and II", Adv. Chem. Ser., 101 and 102, ACS, Washington, D.C., 1971; Proceedings of the 2nd IZC, Worcester, Mass., U.S.A., 1970.
3. "Molecular Sieves", Adv. Chem. Ser., 121, ACS, Washington, D.C., 1973; W.M. Meier and J.B. Uytterhoeven, Eds., Proceedings of the 3rd IZC, Zürich, Switzerland, 1973.
4. "Molecular Sieves-II", ACS Symp. Ser., 40, ACS, Washington, D.C., 1977; J.R. Katzer, Ed., Proceedings of the 4th IZC, Chicago, Ill., U.S.A., 1977.
5. "Proceedings of the 5th International Conference on Zeolites", Heyden, London, Philadelphia, Rheine, 1980; L.V.C. Rees, Ed., Proceedings of the 5th IZC, Naples, Italy, 1980.
6. "Proceedings of the 6th International Conference on Zeolites", Butterworths, Guildford, 1984; D. Olson and A. Bisio, Eds., Proceedings of the 6th IZC, Reno, Nev., U.S.A., 1983.
7. "New Developments in Zeolites Science and Technology", Kodansha, Tokyo, Elsevier, Amsterdam, Oxford, New York, Tokyo, 1986, Stud. Surf. Sci. Catal., 28; Y. Murakami, A. Iijima and J.W. Ward, Eds., Proceedings of the 7th IZC, Tokyo, Japan, 1986.
8. "Zeolites: Facts, Figures, Future", Elsevier, Amsterdam, Oxford, New York, Tokyo, 1989, Stud. Surf. Sci. Catal., 49; P.A. Jacobs and R.A. van Santen, Eds., Proceedings of the 8th IZC, Amsterdam, Netherlands, 1989.

- *Synthesis part in recent international conferences*

"Zeolites, Synthesis, Structure, Technology and Application", Elsevier, Amsterdam, Oxford, New York, Tokyo, 1985, Stud. Surf. Sci. Catal., 24; B. Drzaj, S. Hocevar and S. Pejovnik, Eds.

"Innovation in Zeolite Materials Science", Elsevier, Amsterdam, Oxford, New York, Tokyo, 1988, Stud. Surf. Sci. Catal., 37; P.J. Grobet, W.J. Mortier, E.F. Vansant and G. Schulz-Ekloff, Eds.

"Zeolite Synthesis", ACS Symp. Ser., 398, ACS, Washington, D.C., 1989; M.L. Occelli and H.E. Robson, Eds.

- *Journal*

Zeolites, L.V.C. Rees and R. von Ballmoos, Eds., Publishers, Butterworth, Heinemann, Stoneham, MA, U.S.A.

- *Books*

"Zeolite Molecular Sieves", Structure, Chemistry and Use, John Wiley & Sons, New York, London, Sydney, Toronto, 1974; D.W. Breck.

"Hydrothermal Chemistry of Zeolites", Academic Press, London, New York, 1982; R.M. Barrer FRS.

"Synthesis of High-Silica Alumiosilicate Zeolites", Elsevier, Amsterdam, Oxford, New York, Tokyo, 1987, Stud. Surf. Sci. Catal., 33; P.A. Jacobs and J.A. Martens, Eds.

"Molecular Sieves, Principles of Synthesis and Identification", Van Norstrand Reinhold, New York, 1989; R. Szostak.

"An Introduction to Zeolite Molecular Sieves", John Wiley and Sons, Chichester, 1988, A. Dyer.

XIII. REFERENCES

- 1 G. Gottardi and E. Galli, Minerals and Rocks, Natural Zeolites, Springer-Verlag, Berlin, 1985.
- 2 L.B. Sand and F.A. Mumpton, Natural Zeolites, Occurrence, Properties and Use, Pergamon Press, Oxford, 1978.
- 3 R.L. Hay, Geologic Occurrence of Zeolites, in: L.B. Sand and F.A. Mumpton (Eds.), Natural Zeolites, Pergamon, Oxford, 1978, pp. 135-143.
- 4 A. Iijima, Geology of Natural Zeolites and Zeolitic Rocks, in: L. Rees (Ed.), Proc. 5th Int. Conf. on Zeolites, Naples, Italy, June 2-6, 1980, Heyden, London, 1980, pp. 103-118.

- 5 R.M. Barrer, Synthesis of Molecular Sieve Zeolites, in: Molecular Sieves, London, England, Soc. Chem. Ind., London, 1968, pp. 39-46.
- 6 W.M. Meier and D.H. Olson, Atlas of Zeolite Structure Types, 2nd edn., Butterworths, London, 1987.
- 7 C.A.G. Konings, Delft University of Technology, Central Library. The Library search was performed using Controlled Vocabulary Index Terms of the Chemical Abstracts.
- 8 C.J. Brinker, D.E. Clark and D.R. Ulrich (Eds.), Symp. Proc. Mat. Res. Soc., Vol. 32, Better Ceramics through Chemistry, Albuquerque, U.S.A., February, 1984, Elsevier, New York, 1984.
- 9 C.J. Brinker, J. Non-Crystalline Solids, 100, 1988, 31-50.
- 10 C.J. Brinker, D.E. Clark and D.R. Ulrich (Eds.), Symp. Proc. Mat. Res. Soc., Vol. 73, Better Ceramics through Chemistry II, Palo Alto, U.S.A., April 15-19, 1986, Mat. Res. Soc., Pittsburgh, 1986.
- 11 S.D. Kinrade and T.W. Swaddle, Inorg. Chem., 27, 1988, 4253-4259.
- 12 A.V. McCormick, A.T. Bell and C.J. Radke, J. Phys. Chem., 93, 1989, 1741-1744.
- 13 R.A. van Santen, G. Ooms, C.J.J. den Ouden, B.W. van Beest and M.F.M. Post, Computational Studies of Zeolite Framework Stability, in: M.L. Occelli and H.E. Robson (Eds.), Zeolite Synthesis, ACS Symp. Ser. 398, ACS, Washington, DC, 1989, pp. 617-633.
- 14 A.G. Pelmenshchikov, G.M. Zhidomirov and K.I. Zamaraev, Quantum-chemical Interpretation of Intrazeolite Chemistry Phenomena, in: P.A. Jacobs and R.A. van Santen (Eds.), Stud. Surf. Sci. Catal., 49B, Elsevier, Amsterdam, 1989, pp. 741-752.
- 15 D.C. Bradley, Chem. Rev., 89, 1989, 1317-1322.
- 16 J.L. Guth, H. Kessler, J.M. Higel, J.M. Lamblin, J. Patarin, A. Seive, J.M. Chezeau and R. Wey, Zeolite Synthesis in the Presence of Fluoride Ions, in: M.L. Occelli and H.E. Robson (Eds.), Zeolite Synthesis, ACS Symp. Ser., 398, ACS, Washington, DC, 1989, pp. 176-195.
- 17 L.B. Sand, A. Sacco, Jr., R.W. Thomson and A.G. Dixon, Zeolites, 7, 1989, 387-392.
- 18 D.T. Hayhurst, P.J. Melling, Wha Jung Kim and W. Bibbey, Effect of Gravity on Silicalite Crystallization, in: M.L. Occelli and H.E. Robson (Eds.), Zeolite Synthesis, ACS Symp. Ser., 398, ACS, Washington, DC, 1989, pp. 233-243.
- 19 M. Niwa and Y. Murakami, J. Phys. Chem. Solids, 50, 1989, 487-496.
- 20 Chu Pochen, F.G. Dwyer and V.J. Clarke, Crystallization Method Employing Microwave Radiation, E.P. 0358827.
- 21 R.W. Thomson and A. Dyer, Zeolites, 5, 1985, 202-210.
- 22 F. Di Renzo, F. Fajula, F. Figueras, S. Nicolas and T. des Courieres, Are the General Laws of Crystal Growth Applicable to Zeolite Synthesis?, in: P.A. Jacobs and R.A. van Santen (Eds.), Stud. Surf. Sci. Catal., 49A, Elsevier, Amsterdam, 1989, pp. 119-132.
- 23 L.Y. Hou and L.B. Sand, Determinations of Boundary Conditions of Crystallization of ZSM-5/ZSM-11 in one System, in: D. Olson and A. Bisio (Eds.), Proc. 6th Int. Conf. on Zeolites, Reno, U.S.A., July 10-15, 1983, Butterworths, London, 1984, pp. 887-893.
- 24 E.G. Derouane, L. Baltusis, R.M. Dessau and K.D. Schmitt, Quantitation and Modification of Catalytic Sites in ZSM-5, in: B. Imelik (Ed.), Catalysis by Acids and Bases, Elsevier, Amsterdam, 1985, pp. 135-146.
- 25 C.T-W. Chu, G.H. Kuehl, R.M. Lago and C.D. Chang, J. of Catal., 93, 1985, 451-458.
- 26 M.F.M. Post, T. Huizinga, C.A. Emeis, J.M. Nanne and W.H.J. Stork, An Infrared and Catalytic Study of Isomorphous Substitution in Pentasil Zeolites, in: H.G. Karge and J. Weitkamp (Eds.), Stud. Surf. Sci. Catal., 46, Proc. of an Int. Symp., Sept. 4-8, 1988, Würzburg, F.R.G., Elsevier, Amsterdam, 1988, pp. 363-375.
- 27 W.O. Haag, R.M. Lago and P.B. Weisz, Faraday Discuss. Chem. Soc., 72, 1981, 317-330.

- 28 R.L. Bedard, S.T. Wilson, L.D. Vail, J.M. Bennett and E.M. Flanigen, The Next Generation, Synthesis, Characterization, and Structure of Metal Sulfide-based Microporous Solids, in: P.A. Jacobs and R.A. van Santen (Eds.), Stud. Surf. Sci. Catal., 49A, Elsevier, Amsterdam, 1989, pp. 375-387.
- 29 F. Liebau, H. Gies, R.P. Gunawardane and B. Marler, Zeolites, 6, 1986, 373-377.
- 30 L.V.C. Rees, Nature, 296, 1982, 491-492.
- 31 P.B. Weisz and J.N. Miale, J. Catal., 4, 1965, 527-529.
- 32 R.M. Barrer, Hydrothermal Chemistry of Zeolites, Academic Press, London, 1982, p. 106.
- 33 Ref. 32, p. 105.
- 34 L. Rees (Ed.), Proc. 5th Int. Conf. on Zeolites, Naples, Italy, June 2-6, 1980, Heyden, London, 1980.
- 35 D. Olson and A. Bisio (Eds.), Proc. 6th Int. Conf. on Zeolites, Reno, U.S.A., July 10-15, 1983, Butterworths, London, 1984.
- 36 Y. Murakami, A. Iijima and J.W. Ward (Eds.), New Developments in Zeolite Science and Technology, Proc. 7th Int. Conf. on Zeolites, Tokyo, Japan, August 17-22, 1986, Kodansha, Tokyo, and Elsevier, Amsterdam, 1986.
- 37 P.A. Jacobs and R.A. van Santen (Eds.), Stud. Surf. Sci. Catal., 49, Zeolites, Facts, Figures, Future, Proc. 8th Int. Conf. on Zeolites, Amsterdam, The Netherlands, July 10-14, 1989, Elsevier, Amsterdam, 1989.
- 38 B. Drzaj, S. Hocevar and S. Pejovnik (Eds.), Stud. Surf. Sci. Catal., 24, Zeolites, Synthesis, Structure, Technology and Application, Portoroz, Yugoslavia, September 3-8, 1984, Elsevier, Amsterdam, 1985, Synthesis Part.
- 39 P.J. Grobet, W.J. Mortier, E.F. Vansant and G. Schulz-Ekloff (Eds.), Stud. Surf. Sci. Catal., 37, Innovation in Zeolite Materials Science, Nieuwpoort, Belgium, September 13-17, 1987, Elsevier, Amsterdam, 1988, Synthesis Part.
- 40 M.L. Occelli and H.E. Robson (Eds.), Zeolite Synthesis, ACS Symp. Ser., 398, Los Angeles, U.S.A., September 25-30, 1988, ACS, Washington, DC, 1989.
- 41 P.A. Jacobs and J.A. Martens, Stud. Surf. Sci. Catal., 33, Synthesis of High-silica Aluminosilicate Zeolites, Elsevier, Amsterdam, 1987, p. 71.
- 42 Ref. 40, Crystal Growth Regulation and Morphology of Zeolite Single Crystals of the MFI Type, pp. 257-273.
- 43 J.C. Pouxviel and J.P. Boilot, J. Mat. Sci., 24, 1989, 321-327.
- 44 B.M. Lok, T.R. Cannan and C.A. Messina, Zeolites, 3, 1983, 282-291.
- 45 E. Moretti, S. Contessa and M. Padovan, La Chimica e l'Industria, 67, 1985, 21-34.
- 46 (a) E.M. Flanigen and R.L. Patton, US Pat. 4073865, 1978. (b) J.L. Guth, H. Kessler, M. Bourgogne, R. Wey and G. Szabo, Fr. Pat. 2567868, 1986.
- 47 W. Meise and F.E. Schwochow, Kinetic Studies on the Formation of Zeolite A, in: W.M. Meier and J.B. Uytterhoeven (Eds.), Molecular Sieves, Proc. 3rd Int. Conf. on Zeolites, ACS Symp. Ser., 121, Zürich, Switzerland, September 3-7, 1973, ACS, Washington, DC, 1973, pp. 169-178.
- 48 J.B. Nagy, P. Bodart, H. Collette, J. El Hage-Al Asswad, Z. Gabelica, R. Aiello, A. Nastro and C. Pellegrino, Zeolites, 8, 1988, 209-220.
- 49 (a) M.R. Rubin, E.J. Rosinski and C.J. Plank, US Pat. 4151189, 1979. (b) G.F. Dwyer and P. Chu, Eur. Pat. 11362, 1980.
- 50 J.M. Nanne, M.F.M. Post and W.H. Stork, NL Pat. 4251499, 1981.
- 51 G.T. Kerr, US Pat. 3459676, 1969.
- 52 (a) D.A. Hickson, BE Pat. 8886833, 1981. (b) L.D. Rollman, US Pat. 4296083, 1981. (c) L. Marosi, M. Schwarzmman and J. Stabenow, Eur. Pat. 49386, 1982. (d) L.D. Rollman and E.W. Valyocsik, US Pat. 4139600, 1979. (e) L.D. Rollman and E.W. Valyocsik, US Pat. 4108881, 1978. (f) L.D. Rollman and E.W. Valyocsik, Eur. Pat. 15132, 1980.
- 53 M.K. Rubin and E.J. Rosinski, US Pat. 4331643, 1982.

- 54 R.J. Argauer and G.R. Landolt, US Pat. 3702886, 1972.
- 55 R. Le Van Mas, O. Pilati, E. Moretti, R. Covini and F. Genoni, US Pat. 4366135, 1982.
- 56 A.J. Tompsett and T.V. Whitham, Eur. Pat. 107457, 1984.
- 57 W. Sieber and W.M. Meier, *Helv. Chim. Acta*, 57, 1974, 1533.
- 58 J.L. Casci, Bis-quaternary Ammonium Compounds as Templates in the Crystallization of Zeolites and Silica Molecular Sieves, in: Y. Murakami, A. Iijima and J.W. Ward (Eds.), *Proc. 7th Int. Conf. on Zeolites*, Tokyo, Japan, August 17-22, 1986, Kodansha, Elsevier, Tokyo, Amsterdam, 1986, pp. 215-222.
- 59 (a) G.T. Kerr, *Science*, 140, 1963, 1412. (b) G.T. Kerr, *J. Inorg. Chem.*, 5, 1966, 1539.
- 60 J. Ciric, US Pat. 3950496, 1976.
- 61 G.T. Kerr, US Pat. 3459676, 1969.
- 62 C.J. Plank, E.J. Rosinski and M.K. Rubin, US Pat. 4175114, 1979; US Pat. 4199556, 1980.
- 63 J.L. Casci, B.M. Lowe and T.V. Whittam, Eur. Pat. 42225, 1981.
- 64 M. Taramasso, G. Perego and B. Notari, *Bel. Pat.* 887897, 1981.
- 65 T.V. Whittam, Eur. Pat. 0054386, 1982.
- 66 E. Moretti, M. Padovan, M. Solari, C. Marano and R. Covini, *Germ. Pat.* 3301798, 1983.
- 67 M.K. Rubin, C.J. Plank and E.J. Rosinski, US Pat. 4021447, 1977.
- 68 J. Keysper, C.J.J. den Ouden and M.F.M. Post, Synthesis of High-silica Sodalite from Aqueous Systems, in: P.A. Jacobs and R.A. van Santen, *Stud. Surf. Sci. Catal.*, 49A, Zeolites, Facts, Figures, Future, Elsevier, Amsterdam, 1989, pp. 237-247.
- 69 Idenitsu Kosan Co., Ltd. Jpn., JP Pat. 8207816, 1982.
- 70 C.A. Audeh and E.W. Valyocsik, US Pat. 4285922, 1981.
- 71 P. Chu, US Pat. 3709979, 1973.
- 72 See ref. 71 and ref. 41, p. 148
- 73 M. Baacke and P. Kleinschmit, Eur. Pat. 91537, 1983.
- 74 W.R. Moser, J.E. Cnossen, A.W. Wang and S.A. Krouse, *J. Catal.*, 95, 1985, 21-32.
- 75 W.R. Moser, C.C. Chiang and J.E. Cnossen, *Advances in Materials Characterization*, Plenum, New York, 1985.
- 76 R.A. Laudise, *Chemical & Engineering News*, 1987, 30-43.
- 77 Ref. 32, p. 18.
- 78 D.W. Breck, *Zeolite Molecular Sieves*, John Wiley & Sons, New York, USA, 1974.
- 79 W.O. Haag, R.M. Lago and P.B. Weisz, *Nature*, 309, 1984, 589-591.
- 80 F.J. van der Gaag, Thesis Delft, The Netherlands, 1987.
- 81 G. Debras, A. Gourgue, J.B. Nagy and G. de Clippeleier, *Zeolites*, 6, 1986, 161-168.
- 82 L.D. Rollmann, Synthesis of Zeolites, An Overview, in F.R. Ribeiro, A.E. Rodrigues, L.D. Rollmann and C. Naccache, *Proceedings of the NATO ASI on Zeolites, Science and Technology*, Alcabideche, Portugal, May 1-12, 1983, Martinus Nijhoff Publ., The Hague, The Netherlands, 1984, pp. 109-126.
- 83 Ref. 78, p. 270.
- 84 A. Erden and L.B. Sand, *J. Catal.*, 60, 1979, 241-256.
- 85 P. Bodart, J.B. Nagy, E.G. Derouane and Z. Gabelica, Study of Mordenite Crystallization, in: P.A. Jacobs (Ed.), *Structure and Reactivity of Modified Zeolites*, Elsevier, Amsterdam, 1984, pp. 125-132.
- 86 Z. Gabelica, N. Dewaele, L. Maistriau, J.B. Nagy and E.G. Derouane, Direct Parameters in the Synthesis of Zeolites ZSM-20 and Beta, in: M.L. Occelli and H.E. Robson (Eds.), *Zeolite Synthesis*, ACS Symp. Ser., 398, ACS, Washington, DC, 1989, pp. 518-543.
- 87 K. Suzuki, Y. Kiyozumi, S. Shin, K. Fujisawa, H. Watanabe, K. Saito and K. Noguchi, *Zeolites*, 6, 1986, 290-298.

- 88 E. Thilo, W. Wieker and H. Stade, *Z. Anorg. Allg. Chem.*, 340, 1965, 261-276.
- 89 W. Wieker and D. Hoebbel, *Z. Anorg. Allg. Chem.*, 366, 1969, 139-151.
- 90 L.S.D. Glasser and E.E. Lachowski, *J. Chem. Soc. Chem. Comm.*, 1980, 973-974.
- 91 J.L. Guth, P. Caullet, P. Jacques and R. Wey, *Bull. Soc. Chim. Fr.*, 3-4, 1980, 121-126.
- 92 D. Hoebbel, G. Engelhardt, A. Samoson, K. Ujszasky and Yu. I. Smolin, *Z. Anorg. Allg. Chem.*, 552, 1987, 236-420.
- 93 G. Bissert and F. Liebau, *Zeitschrift für Kristallographie*, 179, 1987, 357-371.
- 94 See Chapter 8, in H. van Bekkum, E.M. Flanigen and J.C. Jansen (Eds.), *Stud. Surf. Sci. Catal.* 58, Elsevier, Amsterdam, 1989.
- 95 S. Ueda, N. Kageama and M. Koizumi, Crystallization of Zeolite Y from Solution Phase, in: D. Olson and A. Bisio (Eds.), *Proc. 6th Int. Conf. on Zeolites*, Reno, USA, July 10-15, 1983, Butterworths, London, 1984, pp. 905-913.
- 96 R.K. Iler, *The Chemistry of Silica*, Wiley, New York, 1979.
- 97 J.V. Sanders, *Journal de Physique*, C3, 1985, 1-8.
- 98 C.F. Baes and R.E. Mesmer, *The Hydrolysis of Cations*, Wiley, New York, USA, 1976.
- 99 W.G. Klemperer, V.V. Mainz and D.M. Milar, A Molecular Building-block Approach to the Synthesis of Ceramic Materials, in: C.J. Brinker, D.E. Clark and D.R. Ulrich (Eds.), *Better Ceramics through Chemistry II*, Materials Research Society, Pittsburgh, USA, 1986, pp. 3-13.
- 100 F. Liebau, *Inorg. Chim. Acta*, 89, 1984, 1-7.
- 101 A.V. McCormick and A.T. Bell, *Catal. Rev.-Sci. Eng.*, 31 (1 & 2), 1989, 97-127.
- 102 D.W. Schaefer and K.D. Keefer, Structure of Soluble Silicates, in: C.J. Brinker, D.E. Clark and D.R. Ulrich (Eds.), *Symp. Proc. Mat. Res. Soc.*, 32, *Better Ceramics through Chemistry*, Albuquerque, USA, February 1984, Elsevier, New York, 1984.
- 103 G. Boxhoorn, O. Sudmeijer and P.H.G. van Kasteren, *J. Chem. Soc. Chem. Commun.*, 1983, 1416-1418.
- 104 Z. Gabelica, E.G. Derouane and N. Blom, Factors Affecting the Synthesis of Pentasil Zeolites, in: T.E. Whyte, Jr., A. Dalla Betta, E.G. Derouane and R.T.K. Baker, *Catalytic Materials, Relationship between Structure and Reactivity*, ACS Symp. Ser., 248, ACS, 1984, pp. 219-236.
- 105 A.V. McCormick, A.T. Bell and C.J. Radke, The Influence of Alkali Metal Hydroxides on Silica Condensation Rates, in: C.J. Brinker, D.E. Clark and D.R. Ulrich (Eds.), *Better Ceramics Through Chemistry III*, 1988, Mat. Res. Soc., Pittsburgh, 1988.
- 106 Z. Gabelica, J.B. Nagy, P. Bodart, N. Dewaele and A. Nastro, *Zeolites*, 7, 1987, 67-72.
- 107 Q. Chen, J.B. Nagy, J. Fraissard, J. El Hage-Al Asswad, Z. Gabelica, E.G. Derouane, R. Aiello, F. Crea, G. Giordano and A. Nastro, in: *Proc. NATO Workshop*, April 24-27, 1989, Dourdan, France.
- 108 J.B. Nagy, P. Bodart, H. Collette, C. Fernandez, Z. Gabelica, A. Nastro and R. Aiello, *J. Chem. Soc. Faraday Trans. 1*, 85 (9), 1989, 2749-2769.
- 109 E.J.J. Groenen, A.G.T.G. Kortbeek, M. Mackay and O. Sudmeyer, *Zeolites*, 6, 1986, 403-411.
- 110 G. Engelhardt and D.Z. Hoebbel, *Chem.*, 23, 1983, 33.
- 111 F. Schlenkrich, E. Beil, O. Rademacher and H. Scheler, *Z. Anorg. Allg. Chem.*, 519, 1984, 41.
- 112 O. Rademacher, O. Ziemans and H. Scheler, *Z. Anorg. Allg. Chem.*, 519, 1984, 165.
- 113 R.D. Edelman, D.V. Kudalkar, T. Ong, J. Warzywoda and R.W. Thomson, *Zeolites*, 9, 1989, 496-502.
- 114 R.W. Thompson and A. Dyer, *Zeolites*, 5, 1985, 292-301.
- 115 See ref. 41, Chapter 1, in H. van Bekkum, E.M. Flanigen and J.C. Jansen (Eds.), *Stud. Surf. Sci. Catal.* 58, Elsevier, Amsterdam, 1989.

- 116 See ref. 32, p. 174.
- 117 B. Subotic, D. Skrtic and I. Smit, *J. of Crystal Growth*, 50, 1980, 498-508.
- 118 P. Bodart, J.B. Nagy, Z. Gabelica and E.G. Derouane, *J. Chim. Phys.*, 83, 1986, 777-790.
- 119 Private communication with Profs. P. Bennema and G.M. van Rosmalen.
- 120 E. Grujic, B. Subotic and L.J.A. Deprotovic, Transformation of zeolite A into hydroxysodalite III, in P.A. Jacobs and R.A. van Santen (Eds.), *Stud. Surf. Sci. Catal.*, 49A, Amsterdam, 1989, pp. 261-270.
- 121 W.M. Meier, in: "Molecular Sieves", London, England, Soc. Chem. Ind., London, 1968, p. 10.
- 122 The similarity between the structures of silicate species in solution and the SBU's is too small, e.g. the open five-, six- and eight-membered ring systems of the SBU's are unknown in aqueous solution.
- 123 Ref. 32, p. 122 and 153.
- 124 G.A. Jeffrey, Hydrate Inclusion Compounds, in: J.L. Atwood, J.E.D. Davies and D.D. MacNicol (Eds.), *Inclusion Compounds*, Vol. 1, Structural Aspects of Inclusion Compounds formed by Inorganic and Organometallic Host Lattices, Academic Press, London, 1984, pp. 135-190.
- 125 T.C.W. Mate, *J. Chem. Phys.*, 43, 1965, 2799.
- 126 a) J. Ciric, *J. Colloid Interface Sci.*, 28, 1968, 315-323. b) E.F. Freund, *J. Cryst. Growth*, 34, 1976, 11-15.
- 127 a) R.B. Borade, A.J. Chandvadkan, S.B. Kulkarni and P. Ratnasamy, *Indian J. of Techn.*, 21, 1983, 358-362. b) R. Aiello and R.M. Barrer, *J. Chem. Soc.*, A, 1970, 1470.
- 128 S.P. Zhdanov and N.N. Samlevich, Nucleation and Crystal Growth of Zeolites, in: L.V.C. Rees (Ed.), *Proc. of the 5th Int. Conf. on Zeolites*, Naples, Italy, June 2-6, 1980, Heyden, London, 1980, pp. 75-84.
- 129 a) H. Kacirek and H. Lechert, *J. Phys. Chem.*, 80, 1976, 1291. b) K.-J. Chao, T.C. Tasi, M.-S. Chen and I. Wang, *J. Chem. Soc. Faraday I*, 77, 1981, 465. c) E. Narita, K. Sato, N. Yatabe and T. Okabe, *Ind. Eng. Chem. Prod. Res. Dev.*, 24, 1985, 507-512.
- 130 R. von Ballmoos, Thesis Zürich, 1981.
- 131 C. Baerlocher and W.M. Meier, *Helv. Chim. Acta*, 52, 1969, 1853-1860.
- 132 C. Baerlocher and W.M. Meier, *Helv. Chim. Acta*, 53, 1970, 1285-1293.
- 133 a) H. Nakamoto and H. Takahashi, *Chem. Lett.*, 1981, 1739-1742. b) F. Crea, J.B. Nagy, A. Nastro, G. Giordano and R. Aiello, *Thermochimica Acta*, 135, 1988, 553-557. c) D.T. Hayhurst, A. Nastro, R. Aiello, F. Crea and G. Giordano, *Zeolites*, 8, 1988, 416-422.
- 134 a) See ref. 129c. b) F.-Y. Dai, M. Suzuki, M. Takahashi and Y. Sato, in: Y. Murakami, A. Iijima and J.W. Ward (Eds.), *Proc. 7th Int. Conf. on Zeolites*, Tokyo, Japan, Aug. 17-22, 1986, Kodansha, Tokyo, and Elsevier, Amsterdam, 1986, pp. 223-230. c) V.P. Shiralkar and A. Clearfield, *J. Chem. Soc.*, 1989, 363-370.
- 135 a) R.M. Barrer and P.J. Denny, *J. Chem. Soc.*, 1961, 971. b) R.M. Barrer, P.D. Denny and E.M. Flanigen, US Pat. 3306922, 1967.
- 136 R. Aiello and R.M. Barrer, *J. Chem. Soc. A*, 1970, 1470.
- 137 E.M. Flanigen and E.B. Kellberg, US Pat. 4241036, 1968.
- 138 G.T. Kokotailo and S. Sawruk, US Pat. 4187283, 1980.
- 139 An extensive list of organic templates is given in Table 5 of refs. 44, 45.
- 140 A. Gutze, J. Kornatowski, H. Neels, W. Schmitz and G. Finger, *Cryst. Res. & Technol.*, 20, 1985, 151-158.
- 141 E. de Vos Burchart, J.C. Jansen and H. van Bekkum, *Zeolites*, 9, 1989, 423-435.
- 142 J.F. Charnell, *J. Cryst. Growth*, 8, 1971, 291.
- 143 D.T. Hayhurst, A. Nastro, R. Aiello, F. Crea and G. Giordano, *Zeolites*, 8, 1989, 416-423.
- 144 Ref. 32, p. 145.
- 145 N.N. Feoktistova, S.P. Zhdanov, W. Lutz and M. Bülow, *Zeolites*, 9, 1989, 136-139.

- 146 C.A. Fyfe, G.C. Gobbi, G.J. Kennedy, J.D. Graham, R.S. Ozubho, W.A. Murphy, A. Bothner-By, J. Dadok and A.S. Chesnick, *Zeolites*, 5, 1985, 179-183.
- 147 G.W. Skeels and D.W. Breck, *Zeolite Chemistry V*, in: D. Olson and A. Bisio (Eds.), *Proc. 6th Int. Conf. on Zeolites*, Reno, USA, July 10-15, 1983, Butterworths, London, 1989, pp. 87-96.
- 148 H.K. Beyer and I. Belenijkaja, A New Method for the Dealumination of Faujasite-type Zeolites, in: B. Imelik, C. Naccache, Y. Ben Taarit, J.C. Vedrine, G. Coudurier and H. Praliaud (Eds.), *Stud. Surf. Sci. Catal.*, 5, Elsevier, Amsterdam, 1980, pp. 203-210.
- 149 B. Marler, *Zeolites*, 7, 1987, 393-397.
- 150 R.P. Gunawardane, H. Gies and B. Marler, *Zeolites*, 8, 1988, 127-131.
- 151 H. Gies and R.P. Gunawardane, *Zeolites*, 7, 1987, 442-445.
- 152 E.M. Flanigen, J.M. Bennett, R.W. Grose, J.P. Cohen, R.L. Patton, R.M. Kirchner and J.V. Smith, *Nature*, 271, 1987, 512-516.
- 153 D.M. Bibby, N.B. Inlestone and L.P. Aldridge, *Nature*, 280, 1979, 664-665.
- 154 D.H. Olson, W.O. Haag and R.M. Lago, *J. Catal.*, 61, 1980, 390-396.
- 155 H. Gies, *Zeitschrift für Kristallographie*, 175, 1986, 93-104.
- 156 A. Stewart, D.W. Johnson and M.D. Shannon, *Synthesis and Characterization of Crystalline Aluminosilicate Sigma-1*, in: P. Grobet, W.J. Mortier, E.F. Vansant and G. Schulz-Ekloff (Eds.), *Stud. Surf. Sci. Catal.*, *Proc. Int. Symp.*, September 13-17, 1987, Nieuwpoort, Belgium, Elsevier, Amsterdam, 1988, pp. 57-64.
- 157 A. Stewart, *Zeolites*, 9, 1989, 140-145.
- 158 H. Gies, *Z. Kristallogr.*, 164, 1983, 247-257.
- 159 H. Gies, *Z. Kristallogr.*, 167, 1984, 73-82.
- 160 H. Gerke and H. Gies, *Z. Kristallogr.*, 166, 1984, 11-22.
- 161 D.M. Bibby and M.P. Dale, *Nature*, 317, 1985, 157-158.
- 162 R.M. Barrer, *Porous Crystals: A Perspective*, in: Y. Murakami, A. Iijima and J.W. Ward (Eds.), *Proc. 7th Int. Conf. on Zeolites*, Tokyo, Japan, August 17-22, 1986, Kodansha, Elsevier, Tokyo, Amsterdam, 1986, pp. 3-11.
- 163 F. Liebau, *Structural Chemistry of Silicates*, Springer-Verlag, Berlin, New York, Tokyo, 1985, p. 243.
- 164 W.A. van Erp, H.W. Kouwenhoven and J.M. Nanne, *Zeolites*, 7, 1987, 286-288.
- 165 Xu Wenyang, Li Jianquan, Li Wengyuan, Zhang Huiming and Liang Bingchang, *Zeolites*, 9, 1989, 468-473.
- 166 J.L. Guth, H. Kessler and R. Wey, New Route to Pentasil-type Zeolites using a non Alkaline Medium in the Presence of Fluoride Ions, in: Y. Murakami, A. Iijima and J.W. Ward (Eds.), *New Developments in Zeolite Science and Technology*, *Proc. 7th Int. Conf. on Zeolites*, Tokyo, Japan, Aug. 17-22, 1986, Kodansha, Tokyo and Elsevier, Amsterdam, 1986, pp. 121-128.
- 167 E.W. Valyocsik and L.D. Rollmann, *Zeolites*, 5, 1985, 123-125.
- 168 U. Müller and K.K. Unger, *Zeolites*, 8, 1988, 154-156.
- 169 H. Lermer, M. Draeger, J. Steffen and K.K. Unger, *Zeolites*, 5, 1985, 131-134.
- 170 C.W.R. Engelen, unpublished results.
- 171 D.E.W. Vaughan, Secondary Cation Effects on Sodium and Potassium Zeolite Synthesis at $\text{Si/Al}_2 = 9$, in: M.M.J. Tracy, J.M. Thomas and J.M. White (Eds.), *Mat. Res. Soc. Symp. Proc.*, *Microstructure and Properties of Catalysts*, Vol. 111, Nov. 30-Dec. 3, 1987, Boston, M.R.S., Pittsburgh, U.S.A., 1988, pp. 89-100.
- 172 J.C. Jansen and S.T. Wilson, The preparation of molecular sieves, in: H. van Bekkum, E.M. Flanigen and J.C. Jansen (Eds.), *Stud. Surf. Sci. Catal.*, 58, Elsevier, Amsterdam, 1989, pp. 137-150.

CHAPTER 4

ON THE LOCATION AND DISORDER OF THE TETRAPROPYLAMMONIUM (TPA)-ION IN ZSM-5 WITH IMPROVED FRAMEWORK ACCURACY*

INTRODUCTION

The catalytic and adsorption properties of the highly siliceous ZSM-5 zeolites, crystalline aluminosilicates, and of silicalite, the aluminum free end-member, have received much attention (e.g. Flanigen *et al.*, 1978; Olson, Haag & Lago, 1980; Haag, Lago & Weisz, 1984). Differences in physical and chemical behaviour are often discussed in terms of differences in structure and composition of the zeolites (von Ballmoos, 1981; Auroux, Desepert, Leclercq & Vedrine, 1983; Gilson & Derouane, 1984). Several papers on the crystal structure of ZSM-5 have been published recently using space group Pnma (Olson, Kokotailo, Lawton & Meier, 1981; Price, Pluth, Smith, Bennett & Patton, 1982; Baerlocher, 1984; Lermer, Draeger, Steffen & Unger, 1985; Chao, Lin, Wang & Lee, 1986). The positions of the framework atoms agree well with a tetrahedral environment of oxygen around silicon. The template molecule, tetrapropylammonium(TPA^+)-fluoride or -bromide or -hydroxide, required for growth and stabilization (Keijsper *et al.*, 1986) of the ZSM-5 crystals and present in the crystals as synthesized, is not always located. Two papers (Price *et al.*, 1982; Chao *et al.*, 1986) describe the template ion at the intersection of the straight and sinusoidal channels (Fig. 1). The

* H. van Koningsveld, H. van Bekkum and J.C. Jansen, Acta Cryst. **B43**, 1987, 127-132.

$N(C_3H_7)_2$ -part in the sinusoidal channel is in a folded conformation in the crystallographic mirror plane. The other two (C_3H_7) -groups, pointing into the straight channel, are related by m . Relevant torsion angles, calculated from the published coordinates, are listed in Table 3. The TPA^+ ion has m symmetry rather than 4 as found in solid TPA^+Br^- (Zalkin, 1957). However, the reported refined C-C and C-N bond distances in TPA^+ vary from .79 Å to 1.88 Å, the bond angles are not as can be expected for tetrahedral carbon and nitrogen atoms and several temperature factors are extremely high. In addition, the m symmetry of TPA^+ with extended propyl groups at both sides of m , inevitably leads to very short contacts in the straight channel between terminal C atoms in adjacent ions. And finally, a folded conformation of the propyl-N-propyl group in m (see Fig. 1a) seems very unlikely because of the inherent substantial conformational strain caused by unfavourable short H...H contacts. Two other papers (Olson et al., 1981; Lermer et al., 1985) do not report the location of TPA^+ . These authors describe two non-framework atoms, called Oxl and Ox2, with low occupancy. Baerlocher (1984) refined the silicalite structure, including the TPA^+ ion with m symmetry at $y = 1/4$, on powder data using geometric restrictions on all distances and angles. The author suggests disorder of TPA^+ in m at $y = 1/4$ but does not investigate this possibility any further. This chapter reports a detailed structure analysis of the occluded template ion in ZSM-5, without any constraints on the atoms.

EXPERIMENTAL

Single crystal grown according to a procedure described recently (Lermer et al., 1985). Molar composition reaction mixture: SiO_2 (12.2), $NaAlO_2$ (1.0), $NaOH$ (43.3), $TPABr$ (43.5), H_2O (2452). Al (and possibly Na) content by electron microprobe analysis (EMPA). Homogeneous Al distribution. IR measurements indicate the presence of H_2O , OH^- and possibly Si-OH groups in the channels. Preliminary TGA measurements point to almost full occupancy of TPA^+ at the four channel intersections. Unit cell content: $Na_{0.3}Si_{95.7}Al_{0.3}O_{192} \cdot 4TPAOH + nH_2O$. Full details on the growth experiments, the EMPA measurements, IR and TGA-data will be published elsewhere (Jansen, Van Koningsveld, Schalkoord & Van Bekkum, 1993). Crystal dimensions: 230 x 200 x 150 μm . CAD-4 diffractometer, graphite-monochromated MoK_α radiation, cell parameters from 25 reflections with $10 < \theta < 17^\circ$. Data collected to $\theta_{max} = 30.0^\circ$ (h: 0 \rightarrow 28, k: 0 \rightarrow 27, l: 0 \rightarrow 18), $\omega/2\theta$ scan, width = (0.85 +

$0.35 \tan \theta$)⁰, max. recording time 240 s, $\sigma_{\text{count}} (I)/I < 0.02$ requested in a scan. Three reference reflections measured every 2 h of X-ray measuring time; no change in intensity observed. Lorentz and polarization correction (none for extinction or absorption) applied. 7944 independent reflections, 4528 with $I > 2.0 \sigma (I)$. Initial positions of framework atoms taken from literature (Olson *et al.*, 1981). All T atoms (Al, Si) treated as silicon. Structure refined in Pnma by (blocked) full-matrix least squares on F; all non-C atoms with anisotropic thermal parameters. N and C atoms located from several difference Fourier maps. H atoms not located. Attempts to locate OH⁻, required for electroneutrality, and of Na⁺ failed. Disordered model converged with 4523 observations ($I > 2.0 \sigma (I)$); 5 low order reflections, possibly affected by extinction, left out) to $R = 0.042$, $wR = 0.044$, $w = 1$, $S = 0.48$, 410 parameters; $\Delta/\sigma < 0.14$ for Si, O and N and < 0.40 for C^{*}. Final ΔF synthesis has six peaks above 0.50 eÅ^{-3} near C(5) (0.65 eÅ^{-3}), O(14) (0.61 eÅ^{-3}), C(10) (0.58 eÅ^{-3}), O(11) (0.56 eÅ^{-3}) and O(5) (0.55 eÅ^{-3}). No residual density around Si atoms observed. Twenty peaks (between 0.41 and 0.49 eÅ^{-3}) can all be attributed to O atoms of the framework. A refinement of the framework atoms using space group Pn2₁a failed. Apparently the deviation of the framework symmetry from Pnma is too small to permit refinement in the lower symmetry space group Pn2₁a. Refinement of TPA⁺ in Pn2₁a (with fixed framework atoms in Pnma) results in a difference Fourier map containing the mirror image of TPA⁺. Apparently, the influence of the TPA⁺ ion on the intensity distribution is too small to break the Pnma symmetry or disorder around m really exists. Disorder around m is assumed by refining the whole structure in Pnma. All calculations performed with XRAY72 (Stewart, Kruger, Ammon, Dickinson & Hall, 1972); atomic scattering factors of zero valent Si, O, N and C from Cromer & Mann (1968).

DISCUSSION

The final positional and isotropic thermal parameters of the framework and the template are given in Tables 1 and 2^{*}, respectively. A comparison with the structural data published by several authors on the same kind of structures is given in Table 3, together with some experimental details.

The framework

The geometry of the framework is the same in all structures. The accuracy of the framework distances and angles, reported in this paper, has been significantly improved (Table 3). On the average, all twelve SiO_4 groups agree well with the ideal tetrahedral environment of Si atoms. In each tetrahedron, the average Si-O distance and O-Si-O angle are 1.587 Å and 109.47° , respectively, without any significant scatter. ZSM-5 has a three-dimensional channel system defined by 10-membered rings (of T (= Si, Al) atoms). Straight channels parallel to [010] and sinusoidal channels along [100] (see Fig. 2). The straight channel locally has an approximate mirror plane through the channel axis, Si(1) and Si(7). The pseudo mirror plane contains N as illustrated in Fig. 3a and might explain the observed disorder of TPA^+ . The Si atom numbering is given in Figs. 3a and 4a together with the numbering of some oxygen atoms involved in short framework to TPA^+ contacts (see Table 5). The thermal vibration of the Si atoms* can well be described as isotropic. The O atoms, however, have very anisotropic thermal parameters (see Figs. 3 and 4). These results might indicate a deviation of the O atoms from the assumed Pnma symmetry. The deviation, however, is too small to allow refinement in the lower symmetry space group $\text{Pn}2_1\text{a}$ (see Experimental).

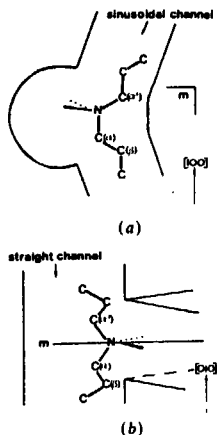


Fig. 1. Conformation of TPA^+ as reported in the literature. (Folded propyl-N-propyl fragment: $\text{C}(\alpha')\text{NC}(\alpha)\text{C}(\beta) = 0^\circ$. (Extended propyl-N-propyl fragment $\text{C}(\alpha')\text{NC}(\alpha)\text{C}$, between 97 and 127° .

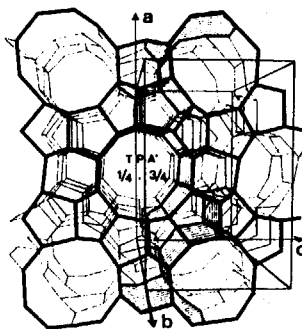


Fig. 2. View of the framework along b . T atoms are at the intersections of lines. O atoms (not drawn) are about midway between T atoms. Ten-membered rings of T atoms in the straight channels are clearly visible. Some ten-membered rings, taking part in the sinusoidal channel, are hatched. Location of TPA^+ ions in the channels indicated by the y coordinate of N atoms.

The TPA⁺ ion

The TPA⁺ ion is located at the intersection of the straight and sinusoidal channels in two different orientations populated in a ratio of 3:2. The two orientations are nearly related by the approximate mirror plane in the straight channel. Bond lengths and bond angles in the two TPA⁺ ions are listed in Table 4. Relevant data are summarized in Table 3. The atom numbering used is depicted in Figs. 3 and 4. Contrary to recently published results (see Table 3) the TPA⁺ ion does not lie exactly in the crystallographic mirror plane. Probably, atom C(4), in both TPA⁺ ions, is refined too far from *m* at $y = 1/4$. In case the refinement would have allowed C(4) to be closer to *m*, the angle C(4)NC(7) would have opened, the angle C(4)NC(10) would have closed and the distance N-C(4) would have become smaller, thus getting values closer to the averaged ones (109° and 1.57 Å). The relatively large *U* values of C(5), C(10) and C(6') (where the prime indicates atoms in the second TPA⁺ ion), reflect the possibility that C(5) and C(10) do not exactly coincide with C(2') (repeated via *m*) and C(10') and that C(6') is not exactly in *m* at $y = 1/4$. A split-atom model for C(5), [C(5) and C(2')], gives larger C(4)-C(5) and C(1')-C(2') distances and smaller C(4)C(5)C(6) and C(1')C(2')C(3') angles, but does not converge satisfactorily.

The propyl-N-propyl fragments pointing into the sinusoidal and straight channel (Figs. 3 and 4), respectively, both are in a non-extended conformation. The relevant CNCC torsion angles are given in Table 3. The observed conformation of the propyl-N-propyl fragment in the sinusoidal channel has considerably less conformational strain (CNCC ≈ 60°) than the reported folded conformation (CNCC = 0). Therefore, the *m* symmetry of TPA⁺, found by Price *et al.* (1982), Baerlocher (1984) and Chao *et al.* (1986) does not really exist. The observed conformation of TPA⁺ in ZSM-5 is completely different from the fully extended conformation of TPA⁺ (symmetry $\bar{4}$) in solid TPA⁺Br⁻ (Zalkin, 1957).

The C---C contacts between terminal C atoms in neighbouring TPA⁺ ions in the straight channel and in the sinusoidal channel are summarized in Table 3. In the present structure disorder is observed and there are three CC contacts in the straight channel: C(9)---C(12): 3.67(3) Å, C(9)---C(9'): 3.70(4) Å and C(12)---C(12'): 3.75(2) Å. Because of the actual conformation and the tilting of the TPA⁺ ion with respect to *m* the contact distances are close to the expected Van der Waals distances and are not as short as given in Table 3 for (b), (c) and (e). There are four CC contacts in the sinusoidal channel: C(6)---C(6'): 3.56(7) Å, C(6)---C(3): 4.01(5) Å, C(3')---C(3):

Table 4. Bond lengths (Å) and bond angles ($^{\circ}$) in the two TPA⁺ ions in ZSM-5.

	(TPA ⁺)	(TPA ⁺)'		(TPA ⁺)	(TPA ⁺)'
N-C(1)	1.57(2)	1.53(5)	C(1)NC(4)	111(1)	112(2)
N-C(4)	1.62(3)	1.64(4)	C(1)NC(7)	106(1)	111(2)
N-C(7)	1.52(3)	1.46(4)	C(1)NC(10)	113(1)	119(2)
N-C(10)	1.59(3)	1.59(3)	C(4)NC(7)	94(1)	93(2)
mean	1.58	1.56	C(4)NC(10)	122(2)	112(2)
			C(7)NC(10)	108(2)	111(2)
			mean	109	110
C(1)-C(2)	1.53(4)	1.46(5)			
C(2)-C(3)	1.63(5)	1.58(6)	NC(1)C(2)	111(2)	116(3)
C(4)-C(5)	1.45(4)	1.52(6)	NC(4)C(5)	111(2)	107(3)
C(5)-C(6)	1.59(4)	1.52(7)	NC(7)C(8)	100(2)	119(3)
C(7)-C(8)	1.61(5)	1.50(6)	NC(10)C(11)	117(2)	117(2)
C(8)-C(9)	1.65(4)	1.62(5)	mean	110	115
C(10)-C(11)	1.53(4)	1.53(4)			
C(11)-C(12)	1.48(3)	1.48(3)	C(1)C(2)C(3)	107(2)	119(3)
mean	1.56	1.53	C(4)C(5)C(6)	114(2)	107(3)
			C(7)C(8)C(9)	105(2)	104(3)
			C(10)C(11)C(12)	106(2)	106(3)
			mean	108	109

Table 5. Framework to TPA⁺ distances less than 3.81 Å.

C(1)-O(15)	3.47(2)	C(11)-O(5)	0(21)
O(21)	3.77(2)	C(12)-O(7)	0(8)
O(26)	3.60(2)	C(1')-O(1)	0(15)
C(2)-O(18)	3.78(3)	C(2')-O(1)	0(26)
O(25)	3.78(3)	C(3')-O(25)	0(2)
C(3)-O(17)	3.73(3)	C(4')-O(5)	0(18)
O(23)	3.80(3)	C(5')-O(5)	0(15)
C(4)-O(2)	3.80(2)	C(8')-O(7)	0(21)
O(20)	3.63(3)		
O(24)	3.77(3)		
C(5)-O(1)	3.71(3)		
O(2)	3.62(3)		
O(20)	3.80(3)		
C(7)-O(5)	3.80(3)		
O(21)	3.76(3)		
C(8)-O(11)	3.37(4)		
O(20)	3.55(4)		
O(22)	3.72(4)		
C(9)-O(11)	3.64(3)		
O(22)	3.56(3)		

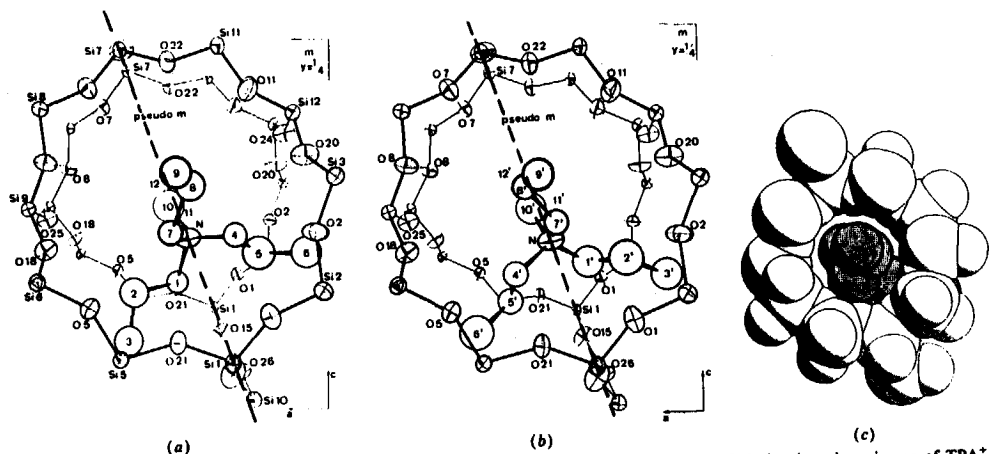


Fig. 3. TPA⁺ at the intersection of channels seen along *b*. Pseudo-*m* is indicated. For reasons of clarity the mirror image of TPA⁺ around *m* at $y = \frac{1}{2}$ is not drawn. (a) Orientation of the first TPA⁺ ion. (b) Orientation of the second TPA⁺ ion. (c) Space-filling drawing (Spek, 1982) of TPA⁺ in first orientation showing the packing in the straight channel. van der Waals radii taken from Bondi (1964).

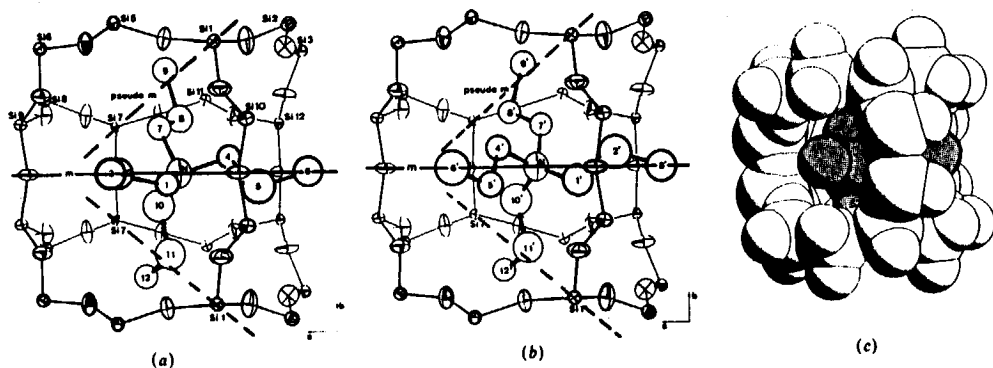


Fig. 4. As Fig. 3, seen along *c*. The packing of terminal C atoms of TPA⁺ in the sinusoidal pores is shown.

Table 1. Fractional coordinates ($\times 10^4$) and U_{eq} values ($\text{\AA}^2 \times 10^3$) for the framework atoms. $U_{eq} = 1/3 (U_{11} + U_{22} + U_{33})$.

	x	y	z	U_{eq}
Si(1)	4223.8(5)	565.0(6)	-3359.8(9)	17.6(3)
Si(2)	3071.6(6)	277.2(6)	-1893.0(9)	20.7(3)
Si(3)	2791.1(6)	612.7(6)	312.0(9)	19.3(3)
Si(4)	1221.5(6)	629.8(6)	267.0(9)	18.1(3)
Si(5)	712.8(6)	272.2(6)	-1855.1(9)	16.0(3)
Si(6)	1864.1(5)	589.6(6)	-3281.8(8)	17.8(3)
Si(7)	4226.5(6)	-1725.0(6)	-3271.8(9)	18.5(3)
Si(8)	3077.8(6)	-1301.6(6)	-1854.8(9)	19.9(3)
Si(9)	2755.4(6)	-1727.9(6)	310.9(9)	17.6(3)
Si(10)	1205.8(6)	-1731.0(6)	297.9(9)	19.3(3)
Si(11)	704.4(6)	-1303.7(6)	-1820.0(9)	19.3(3)
Si(12)	1870.6(6)	-1732.7(6)	-3193.3(9)	20.0(3)
O(1)	3726(2)	534(3)	-2442(3)	49(1)
O(2)	3084(2)	587(2)	-789(2)	40(1)
O(3)	2007(2)	592(3)	289(4)	64(2)
O(4)	969(2)	611(2)	-856(3)	44(1)
O(5)	1149(2)	541(2)	-2763(2)	34(1)
O(6)	2435(2)	553(3)	-2460(3)	46(1)
O(7)	3742(2)	-1561(2)	-2372(3)	47(1)
O(8)	3085(2)	-1552(2)	-728(3)	44(1)
O(9)	1980(2)	-1554(2)	288(3)	40(1)
O(10)	910(2)	-1614(2)	-777(3)	58(2)
O(11)	1169(2)	-1578(2)	-2694(3)	48(1)
O(12)	2448(2)	-1594(3)	-2422(3)	55(2)
O(13)	3047(3)	-510(2)	-1866(4)	71(2)
O(14)	768(2)	-519(2)	-1769(3)	47(1)
O(15)	4161(2)	1276(2)	-3896(3)	44(1)
O(16)	4086(2)	-17(2)	-4136(3)	46(1)
O(17)	4020(2)	-1314(2)	-4239(3)	40(1)
O(18)	1886(2)	1298(2)	-3836(3)	36(1)
O(19)	1940(2)	7(2)	-4082(3)	45(1)
O(20)	1951(2)	-1291(2)	-4190(3)	43(1)
O(21)	-37(1)	502(2)	-2080(2)	33(1)
O(22)	-40(2)	-1528(2)	-2078(3)	40(1)
O(23)	4192(3)	-2500	-3540(4)	44(2)
O(24)	1884(3)	-2500	-3538(4)	34(1)
O(25)	2883(3)	-2500	579(4)	33(1)
O(26)	1085(3)	-2500	611(4)	30(1)

Table 2. Fractional coordinates ($\times 10^3$), U_{iso} values ($\text{\AA}^2 \times 10^3$) and population parameters (PP) of the atoms in the TPA⁺ ions.

	x	y	z	U_{iso}	f
N	476.2(5)	250	-109.5(6)	69(4)	1.
C(1)	495(1)	233(1)	-221(2)	58(8)	0.
C(2)	568(2)	250	-241(2)	97(9)	0.
C(3)	578(2)	250	-362(2)	98(9)	0.
C(4)	399(1)	274(1)	-100(2)	64(8)	0.
C(5)	355(1)	228(1)	-150(2)	136(10)	0.
C(6)	278(2)	250	-147(3)	104(10)	0.
C(7)	505(2)	319(2)	-89(2)	65(8)	0.
C(8)	473(2)	334(2)	19(3)	83(9)	0.
C(9), C(9')	496(1)	412(1)	45(2)	88(6)	0.
C(10), C(10')	508(1)	199(1)	-32(2)	121(9)	0.
C(11), C(11')	490(1)	124(1)	-45(2)	109(7)	0.
C(12), C(12')	529(1)	88(1)	33(1)	72(4)	0.
C(1')	413(2)	229(2)	-166(4)	83(16)	0.
C(2')	355(1)	272(1)	-150(2)	136(10)	0.
C(3')	285(3)	250	-195(4)	110(16)	0.
C(4')	534(2)	279(2)	-185(3)	67(12)	0.
C(5')	546(2)	225(2)	-263(4)	73(13)	0.
C(6')	601(3)	250	-332(5)	129(21)	0.
C(7')	468(2)	315(2)	-60(3)	61(11)	0.
C(8')	516(2)	335(2)	20(3)	61(10)	0.

Table 3. Comparison between several ZSM-5-like structures

Reference	(a)	(b)	(c)	(d)	(e)	This work
Crystal data						
Dimensions (μm)	20 \times 30 \times 40	180 \times 50 \times 50	Powder	260 \times 130 \times 120	200 \times 70 \times 50	230 \times 200 \times 150
Al/unit cell	1-1	0-0	0-0	8-0	3-7	0-3
Reflections with $I \geq 2\sigma(I)$	1026*	1645	2246	2217	1508	4528
θ_{max} (°)	Not given	27.5	45.0	32.5	25.0	30.0
$R(F)$	11.9	6.7	6.9	9.7	7.9	4.2
Framework geometry						
T-O range (Å)	1.50 (4)-1.67 (3)	1.51 (3)-1.69 (3)	1.55-1.65†	1.54 (2)-1.62 (2)	1.52 (2)-1.66 (2)	1.567 (4)-1.605 (4)
O-T-O range (°)	96 (2)-129 (2)	100 (2)-119 (2)	104-113	105-6 (7)-113-7 (8)	103-9 (8)-115-5 (8)	106-0 (2)-112-0 (2)
Av. T-O-tetrahedron (Å)	1.56-1.63	1.57-1.61	1.57-1.62	1.57-1.60	1.57-1.62	1.584-1.591
Av. O-T-O-tetrahedron (°)	109-110	109-110	109-5	109-4-109-5	109-4-109-5‡	109-5
TPA ⁺ ion geometry						
C-N range (Å)	TPA not localized§	1.5 (1)-1.9 (1)	1.54-1.55†	TPA not localized§	1.5 (1)-1.9 (1)	1.46 (3)-1.64 (4)
C-C range (Å)		0.8 (2)-1.8 (2)	1.51-1.55		1.0 (1)-1.7 (1)	1.45 (4)-1.65 (4)
CNC range (°)		73 (12)-140 (12)	106-112		102 (4)-116 (4)	93 (2)-122 (2)
CCN range (°)		140 (12)-179 (12)	108-113		104 (8)-160 (6)	100 (2)-119 (3)
CCC range (°)		134 (12)-174 (12)	109-112		111 (8)-144 (7)	104 (3)-119 (3)
C(O)NC(a)C(β) torsions (°):						
CNCC (straight channel)		124 (15)	127		97 (8)	67 (2), 31 (2)¶
CNCC (sinusoidal channel)		0	0		0	51 (2), 55 (2)¶
C-C** (straight channel)		2.7 (2)	3-16		3-6 (2)	≥ 3-67 (3)
C-C** (sinusoidal channel)		3-1 (2)	4-46		3-6 (2)	≥ 3-56 (7)

References: (a) TPAOH-ZSM-5 (Olson *et al.*, 1981); (b) TPAF-silicalite (Price *et al.*, 1982); (c) TPAOH-silicalite (Baerlocher, 1984); (d) TPAOH-ZSM-5 (Lerner *et al.*, 1985); (e) TPAOH-ZSM-5 (Chao *et al.*, 1986).

* For $F_o \geq 3\sigma(F_o)$.

† Constraint values; standard deviations doubtful, assumed by the author to be of the same order of magnitude as in (a) and (b).

‡ There is a misprint in the reported av. O-Si-O angle (107.9°) and in the reported x coordinate of C(6): 0.1258; the correct values are 109.5° and 0.5128.

§ Non-framework atoms Ox1 and Ox2 localized instead. [Coordinates of Ox2 are different in reports (a) and (d). See text.]

¶ Values in both TPA⁺ ions are listed. The torsion angles measuring the 'folding' are given: C(8)C(7)NC(10) in the straight channel and C(1)NC(4)C(5) in the sinusoidal channel.

** Contact distances between terminal C atoms in adjacent TPA⁺ ions.

4.21(6) Å and C(3')---C(6'): 3.70(8) Å. The shortest contacts involve C(6') at $y = .250$, an atom with a large temperature factor. The distances enlarge when C(6') is not exactly in m. The framework to TPA^+ distances, less than 3.81 Å, are given in Table 5 and illustrated in Figs. 3 and 4. The C---C and C---O contacts are different for the two TPA^+ ions. This might explain the population difference of the two TPA^+ ions.

The coordinates of the non-framework atoms O_{x1} and O_{x2}, found by Olson *et al.* (1981), correspond to those of the center of gravity of atoms C(3) & C(6') and of atoms C(6) & C(3') in our study, respectively. The O_{x1} and O_{x2} atoms given by Lermer *et al.* (1985), are identical with C(6) (& C(3')) and N in the present work, respectively. These observations strongly suggest the template ion to be present as well in the structures studied by Olson *et al.* and Lermer *et al.*

REFERENCES

- Auroux, A., Deseper, H., Leclercq, C. & Vadrine, J. (1983). Appl. Catal. 6, 95-119.
- Baerlocher, C. (1984). Proc. 6th Int. Zeolite Conf. Reno, edited by D. Olson & A. Bisio, pp. 823-833. Guildford: Butterworths.
- Ballmoos, R. von (1981). Thesis, Zürich.
- Bondi, A. (1964). J. Phys. Chem. 68, 441-451.
- Chao, K.J., Lin, J.C., Wang, Y. & Lee, G.H. (1986). Zeolites, 6, 35-38.
- Cromer, D.T. & Mann, J.B. (1968). Acta Cryst. A24, 321-324.
- Flanigen, E.M., Bennett, J.M., Grose, R.W., Cohen, J.P., Patton, R.L., Kirchner, R.L. & Smith, J.V. (1978). Nature, 271, 512-516.
- Gilson, J.P. & Derouane, E.G. (1984). J. Catal. 88, 538-541.
- Haag, W.O., Lago, R.M. & Weisz, P.B. (1984). Nature, 309, 589-591.
- Jansen, J.C., van Koningsveld, H., Schalkoord, D. & van Bekkum, H. Zeolites, to be submitted.
- Johnson, C.K. (1965). ORTEP. Report ORNL-3794, revised June 1970. Oak Ridge National Laboratory, Tennessee.
- Keijsper, J., Mackay, M., van den Berg, J., Kortbeek, A.G.T.G. & Post, M.F.M. (1986). KNCV Katalyse Symposium (Catal. Symp. of the Royal Dutch Chem. Soc.). 17, 18 April, TH Twente, The Netherlands, p. 39.

- Lermer, H., Draeger, M., Steffen, J. & Unger, K.K. (1985). Zeolites, 5, 131-134.
- Olson, D.H., Haag, W.O. & Lago, R.M. (1980). J. Catal. 61, 390-396.
- Olson, D.H., Kokotailo, G.T., Lawton, S.L. & Meier, W.M. (1981). J. Phys. Chem. 85, 2238-2243.
- Price, G.D., Pluth, J.J., Smith, J.V., Bennett, J.M. & Patton, R.L. (1982). J. Am. Chem. Soc. 104, 5971-5977.
- Sheldrick, G.M. (1976). SHELX76. Program for crystal structure determination. Univ. of Cambridge, England.
- Spek, A.L. (1982). The EUCLID Package. In Computational Crystallography, edited by D. Sayre, p. 528. Oxford: Clarendon Press.
- Stewart, J.M., Kruger, G.J., Ammon, H.L., Dickinson, C.W. & Hall, S.R. (1972). XRAY72 system. Tech. Rep. TR-192. Computer Science Center, Univ. of Maryland, College Park, Maryland.

CHAPTER 5

ISOMORPHOUS SUBSTITUTION OF Si BY B, Al, Ga AND Be DURING CRYSTALLIZATION OF LARGE SINGLE CRYSTALS OF ZEOLITE. PART I. ON THE MAXIMUM BORON CONTENT OF ZSM-5*

INTRODUCTION

Isomorphous substitution of Si by other T-atoms has been studied on powders of the zeolite ZSM-5 [1-6]. Apart from the crystal structure analysis of as synthesized [Al]-ZSM-5 [7-10] and recently of the detailed study of the template TPA⁺ therein [11], no single crystal studies on ZSM-5 with Si replaced by T-atoms other than Al are known.

Differences between products consisting of powders (crystals < 10 μm) and/or large crystals (> 60 μm) as well as differences in the typical analyses techniques used may lead to ambiguous conclusions with respect to T-atom replacements.

Homogeneous [12] but more frequently heterogeneous [13] T-atom distributions in powders of ZSM-5 have been reported. The heterogeneous distributions indicating non optimal syntheses conditions, might be related to the relatively high concentration of silicon applied. Also in more diluted solutions required to obtain large crystals, a strong Al gradient, showing heterogeneity, was observed within multiple twinned crystals [14]. Later on, a homogeneous Al distribution within single crystals but not among single crystals of the same batch could be prepared [15]. Recently, a homogeneous Al distribution within the single crystals and among the single crystals of the same batch, indicating a pure material has been found [16].

* J.C. Jansen, E. Biron and H. van Bekkum, Stud. Surf. Sci. Catal. 37, 1988, 133-137.

Isomorphous replacement of Si in zeolites is often studied by XRD and IR [1,2,5]. The unit-cell variation as a function of the T-content ion powders can be measured by XRD; however, broadening of the X-ray diffraction peak profiles is caused by particle size and/or heterogeneously substituted T-atoms. In contrast, the unit cell variation can be accurately determined with a single crystal on a single crystal diffractometer [17].

Measurements on powders using IR in transmission mode with KBr pellets or as self supported wafer show gradual shifts of the lattice vibrations with the degree of substitution [18]. To avoid scattering of the IR radiation on the particles [19] single crystal sheets of 6 μm or less can be used [16]. An additional advantage of single crystal XRD studies with respect to powders is the possibility of single crystal structure analysis. However, to detect any influence resulting from the replacement of Si by other T-atoms in high Si/T zeolites like ZSM-5 the concentration of the replacing T-atom must be high.

In order to gain more insight into the isomorphous substitution of certain hetero T-atoms, i.e. the maximum number, the distribution and the framework distortion with respect to silicalite, single crystalline material of ZSM-5 has been chosen for this study.

Here we report results on the synthesis and characterization of single crystals of [B]-, [Be]-, [Al]- and [Ga]-ZSM-5. Special attention is given to the maximum incorporation of boron in ZSM-5 single crystals.

EXPERIMENTAL

Single crystals of [B]-, [Be]-, [Al]- and [Ga]-ZSM-5 were synthesized in a 50 ml Teflon lined stainless steel autoclave at 180 $^{\circ}\text{C}$ during 5-8 days without stirring. Starting chemicals used were: silica, Aerosil 200 (Degussa), TPABr supplied by Chemfaza B.V., sodium aluminate and sodium hydroxide both reagent grade chemicals from Riedel de Haen and Merck, respectively.

The molar oxide ratio used was as follows:

SiO_2	$\text{TO}_{(2)}$	Na_2O	$(\text{TPA})_2\text{O}$	H_2O
4-12	0.01-2(0)*	20	20	2000

* in the case of boron

Crystals were used as-synthesized and were powdered for part of the XRD and the IR measurements. The elemental analysis was performed on a Perkin Elmer Plasma II ICPAES apparatus equipped with a PE 7500 computer. Crystals were selected and dissolved in 1-4% HF. The solutions were stored and measured in plastic vessels. Crystals were also selected for Guinier-de Wolff powder diffraction photographs, using Cu-K α radiation and quartz as an internal standard. The line shift of three lines, i.e. the 552; 804/1000 and 536/356 were used to calculate the final unit cell dimension variation. Infrared data of [B]-ZSM-5 were collected on a Perkin Elmer 521 apparatus using KBr pellets. FTIR measurements were performed, using a Bruker IFS 85 IR spectrometer with a microscope in both the transmission and reflection mode. The unit cell dimensions of a single crystal of silicalite and of four [B]-ZSM-5 single crystals have been measured on an Enraf Nonius CAD-4 diffractometer.

RESULTS AND DISCUSSION

Two types of ZSM-5 crystals were observed, as shown in Fig. 1, for all substituting T-atoms studied: (i) Long shaped prismatic single crystals up to a maximum of 600 μm in length (Fig. 1a), of which twinned and multicrystalline forms (Fig. 1b) often occur; (ii) Cube shaped single crystals with maximum dimensions of 500 x 500 x 500 μm (Fig. 1c).

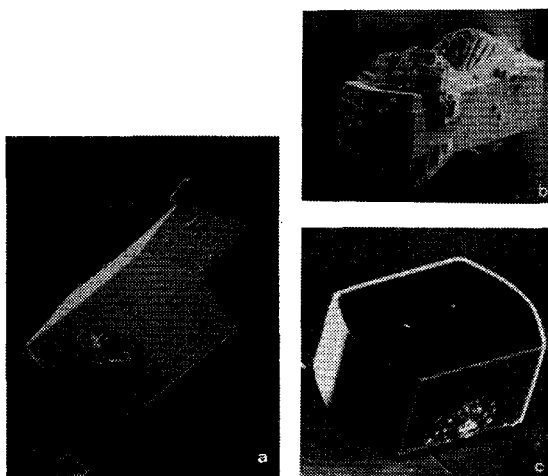


Fig. 1. ZSM-5 crystal morphologies.

The prismatic crystals were particularly found when reaction syntheses mixtures contained relatively high T-atom concentrations. In these mixtures a relative fast crystal growth is assumed. Cube-shaped crystals generally form when using low concentrations. In some synthesis experiments both types of crystal morphologies were observed which may have been due to local concentration differences resulting from heterogeneity of the synthesis mixtures (gel formation). The cube shaped single crystals (Fig. 1c) were invariably accompanied by side products, as listed in Table I. Depending upon the T atom chosen, different side products were found. In the case of [B]-ZSM-5 only boron-free quartz was found as a side product according to ICPAES analysis. The beryllosilicate ($\text{Si/Be} = 4$, analysed by ICPAES), formed as a side product of a [Be]-ZSM-5 synthesis, has the gismondine structure [20]. Single crystals of analcime, sometimes accompanied by quartz, were found as a side product in the [Al]-ZSM-5 synthesis. The amount of analcime (reported Si/Al ratio 2 [21]) was found to increase with increasing Al content of the synthesis formulation. In the case of [Ga]-ZSM-5, single crystals of Ga-natrolite and Ga-analcime were formed, together with a quartz phase. A comparison between Al-analcime and Ga-analcime by studying their crystals is in progress. For [Al]-natrolite a Si/Al ratio of 1.5 has been reported [21].

Table I. Single crystals of ZSM-5 and side products

Morphology T-atom	Cube				Prismatic			
	B	Be	Al	Ga	B	Be	Al	Ga
Single crystal of ZSM-5	+	+	+	+	+	+	+	+
Gismondine type		+						
Natrolite type				+				
Analcime type			+	+				
Quartz	+		+	+				

If cube crystals are absent, the long shaped [T]-ZSM-5 crystallized without any side products. This holds for all four T atoms studies.

As to the incorporation of Be into ZSM-5 a Si/Be ratio of 37 was found both for cube- and long-shaped as-synthesized [Be]-ZSM-5 single crystals starting from a synthesis mixture with $\text{Si/Be} = 8$. In a series of experiments on [Al]-ZSM-5, synthesis mixtures with $20 < \text{Si/Al} < 95$, yielded cube shaped crystals

with $48 < \text{Si/Al} < 260$. Quantitative results on both morphologies of [Ga]-ZSM-5 are presently under study. In a study of the maximum boron content in [B]-ZSM-5 crystals, *vide infra*, Si/B ratios down to 16 were observed. Elemental analyses results and [B]-ZSM-5 unit cell volumes are given in Table II. Variation of Si/B ratio in the mainly long shaped crystals as a function of the boron concentration in the starting solution is given in Fig. 2. From the asymptotic nature of the graph in Fig. 2 a Si/B ratio of 18, i.e. ~ 5.0 B/uc would seem to be the maximum content of boron that can be incorporated into ZSM-5 crystals grown in hydrogel systems with $\text{H}_2\text{O/SiO}_2 = 167$. In an attempt to incorporate more than ~ 5 B/uc in the ZSM-5 framework, concentrated ($\text{H}_2\text{O/SiO}_2 = 17$) and diluted ($\text{H}_2\text{O/SiO}_2 = 501$) synthesis mixtures were used. However, all products contained less than 5 B/uc.

Table II. Si/B ratio of species obtained in [B]-ZSM-5 synthesis

Sample code	Reaction mixture		Si/B in the end-product		
	B/Si+B * 96	Si/B	[B]-ZSM-5	Gel	Filtrate
Z-31-6	0.8	119	79		
Z-26-6	0.8	119	106		
Z-44-11	3.8	24.3	119		
Z-24-1	7.3	12.2	52.3		
Z-26-1	7.3	12.2	44.7		
Z-26-4	23.7	3.1	32.1		
Z-31-49	23.7	3.1	28.1		
Z-24-5	27.9	2.4	35.9		
Z-49-11	43.2	1.2	22.4		
Z-44-15	59.6	.6	16.1		
Z-51-13	23.7	3.1	29.5	16.2	0.4
Z-51-14	31.6	2.0	25.3	16.5	0.3
Z-54-1	48.0	1.0		2.2	0.6
Z-54-2	48.0	1.0		4.0	0.1
Z-53-15	8.6	10.1		281.6	6.5
Z-53-16	15.8	5.1		212.1	3.7
Z-53-17	48.0	1.0		5.8	0.9
Z-53-18	64.0	.5		2.8	0.2
Z-39-3	48.0	1.0	13.5		
Z-44-15	59.6	.6	15.4		

To gain more insight in the boron distribution of the synthesis mixture in two typical experiments the Si/B ratio of the crystals, the gels and the final solutions were measured. As shown in Fig. 2 (o, Δ , \square) the Si/B data indicate a higher boron content of the gel and of the final solution than of the crystals. Data from solutions with higher boron concentrations show the same trend as depicted in Fig. 2. Thus the limiting factor of boron substitution in ZSM-5 crystalline material appears to be not the remaining solution and capacity of the gel but the ZSM-5 framework, assuming that no interstitial, intercrystalline and/or cationic boron is present.

Fig. 3 gives the variation in the unit cell volume of [B]-ZSM-5 as a function of the boron content per unit cell in the crystals. A linear relationship between unit-cell volume and the substituting T-atom content in the unit-cell is generally assumed [3,4,6]. In the present work the unit-cell volume was determined both for single crystals (dimensions $\sim 200 \times 200 \times 100 \mu\text{m}$) and for powdered material (diameter $\sim 4 \mu\text{m}$). The slopes of the lines in Fig. 3 deviate from the data reported by Taramasso et al. [4] but are consistent with recently published data by Meyers et al. [6].

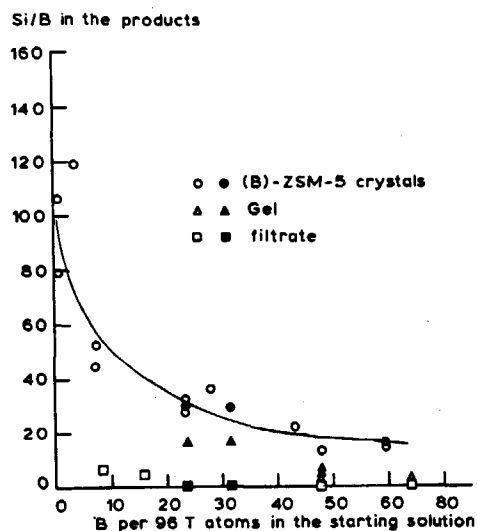


Fig. 2. Si/B in products as a function of $B/(Si+B \cdot 96)$ T in starting solution. Lowest Si/B values between .2 and 1.6. Filled symbols refer to two independent completely analyzed experiments.

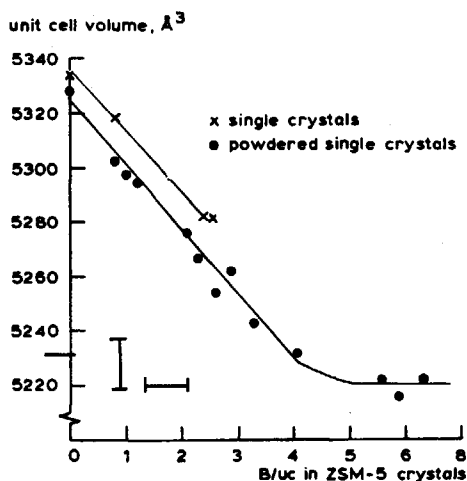


Fig. 3. Unit-cell volume as a function of B/uc in the crystals. Measured on powdered crystals (o) as well as on single crystal (x).

The homogeneously distributed data of Fig. 3 show a linear relationship up to 4 B/uc. The graph then continues however, horizontally to higher B/uc contents up to 6.6 B/uc. We assume the higher B content measured in the horizontal part to be due to extra-lattice boron. Thus a maximum incorporation of around 5.0 B/uc in Fig. 3 is also reflected by the curve of Fig. 2. The expansion of the [Al]-ZSM-5 unit cell caused by 9.5 Al/uc, as published recently [6], indicates that relatively high amounts of three-valent heteroatoms can be built into the framework of ZSM-5. However from the ionic radii of Al^{3+} (~ 0.5 Å), Si^{4+} (~ 0.4 Å) and B^{3+} (~ 0.2 Å).

Such a distortion is less pronounced in less porous systems which therefore can accommodate more B/uc. This trend is illustrated in Table III for three borosilicates.

Substitution of boron in zeolites A, X and Y is reported by Barrer et al., to be insignificant [22]. The minimum Si/B ratio and density of [B]-ZSM-5 are in line with the trend of the data in Table III.

Table III. Si/B ratio and density of borosilicates.

Silicate	Si/B	D (g/cm ³)
A, X and Y	∞	1.4
ZSM-5	~ 18	2.0
Reedmergnerite	3	2.8
Datolite*	1	3.1
Danburite	1	3.3

* BO_3OH tetrahedra.

Apart from the powder data on crystals, four points (x) are added in Fig. 3 from single crystal analyses: silicalite and three [B]-ZSM-5 species. A linear relationship, not coinciding, but parallel to the data of the powdered crystals, is shown through the first four points (one of which represents measurements on two crystals with different morphologies) of the single crystals.

The non-coincidence of the data on the powdered- and single crystals might be due to systematic errors. However, the parallelism of both lines indicates a consistent evidence for the influence of B on the unit cell reduction. A single crystal structure analysis on a [B]-ZSM-5 crystal will be performed in due time.

Powdered single crystals of silicalite in KBr pellets depicted the well known mid infra-red spectrum with absorptions near 1225, 1090, 800, 550, and 450 cm^{-1} . The 550/450 cm^{-1} optical density ratio being 0.8 as expected for pure as-synthesized material. In the spectrum of a [B]-ZSM-5 with 4.1 B/uc the asymmetric T-O-T stretch vibration at 1090 cm^{-1} of silicalite was shifted to 1080 cm^{-1} . The intensity of an additional absorption at 900 cm^{-1} present in different [B]-ZSM-5 spectra increases with the B content of the crystals. In a recent publication [5] this is ascribed to an asymmetric stretching B-O-Si mode, indicating the presence of boron in the framework.

CONCLUSIONS

Single crystals of [B]-, [Be]-, [Al]- and [Ga]-ZSM-5 can be prepared. In the case of B-ZSM-5 sizes up to a maximum of 500 μm in size. Two morphologies are observed, prismatic- and cube-shaped with the cubes being accompanied by identified side products. The maximum number of boron atoms per unit cell that can be accommodated in the framework of ZSM-5 is about 5. It appears that the framework distortion is the main limiting factor for the Si replacement by boron.

A linear relationship between unit cell reduction up to 4 B/uc is observed. Single crystals of [Ga]-analcite have been prepared.

REFERENCES

1. R.M. Barrer, Hydrothermal chemistry of zeolites, Academic Press, London, 1982, pp. 251.
2. C.T-W. Chu and C.D. Chang, J. Phys. Chem. 89 (1985) 1569.
3. M. Tielen and P.A. Jacobs, Proc. Int. Symp. Zeol. Catal. Siófok, Hungary, 1985, p. 1.
4. M. Taramasso, G. Perego and B. Notari, in L.V. Rees (editor), Proc. 5th Int. Conf. on Zeolites, Naples, 1980, Heyden, London, 1980, p. 40.
5. G. Coudurier and J.C. Vedrine, in Y. Murakami, A. Lyima and J.W. Ward (editors), Proc. 7th Int. Conf. on Zeolites, Tokyo, 1986, Kodansha/Elsevier, Tokyo, 1986, p. 643.
6. B.L. Meyers, S.R. Ely, N.A. Kutz, J.A. Kaduk and E. van den Bossche, J. Catal. 91 (1985) 352.
7. H. Lerner, M. Draeger, J. Steffen and K.K. Unger, Zeolites 5 (1985) 131.
8. K-J. Chao, J.C. Lin, Y. Wang and G.H. Lee, Zeolites 6 (1986) 35.
9. D.H. Olson, G.T. Kokotailo, S.L. Lawton and W.M. Meier, J. Phys. Chem. 85 (1981) 2238.
10. G.D. Price, J.J. Pluth, J.V. Smith, J.M. Bennett and R.L. Patton, J. Am. Chem. Soc. 104 (1982) 5971.
11. H. van Koningsveld, J.C. Jansen and H. van Bekkum, Acta Cryst. B43 (1987) 127.
12. S.I. Suib, G.D. Strucky and R.J. Blattner, J. Catal. 65 (1980) 174.

13. Z. Gabelica, E.G. Derouane and N. Blom, in T.H.E. Whyte, Jr., R.A. Dalla Betta, E.G. Derouane and R.T.K. Baker (Editors), ACS symposium series, no. 248, p. 219.
14. R. von Ballmoos et al., in D. Olson and A. Bisio (editors), Proc. 6th Int. Conf. on Zeolites, Reno, 1983, Butterworths, 1984, p. 803.
15. K-J. Chao et al., Preprints of poster papers of the 7th Int. Conf. on Zeolites, Japan Association of Zeolite, Tokyo, 1986, p. 145.
16. J.C. Jansen, H. van Koningsveld and H. van Bekkum, Ref. 15, p. 147.
17. H. van Koningsveld, 1988, private communication.
18. E.M. Flanigen, in J.A. Rabo (editor), Zeolite Chemistry and Catalysis, ACS 171, 1976, p. 80.
19. R.A. le Févre, J.C. Jansen and H. van Bekkum, Zeolites 7 (1987) 471.
20. S. Ueda and M. Koizumi, Nature 238 (1972) 139.
21. Ref. 1, p. 18.
22. Ref. 1, p. 285.

CHAPTER 6

FIRST STM SURFACE CHARACTERIZATION OF A ZEOLITE*

INTRODUCTION

Images of surfaces of conducting materials can be obtained by STM in air⁴. Spatial positions and patterns of atoms can be recognized from the topography of the sample surface⁵.

Zeolites, crystalline aluminosilicates used as catalysts and sorbents⁶ contain nano pores which are uniformly distributed. In case of conductance, STM images of the zeolite crystal surface are supposed to reveal the pore distribution together with the pore wall topography.

EXPERIMENTAL

For this work a cube like $300 \times 250 \times 200 \mu\text{m}$ single crystal of silicalite-1, see Fig. 1a, was hydrothermally grown from a $\text{Na}_2\text{O} \cdot \text{TPA}_2\text{O} \cdot \text{SiO}_2 \cdot \text{H}_2\text{O}$ gel (TPA, tetrapropylammonium ion)³. After cleavage perpendicular to [001] of the calcined crystal the fresh crystal surface was used for exploration by STM as shown in the schematic view in Fig. 1b. The wire model shown in Fig. 1c represents a detail of the arrangement of the two dimensional pore system and silicate framework alternating in [001]. The STM experiments were conducted using air as ambient. The zeolite crystal was glued on a platelet with carbon lacquer. No metallization was applied. The image in Fig. 2a was obtained with a 4.6 mV bias voltage; 7.2 nA of setpoint current and Pt-Ir tip. The scanning was 3.4 nm in X and Y direction and performed in the constant current mode of 3 nA full scale. The image was further enhanced by 2 dimensional Fast Fourier Transform filter.

* J.C. Jansen, J. Schoonman, V. Pinet and H. van Bekkum, Zeolites 11, 1991, 306-308.

RESULTS AND DISCUSSION

As depicted in the lower half of Fig. 2a, an almost atomic resolution STM-image of the fresh surface of the silicalite-1 crystal could be made. The image clearly shows rows in three directions (indicated by arrows) together with bright spots. The more or less straight row, arrow 1, the zig-zag rows, arrows 2 and 3, and the local row angles of 120° and 65° , between 1-2 and 1-3, respectively, form a pattern which is in agreement with the wire model depicted in Fig. 2b. This model, based on the single crystal structure analysis², shows a part of the framework of silicalite-1 perpendicular to [001]. At the same time the ~ 2.5 Å diameter, and the ~ 4 Å repeated distance of the dark areas in [100] can be compared with the geometry of the bold section of the wire model. Together with the ring image shown in Fig. 2a and Fig. 3 (indicated by an asterisk) it appears that the STM image of Fig. 2a reflects the surface of a sheet composed of 6-rings of Si-tetrahedra. Though this sheet is flat in [100], a crenel-like configuration, with a repeating unit of three 6-rings, and differences in height of ~ 10 Å is present in [010]¹. It is thus possible that the image in Fig. 2a has not a constant pattern in [010] as the STM tip does not approach close enough to provide a clear picture. As shown schematically in Fig. 1c, high tetrahedral density (S) containing the 6-ring sheets alternates with low tetrahedral density (T) containing both tunnel directions. It is therefore most plausible that perfect cleavage for {001} in silicalite-1 results in flat three-6-ring-wide alternating crystal faces⁷. A slight curvature of the rows can be observed which is probably due to thermal drift of the piezoelectric tube of the STM apparatus.

Of other zeolites containing 6-ring sheets it is well known that the crystal morphology can be related to these sheets⁸.

The cube type, as well as the elongated prismatic crystal form of silicalite-1 do not show {001}. However, additives to the synthesis mixture, like boric acid, result in a crystal morphology showing {001}³. As a few percent of silicon is, under these conditions, isomorphously substituted by boron in the framework the crystals with {001} morphology belong to the ZSM-5 type. The bright spots in the rows of Fig. 2a above mentioned are supposed to reflect the positions of the topmost atoms since tunneling is expected to occur predominantly from dangling bonds⁴. Details of the {001} shown in the relief form in Fig. 3 further support the interpretation given to Fig. 2a. As shown in Fig. 3 the above mentioned rows can be recognized as well as

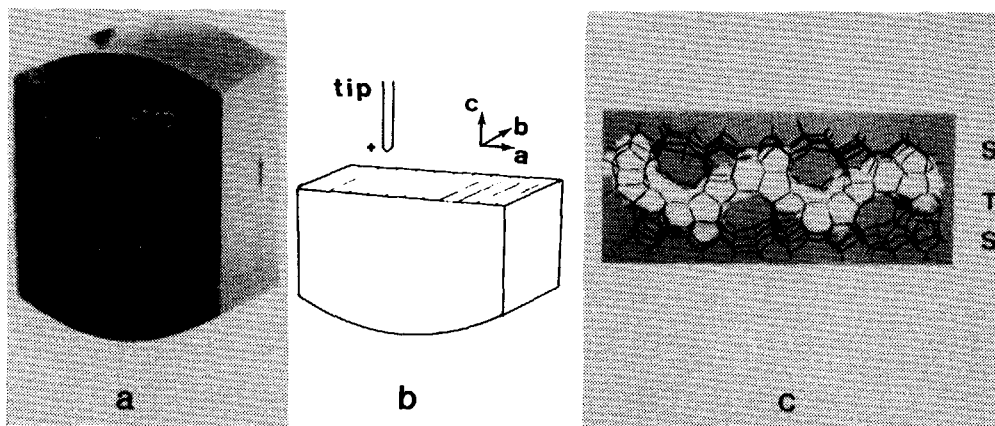


Figure 1 Sample orientation. a) SEM picture of a cube-like single crystal of silicalite-1. b) Schematic drawing of the crystal form after cleavage. The fresh crystal surface (hatched) and the tip orientation are given. c) Wire model of the framework topology corners occupied by Si; O omitted. Sheets (S) of SiO₄ tetrahedra are alternated by sinusoidal (filled) and straight (empty) tunnels (T) in [001].

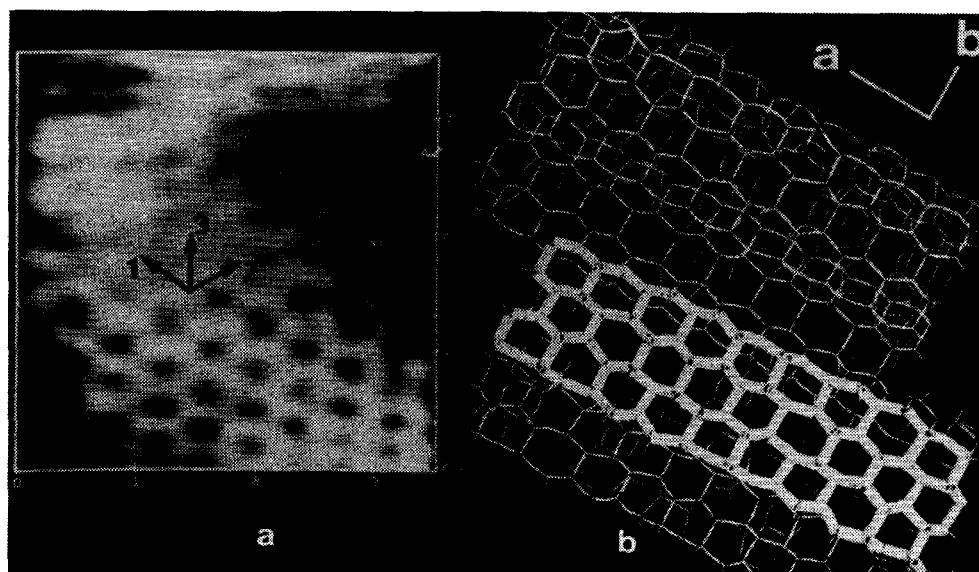


Figure 2 A typical fresh exposed surface of silicalite-1 perpendicular to [001]. a) A 3.4 nm wide STM electronic iso-density map of the exposed surface, arrows indicate directions of repeating tetrahedra connections. b) Wire model, based on single crystal structure analysis. The bold part of this model shows a three-6-ring-wide sheet of the framework perpendicular to [001].

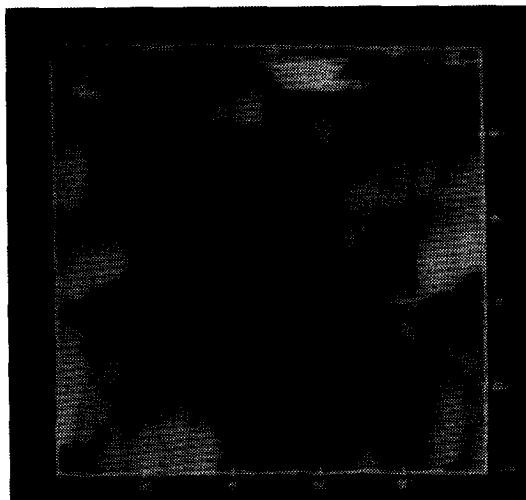


Figure 3 STM relief form with a 60° pitch angle of the same surface region as shown in Figure 2a. 6-Ring of Si-tetrahedra shown by asterisk.

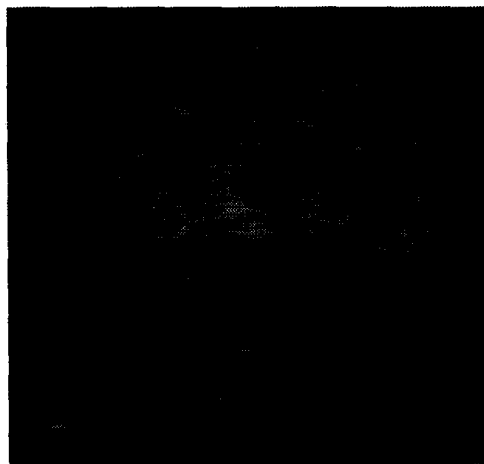


Figure 4 100 nm wide STM image of original, external crystal surface of silicalite-1. Bias 53.4 mV; 4.1 nA of setpoint current; constant current scanning mode of 100 nA full scale.

particular 6-rings (indicated by asterisk). The number of 6-rings in line indicate that at least two unit cells are displayed in Figs. 2a and 3.

Though cleavage along the characteristic (100) and (010) pentasil sheets⁹ might be possible the corrugation on nano-scale of those sheets will be much greater compared to the 6-ring sheet shown in Fig. 2a.

In order to obtain a STM image of a surface of zeolite framework on atomic scale it seems to be essential to prepare a clean and flat surface. As shown in Fig. 4 the external surface of the silicalite-1 single crystal contains ~ 50 Å silica particles which obstruct the opportunity to scan a flat region. As the silica particles must be chemically bonded to be subject to characterization with STM, it is believed that intrinsically in common zeolite synthesis procedures silicate particles are deposited or chemically bonded on the crystal surface upon cooling. The roughness of the external crystal surfaces is in agreement with recent nitrogen adsorption measurements yielding relatively high external surface areas¹⁰. Experiments to remove the silica(te) particles of the external surface with physical and chemical procedures were not successful. The pattern of the silica particles was, however, not always constant under scanning indicating a mechanical tip interaction with the substrate.

Scanning tunneling microscopy needs a sample with an electrical conduction pathway. As SiO_2 is an electrical insulator one should expect STM on silicalite-1 not to lead to an image. Two different surface pathways can be envisaged, however, for the observed conductivity of this zeolite.

Firstly, electrical conductivity via the fresh and subsequently the external crystal surface. The fresh exposed surface, after cleavage, can contain neutral, charged and radical species like SiOH , SiO^- and SiO^\cdot ¹¹, respectively, whereas the original external crystal surface has a hydrophilic nature due to terminal silanol groups¹². Together with water molecules attached via hydrogen bonding a surface conduction pathway will be likely.

Secondly, conductivity via the pore surface of the zeolite. Though a pure calcined silicalite-1, comprising $(\text{SiO}_2)_n$ shows a hydrophobic character, most silicalite-1 species contain structural defects in terms of non-intact Si-O-Si bonds resulting in internal silanol and Si-O^- groups and thus leading to local hydrophilic properties. Depending upon the zeolite crystal growth history, the calcination and steaming procedure and the types of guest molecules used, the percentage of non-intact siloxane bonds may vary. The framework defects then promote the accommodation of water molecules in

the pore system. In the case of e.g. 8% bond failure, a calcined silicalite-1 species synthesized by TPA⁺, can contain 12 water molecules per unit cell¹³. It is then possible to realize a continuously hydrogen bridged structure through each pore of the zeolite structure in which twelve water molecules and eight Si-OH groups are involved per unit cell. As silicalite-1 is a uniform highly porous system with each tetrahedral unit exposed to a pore channel, the zeolite pore volume might have conducting capacity. It is further suggested that electrolysis of water molecules under the tip in ambient conditions generates protons which can migrate, via e.g. the Grotthuss mechanism¹⁴ along one of the above-mentioned conduction pathways. However, we are inclined to believe that the external surface conductivity is of more importance than the usually lower conductivity exhibited by the pores.

REFERENCES

1. Flanigen, E.M. et al., Nature 271, 512-516 (1978).
2. Olson, D.H., Kokotailo, G.T., Lawton, S.L. & Meier, W.M., J. Phys. Chem. 85, 2238-2243 (1981).
3. Jansen, J.C., Engelen, C.W.R. & van Bekkum, H. in Zeolite synthesis, ACS Symp. Ser. 398 (eds. Occelli, M.L. & Robson, H.E.) 257-273 (1989).
4. Binnig, G., Rohrer, H., Gerber, C. & Weibel, E., Phys. Rev. Lett. 50, 120-123 (1983).
5. Bryant, A., Smith, D.P.E. & Quate, C.F., Appl. Phys. Lett. 48, 832-834 (1986).
6. Corma, A. in Stud. Surf. Sci. Cat. 49A (eds. Jacobs, P.A. & van Santen, R.A.) 49-67 (Elsevier, Amsterdam, 1989).
7. Hartman, P. in Crystal growth: an introduction (ed. Hartman, P.) 367-402 (NHC, Amsterdam, 1973).
8. Meier, W.M. in Natural zeolites (eds. Sand, L.B. & Mumpton, F.A.) 99-103 (Pergamon Press, Oxford, 1976).
9. Kokotailo, G.T. & Schlenker, J.L. in Advances in X-ray analysis, vol. 24 (eds. Smith, D.K. et al.) 49-61 (Plenum, 1981).
10. Voogd, P., Scholten, J.J.F. & van Bekkum, H., Colloids surfaces, 55, 163 (1991).
11. Steinike, U., et al. in Reactivity of Solids 4, 1-21 (1987).
12. Hill, S.G. & Seddon, D., Zeolites 5, 173-178 (1985).

13. Hunger, M. et al., J. Chem. Soc. Far. Trans. 1 83 (11), 3459-3468 (1987).
14. Poulson, F.W., in High conductivity solid ionic conductors (ed. Takahashi, T.) 166-200 (World Scientific, London, 1989).

CHAPTER 7

CRYSTAL GROWTH REGULATION AND MORPHOLOGY OF ZEOLITE SINGLE CRYSTALS OF THE MFI TYPE*

INTRODUCTION

Synthesis procedures to obtain large zeolite crystals are well developed (1,2). In particular much attention has been paid to the synthesis of ZSM-5 crystals (3-6). Elongated prismatic (Fig. 1a) and cubic-shaped orthorhombic (Fig. 1b) ZSM-5 crystals of sizes between 2-50 μm were reported in the first recipes (7) in the patent literature. Later on, systematic studies have led to excellent synthesis prescriptions for the growth of large crystals of the prismatic (8) as well as of the orthorhombic form (9). The synthesis parameters which are dominant in the crystallization of pure ZSM-5 single crystals, are still under study (10,11).

A full understanding of zeolite growth principles is difficult because hydrothermal crystallization of zeolites takes place in heterogeneous reaction media. Domains differing in composition and in viscosity exist in the same reaction mixture and can give rise to different products due to local differences in supersaturation, in ion transport velocity, etc. For this reason it is often difficult to correlate the crystal shape and type to the starting synthesis parameters because the crystal morphology, composition and size will reflect the local crystal growth conditions. So far only the crystal growth history of crystals with the elongated prismatic form is well described. The objective of our studies is to identify local crystal growth conditions which lead to different crystal forms of ZSM-5 by influencing nucleation and growth behaviour. In this chapter are reported two new morphologies (Fig. 1c, 1d) of single crystals of the MFI type.

* J.C. Jansen, C.W.R. Engelen and H. van Bekkum, in "Zeolite Synthesis", M.L. Occelli and H.E. Robson (Eds.), ACS Symposium Series 398, 1989, pp. 257-273.

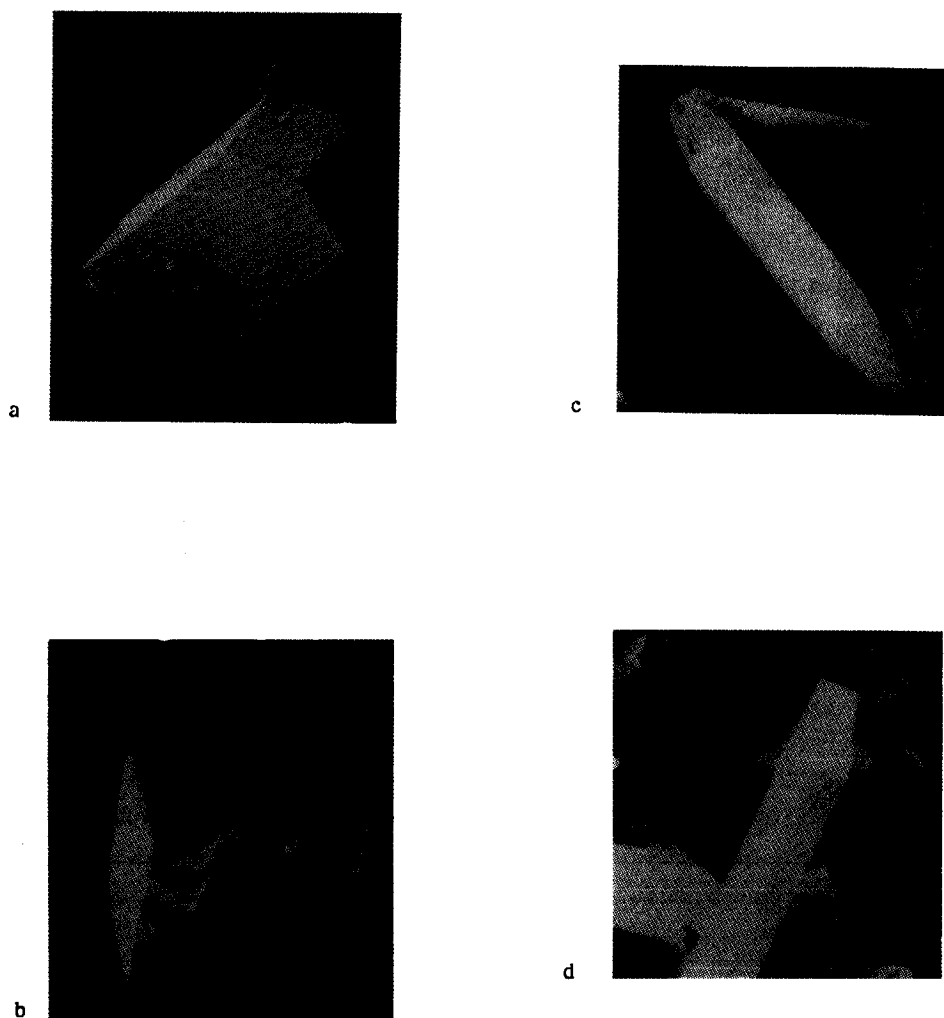


Figure 1. Four different single crystal forms of ZSM-5.
(a) Elongated prismatic; (b) cubic-shaped orthorhombic.
(c) Pyramidal shaped and (d) shelf-like shaped.

Growth history as well as relation to the morphologies reported earlier (Fig. 1a, b) will be discussed.

EXPERIMENTAL

Materials. Table I lists the starting chemicals together with the concentration of the main inorganic impurities.

Table I. Inorganic impurity contents (in ppm) of source chemicals applied.

	Al	Ti	Cr	Fe
SiO ₂ , Aerosil 200,* Degussa	440	90	10	110
SiO ₂ , FO Optipur, Merck*			< 10 ¹³	< 0.01
NaOH, Merck	< 5			< 5
aq. NaOH, Suprapur, Merck	< 0.05			< 0.05
TPA.Br, Janssen*	0.2	0.18	0.004	0.2

* Regularly used chemicals.

Synthesis. Two types of synthesis formulations were applied. The first one is the synthesis procedure as described by Lerner et al. (9) resulting in large cubic ZSM-5 crystals (Fig. 1b) with composition (molar ratio) in the clear starting solution as follows:

SiO ₂	Al ₂ O ₃	Na ₂ O	TPA ₂ O	H ₂ O	(I)
12	<0.5	20	20	2000	

The other formulation yielding elongated or shelf-shaped ZSM-5 crystals (Fig. 1a and d, respectively) has the following molar composition:

SiO ₂	B ₂ O ₃	Na ₂ O	TPA ₂ O	H ₂ O	(II)
12	0-2.5	4.5	4.5	2000	

Crystallizations were performed at 180 °C, in Teflon-lined autoclaves of 35 ml capacity.

Characterization. The TPA concentration in the reaction mixtures was determined by Induced Coupled Plasma Atomic Emission Spectroscopy (ICPAES) carbon analysis, which was preceded by n-hexane extraction in order to remove tripropylamine.

- Al, Cr, Fe, Ti were analyzed in the reactants and intermediate products with ICP and Atomic Absorption Spectroscopy (AAS).

- Al-ZSM-5 single crystals were characterized by Electron Probe Micro Analysis (EPMA) on a JEOL XRAY microanalyzer (Superprobe 733).
- B-ZSM-5 as well as Al-ZSM-5 single crystals were for particular characterization embedded in resin and subsequently polished.

RESULTS AND DISCUSSION

Growth of ZSM-5 crystals from gel spheres. The events that take place during the hydrothermal treatment of synthesis mixture (I), with regularly used chemicals, see Table I, but *without* added alumina, are shown in Figures 2a and 2b. Initially the silica is, considering the high OH/SiO₂ ratio of the synthesis mixture, mainly present as monomers (12). During the first day about two thirds of the TPA⁺ reacts with OH⁺ according to the Hoffmann degradation reaction yielding tripropylamine and propene. The decrease in pH accompanying this reaction induces polymerization of the silica monomers to silica sol particles. When Aerosil 200 silica is used, transparent silica bodies up to several mm in size are formed after the first day (see Figure 3a). According to SEM observations (see Figure 3b) these gel spheres are composed of close-packed particles of about 200-400 Å in diameter. The silica bodies therefore have been formed by aggregation of the earlier formed sol particles. As estimated from the decrease in SiO₂ concentration, some 5-10 percent of the original silica is converted into the gel bodies. During hydrothermal treatment of a very pure synthesis mixture composed of Optipur SiO₂, Ultrapure NaOH (both of Merck), TPA-Br, and water with a resistance higher than 10¹⁸ ohm, no gel bodies were formed at 180 °C, not even after two weeks. This implies (13) that the aggregation of the silica sol particles to gel bodies is facilitated by the presence of T atoms other than Si. It has been proposed (14) that trivalent cations - which are present in the Aerosil source (cf. Table I), adsorb onto the sol surface and cause the formation of interparticle bonds which is observed as gelation. Indeed chemical analysis by AAS showed the following non-Si elements to be present in the gel bodies: Cr - 63 ppm, Fe - 538 ppm, Al - 588 ppm, Ti - 513 ppm (concentrations relative to Si); the total ratio Si/T being 588 (T = Cr³⁺, Fe³⁺, Ti⁴⁺, and Al³⁺). Assuming that the T atoms are adsorbed onto the surfaces of the sol particles, this would mean for a 400 Å particle with density 2 g/cm³ that each T atom occupies 440 Å² outer surface, which is a

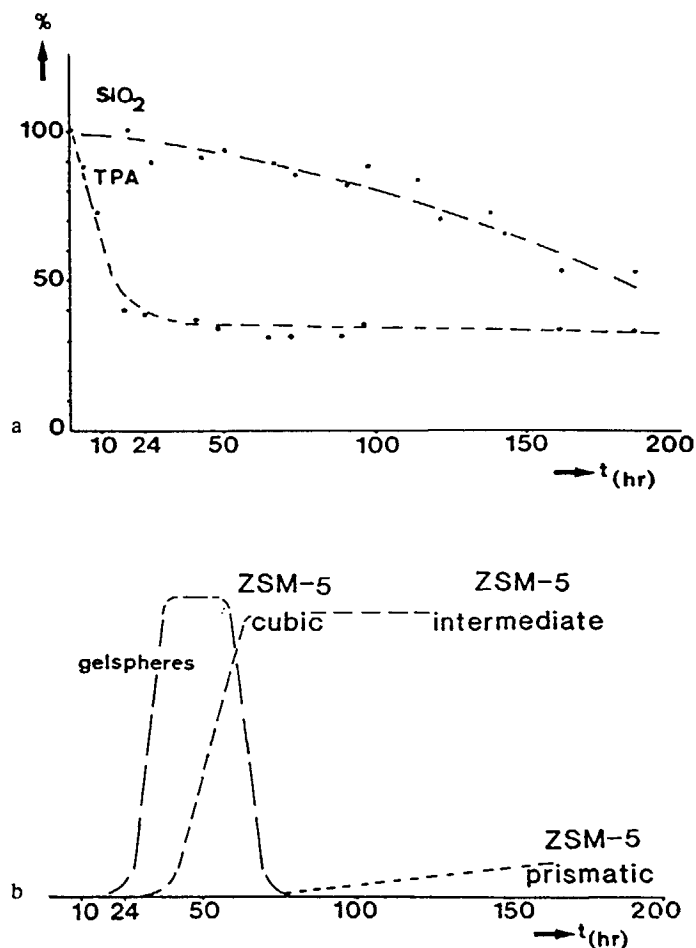


Fig. 2. Hydrothermal treatment of synthesis mixture I without added alumina at 180 °C.

- The solution concentrations of silica and tetrapropylammonium ion (TPA) as measured by ICP versus time;
- The formation of solid phases as observed by light-microscope.



Fig. 3. a. Light micrograph (50 x) of silica bodies formed during the first days of hydrothermal treatment of synthesis mixture I without added alumina at 180 °C;
b. SEM picture (30,000 x) of a fracture plane of a silica body.

realistic figure (15). The concentration of Al in the gel bodies is about equal to the corresponding concentration in the silica source (Aerosil) which is according to Table I the main supplier of inorganic impurities. By contrast, the concentrations of Cr, Fe and Ti are higher than the initial ones mentioned in Table I. The water content of the gel bodies as determined by AAS and TGA measurements ranged from 30 to 50%. Surprisingly, neither on the outer surface, in the diffuse reflection mode, nor in flakes from the interior of the gel spheres in the transmission mode, TPA could be detected by FTIR.

After about two days, see Figures 4 and 5a, crystallization is observed at the surface of the gel spheres. Pyramids of which the basal plane coincides with the sphere surface penetrate into the sphere body. Despite the supersaturation of the silica source no abundant nucleation is observed on the sphere surface. According to XRD and FTIR measurements the pyramids consist of ZSM-5 framework with TPA as guest molecules.

The fact that ZSM-5 framework formation is strongly promoted by TPA^+ and the observation that just a relatively low number of pyramids is present in the sphere surface are in harmony with DRIFT measurements on the sphere surface which do not indicate the presence of TPA. Thus it is concluded that the concentration of TPA^+ is low in the cation layer of the gel sphere surface.

The orientation of the pyramids, see Figure 4, is unique. Generally, the ac plane which is the largest crystal plane, is parallel to the surface of the gel sphere. As shown in Scheme I(a) the crystal a direction is initially relatively large with respect to the crystal c direction. Apparently crystallization proceeds favorably in the a direction under the actual crystal growth conditions. The continuous TPA strings and silica layers in the crystal a direction might be the stabilizing factor (16). The c direction, under more homogeneous crystal growth conditions the longest ZSM-5 crystal dimension, is initially relatively small as shown in Scheme I(a) and Figure 4. The absence of flat crystal faces in the c direction of the pyramid crystal and the smoothly curved ends of the crystal suggest a volume diffusion controlled crystallization mechanism. The mechanism is most likely imposed (17) by the extremely high supersaturation prevailing.

After some time a new ac plane is observed at the top of the pyramid as shown in Figure 5b (by arrows) and Scheme I(b). The new a/c crystal dimension ratio deviates strongly from the a/c ratio of the plane. It is therefore suggested that the local crystal growth conditions are changed.

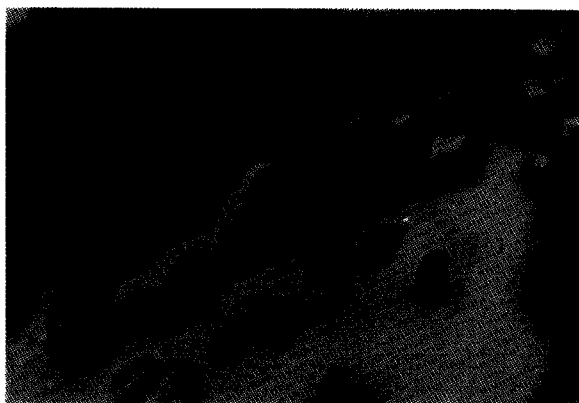


Fig. 4. Light micrograph (50 x) of the lower surface of a silica gel body present after 2 days hydrothermal treatment; ZSM-5 crystals with a pyramidal shape penetrate (upwards) into the body. The a-c plane is for all depicted crystals parallel to the outer surface of the silica body.

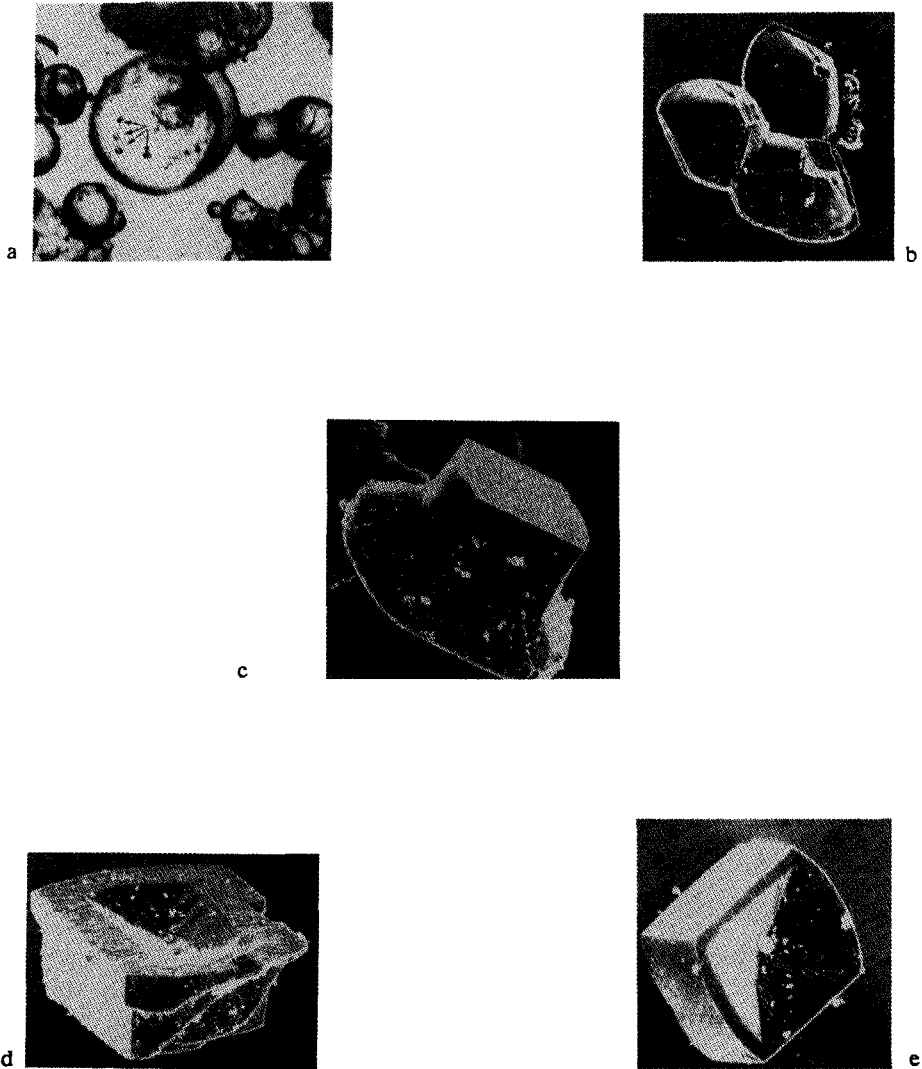
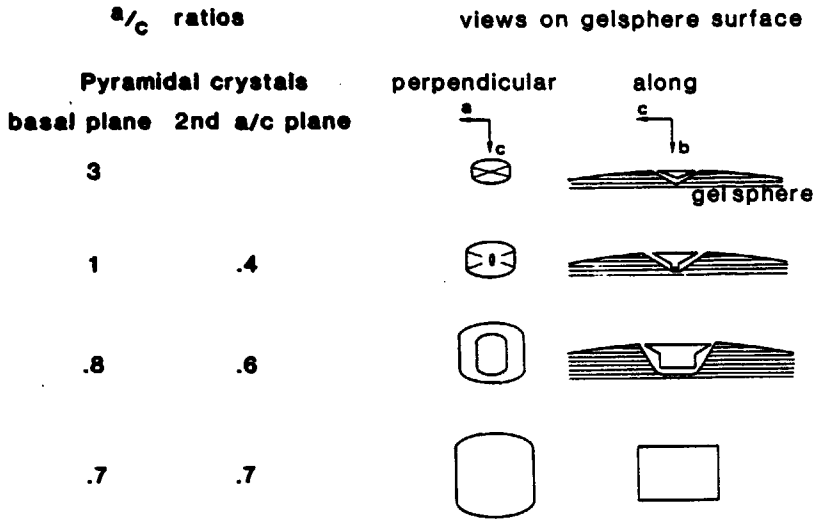


Fig. 5. Genesis of a cubic ZSM-5 crystal.

- a. Small ZSM-5 pyramids (light micrograph - 30 x) present on surface of gel bodies, see arrows;
- b. Development of a new a-c plane on the top of the pyramids (SEM picture - 150 x), see arrows;
- c and d. Growth of the pyramids mainly in the a and c direction (SEM - 600 x);
- e. Full grown hollow cubic ZSM-5 crystal (SEM - 240 x).



Scheme I. Average a/c ratios of developing pyramid crystals with transition into cubes and schematic drawing of growth process in the gel spheres.



Fig. 6. SEM picture (360 x) of a pyramidal ZSM-5 crystal with pyramid-shaped hole.

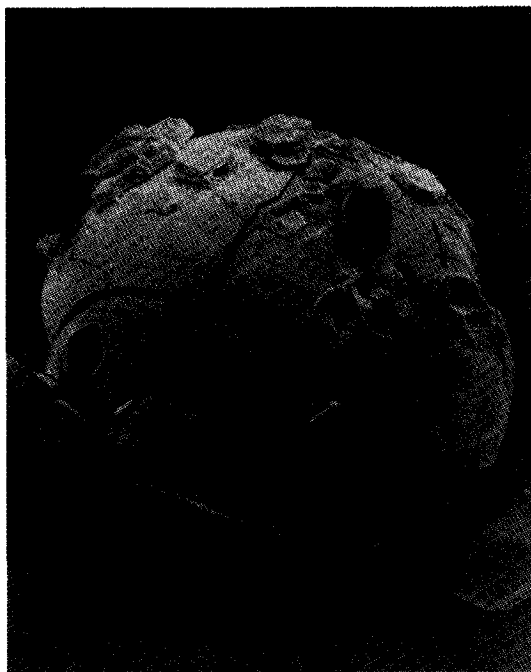


Fig. 7. SEM picture (100 x) of a gel sphere covered with ZSM-5 pyramids penetrating the gel surface (only the ac planes are visible) and holes (see arrows) where pyramids have been present.

The new a/c ratio resembles the a/c ratio of the final cube-shaped crystals. As shown in Figure 5c,d and Scheme 1c the pyramidal crystal is now growing in the a and c crystal direction, apparently in the liquid interface which also provides supply of TPA from the liquid phase. At last the well-known cubic-shaped ZSM-5 crystal is formed, Figure 5e and Scheme 1(d).

Two types of crystals can be grown, depending upon the history of the pyramid. As depicted in Figure 1c and Figure 6 massive and hollow pyramids are observed, respectively. The massive as well as the hollow pyramids both result in ZSM-5 cubic-shaped crystals, shown in Figure 5d for the hollow species. As separate pyramids are observed in the synthesis mixture, after 48 h, holes of such pyramids must be present in the surface of the gel spheres, as marked in Figure 7. It is postulated that a preorientation of silica with TPA in the wall of such holes restarts a pyramid crystallization. The pyramid growth process is then analogous to the solid pyramid growth. At last a ZSM-5 crystal with a hollow ac plane is observed, see Figure 5e. As shown in Figure 8 several intermediate crystal forms of ZSM-5 elongated and cubic-shaped crystals are possible. Extreme forms with respect to a/c crystal dimension ratio and crystal faces in c direction are the left and right crystals in this series. The well-known elongated prismatic crystal form of ZSM-5 is observed in relatively homogeneous crystal-growth conditions. As described above the cubic form is grown in heterogeneous crystal-growth conditions. Intermediate crystal forms might be developed when both crystal growth conditions have been present, the probable growth order being from cubic to elongated. As cubic crystals are developed in gel spheres an enrichment of crystal faces in the c direction is possible when the gel spheres are consumed and the crystal growth conditions become more homogeneous. It is supposed that a change from heterogeneous to homogeneous crystal growth conditions, thus crystal growth in a gel sphere to crystal growth in solution, influences the concentration and gradient of isomorphously substituted framework Si. The Al gradient occurring in elongated shaped ZSM-5 crystals is well documented (17). By contrast the Al distribution *among* and within the cube-shaped crystals, shows a more homogeneous pattern as depicted in Figure 9. Figure 9a presents the Al/uc of seven crystals, with different sizes, of the same batch prepared according to Lermer et al. (9). According to linear crystal growth theory small crystals are formed later than large crystals. A homogeneous distribution among the crystals was observed. Figure 9b presents the EMPA

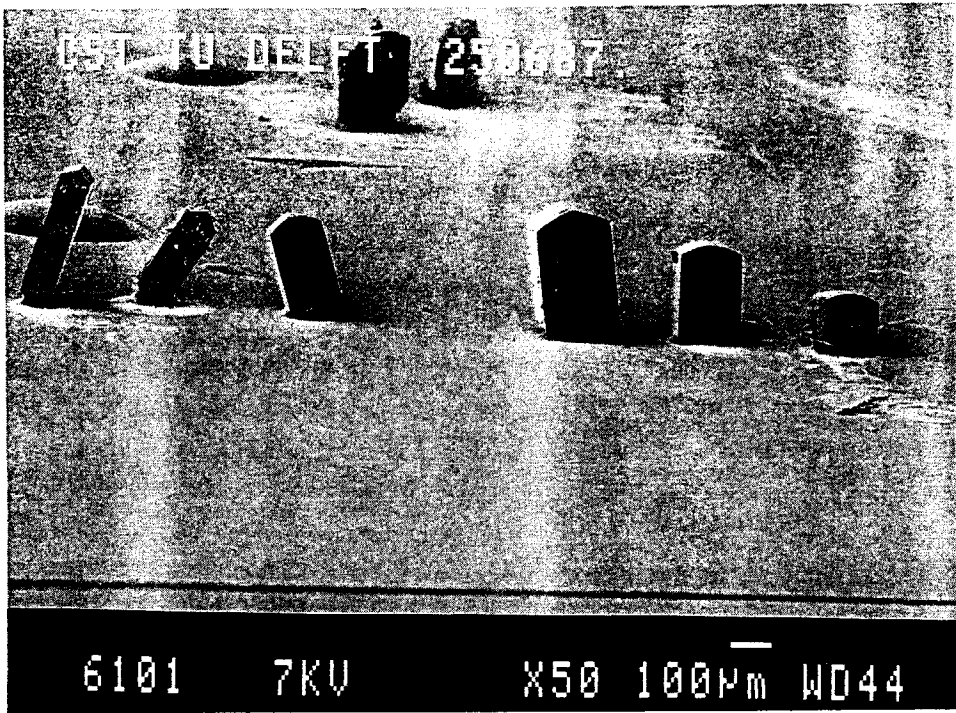


Fig. 8. Scala of shapes of ZSM-5 crystals.

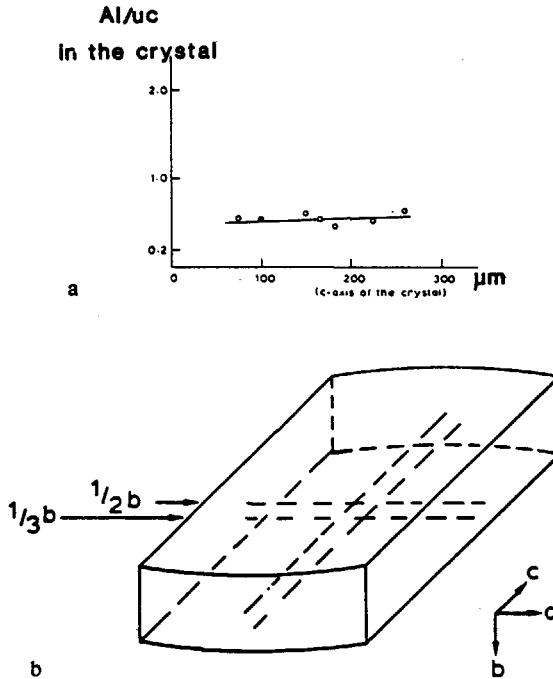


Fig. 9. Al distribution among and within cubic-shaped ZSM-crystals.

- a. Al/u.c. of cubic ZSM-5 crystals grown from the same synthesis mixture as function of the c-dimension;
- b. EMPA Al-scanning pattern at half and one third height within a cubic ZSM-5 crystal. The ac planes were exposed by polishing the crystal in the b direction.

scanning pattern on two planes of the largest crystal. No heterogeneity was found, regarding the Al distribution. The homogeneous pattern might be due to crystal-growth in a gel phase with a homogeneous Al distribution. To establish T-atom distribution in the cube-shaped crystals it is imperative that no homogeneous crystal growth conditions have been started in the last period of the hydrothermal crystallization. As the cube crystallization is finished when the gel spheres are consumed the actual [Si] and Si/Al ratio of the remaining synthesis mixture will then be opportune. Consequently a further growth of the original cube crystal will change the crystal shape and the Al distribution. The crystallization time of the cube crystals in this study was 4 days and no Al gradient was found. On the other hand cubic crystals which were grown 10 days indeed were reported to exhibit an Al gradient (18).

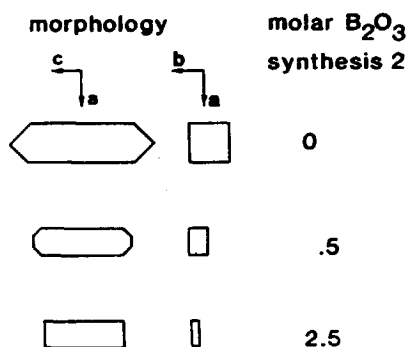
The main differences between the elongated and cube-shaped crystal forms are in the different faceting in the crystal c direction and the relatively short crystal c dimensions of the cubic crystal. In terms of crystal growth it is plausible that the elongated crystal growth is governed by the framework topology. The growth is relatively slow in directions perpendicular to framework layers with high tetrahedral density, the pentasil layers in the ac and bc plane being examples (16). A 001 plane is generally not observed. The crystal c direction flat facets are $h0l$ planes, though hkl planes have also been observed. It is well known that increasing supersaturations of crystal building molecules can change the crystal form. In the gel sphere crystallization it appears that the crystal form is a function of the above mentioned mechanism which is, however, partly overruled by the extremely high silica supersaturation resulting in smooth curved ends of the crystal in the relative short c direction.

Effect of borate additive on ZSM-5 morphology. If crystal morphology is studied in relation to isomorphous substitution of Si by T atoms in the framework then it looks like homogeneous crystal growth conditions should be present. By adding boric acid to the reaction mixture (II) the elongated crystal morphology of Figure 1a was found to be changed as a function of the concentration of the borate source. Scheme II presents schematically the crystal morphology changes observed. At higher boron concentrations the ac plane develops strongly with respect to the bc plane. At the higher boron concentration applied shelf-type crystals (Fig. 1d) are formed. It is

suggested that all crystal faces are involved in a crystal growth inhibition by the presence of $B(OH)_3/B(OH)_4^+$, as the build-in of B as a T atom - trigonal or tetrahedral - will constitute an irregularity at the growing crystal surface which will hamper.

It is well described that crystal growth inhibition is caused by special additives. The pentasil layers of the ac plane and bc plane are more or less identical. The ac plane pentasil layers, however, are generated via a crystallographic mirror plane operation, the bc plane pentasil layers not. As the crystal growth rate of both layers is decreased by the BO_3/BO_4 presence the above mentioned difference in the stacking of the pentasil layers will be reflected in the a/b crystal dimension ratio (16). Presently a detailed study is being carried out regarding this interesting effect on morphology exerted by borate (19).

In conclusion two new single crystal forms of zeolites of the MFI type have been observed which can be interrelated on the basis of crystal growth consideration with two existing morphologies.



Scheme II. Morphology of B-ZSM-5 crystals as a function of the boron concentration in the synthesis formulation.

REFERENCES

1. Ciric, J. Science 1967, 689.
2. Charnell, J. F. J. of Cryst. Growth 1971, 8, 291-294.
3. Erdem A.; Sand, L. B. Proc. 5th IZC; Rees, L. V., Ed.; Heyden, 1980, 64-72.
4. Gabelica, Z.; Derouane, E. G. A.C.S. Symposium Series 1987, 248, 219-251.
5. Mostowicz, R.; Berak, J. M. Stud. Surf. Sci. Cat. ; Drzaj, B.; Hocevar S.; Pejovnik, S., Eds.; Elsevier: Amsterdam, 1985, Vol. 24, pp 65-72.
6. Kuehl, G. H. Eur. Pat. Appl. 0,0093519 (1983).
7. Argauer R. J.; Landolt, G. R. U.S. Patent 3,702,886 (1972).
8. Hayhurst D. T.; Lee, J. C. Proc. 7th IZC; Murakami, Y.; Iijima A.; Ward, J. W., Eds.; Elsevier: Tokyo, 1986, pp 113-120; Hayhurst, D. T.; Aiello, R.; Nagy, J. B.; Crea, S.; Giordano, G.; Nastro, A.; Lee, J.C. A.C.S. Symp. Series 1988, 368, 277-291.
9. Lermer, H.; Draeger, M.; Steffen, J.; Unger, H. K. Zeolites 1985, 5, 131-134.
10. Bodart, P.; Nagy, J. B.; Gabelica, Z.; Derouane, E. G. J. Chem. Phys. 1986, 83, 777-790 and literature cited therein.
11. Lowe, B. M. Stud. Surf. Sci. Cat.; Goubet, P. G.; Mortier, W. M.; Vansant, E. F.; Schulz-Ekloff, G., Eds.; Elsevier: Amsterdam, 1988, 37, 1-12.
12. Dentglasser, L. S.; Lachowski, E. E. J. Chem. Soc. Dalton 1980, 393-398.
13. O'Melia, C. R.; Stumm, W. J. Colloid and Interface Sci. 1967, 23, 437-477. Allen, L. H.; Matijevic, E. J. Colloid and Interface Sci. 1970, 35, 67-76.
14. Lamer, V. K.; Healy, T. W. Rev. Pure Appl. Chem. 1963, 13, 112. Hahn, H. H.; Stumm, W. Adv. Chem. Ser. 1968, 79, 91 (American Chemical Society).
15. Iler, R.K. J. Colloid Interface Sci. 1976, 55, 25.
16. A more theoretical study has been undertaken and will be published.
17. Ballmoos R. von; Meier, W. M. Nature 1981, 289, 782-783.
18. Chao, K.-J.; Chern, J.-Y. Zeolites 1988, 8, 82-85.
19. Jansen, J. C.; Ruiter, R. de; Bekkum, H. van, Stud. Surf. Sci. Catal. 1989, 49A, 679.

CHAPTER 8

CONTROLLED GROWTH OF THIN FILMS OF MOLECULAR SIEVES ON VARIOUS SUPPORTS*

INTRODUCTION

The preparation of layers, films and coatings of zeolites has been reported recently.^[1-3] The polycrystalline material with a thickness between 3 and 30 μm was precipitated on metallic-, monolithic ceramic-, teflon-, and silica substrates. The main objectives to prepare these composite products are the potential application as catalyst, membrane and sensor.

For certain catalyst uses the axial orientation of zeolite crystals on a support is of interest in order to expose the zeolite pores as good as possible. In the case of membrane application a lateral orientation of the crystals on a macroporous support is required.

In this work the parameters to achieve either type of orientation of the zeolite crystals have been studied for MFI-type zeolite.

EXPERIMENTAL

Crystal supports and set-ups

Metal supports were horizontally positioned on the bottom of a 3 ml teflon lined autoclave with a diameter of 20 mm which was filled with 2 ml synthesis mixture. The metals chosen were: aluminum foil, aluminum-, nickel-, copper- and titanium platelets of 10x10x2 mm. All metal supports were cleaned with ethyl alcohol before use.

The following supports were vertically positioned against the wall of a 35 ml teflon lined autoclave:

* J.C. Jansen, W. Nugroho and H. van Bekkum, accepted 9th IZC, Montreal, 1992.

- Stainless steel gauze (50x50 mm) with a wire diam. of 0.08 mm and a spacing of 0.1 mm.
- Modules of cordierite and mullite, 10x10x40 mm.
- Mica.
- Quartz platelets, diameter 15 mm.

Silicon [100] wafers were used in particular model studies. They were obtained from a silicon single crystal, grown by a crystal pulling method. The wafers were 0.7 mm thick and 98 mm in diameter. Prior to cutting to provide platelets of 10x10 mm, the wafers were chemically and mechanically treated and polished on one side down to atomic scale.

Contaminants will be present on the surface after these operations, so in order to provide a clean hydrophilic silicon surface, the platelet has to be cleaned. Firstly, gross organic contaminants were removed by treating of the platelets in boiling xylene. Solution RCA-1, see Table 1, is thereafter used to remove residual organic contaminants. In this step, the platelets are already placed vertically in teflon holders, see Figure 1. Inorganic contaminants were removed with RCA-2 solution.^[4,5] As final step, the platelets were exposed to sonification in water. These cleaning operations are given in Table 1.

Table 1: Cleaning operations data of the silicon platelets.

Cleaning sequence	Composition	Conditions
Xylene	Xylene	Boiling point 30 minutes
RCA-1	H ₂ O: H ₂ O ₂ : NH ₄ OH 5: 1: 1*	80°C ± 5°C 15 minutes water rinse
RCA-2	H ₂ O: H ₂ O ₂ : HCl 6: 1: 1*	80°C ± 5°C 15 minutes water rinse
Ultra sonic	H ₂ O	Room temperature 10 minutes water rinse
<div style="display: flex; justify-content: space-between;"> <div> H₂O : distilled deionized water. NH₄OH : 25%, JT Baker. </div> <div> H₂O₂ : 30%, stabilized, Merck. HCl : 36 - 38%, JT Baker. </div> </div>		

*parts by volume

Without drying (to prevent any contamination by the atmosphere), the holder with the platelet was placed in a teflon-lined autoclave containing 32 ml synthesis mixture in such a way that the platelet was positioned in the upper part of the liquid.

Synthesis

The syntheses are summarized in Table 2 and 3.

Table 2: Synthesis conditions using various supports.

Support	Synthesis mixture molar ratio			Temp. (K)	Time (h)
	SiO ₂	TPA ₂ O	H ₂ O		
Al-foil	2	1	5600	453	6-8
Al/Ti/Ni/Cu platelets	2	1	13800	448	10
Stainless steel gauze	2	1	1400	443	8
Cordierite	2	1	1400	443	8
Quartz	2	1	2000	453	5

Si : Aerosil 200, Degussa. TPA : TPAOH, 40%, CFZ.

Table 3: Synthesis conditions using Si-platelet support, at 436 K

Code	Synthesis mixture molar ratio					Time (h)
	SiO ₂	Al ₂ O ₃	TPA ₂ O	Na ₂ O	H ₂ O	
¼A	10.0	-	1.4	-	16800	20.0*
½A	21.2	-	3.0	-	16800	14.0*
A	39.4	-	5.8	-	16800	12.0*
4A	139.4	-	19.7	-	16800	3.5*
6A	209.1	-	27.3	-	16800	3.5* [‡]
TNA-1	39.4	-	5.5	5.8 ⁺	16800	20.0**
TNA-2	39.4	-	5.5	11.8 ⁺	16800	22.5*
NA	39.4	-	-	5.5 ⁺⁺	16800	20.0**
NAAl	39.4	0.4	-	5.5 ⁺⁺	16800	20.0**

Si : TEOS, 98%, Janssen Chimica. TPA : TPAOH, 40%, CFZ.
Na : NaCl⁺, Merck or NaOH⁺⁺, Lameris Pleuger. Al : Al(NO₃)₃·9H₂O, Merck.

* for complete crystallization

◆ etching of silicon wafer

**** no crystallization observed**

Characterization

XRD, powder X-ray diffraction data were collected on a Philips PW 1840 diffractometer and a Siemens D500 diffractometer, using the Cu-K α line in both cases.

FTIR, infrared spectra were recorded on a Bruker IFS 66 spectrometer in transmission mode in case of the silicon platelets.

SEM, photographs were taken of samples covered with a thin layer of gold by sputtering. The microscope used was a JEOL JSM-35 scanning electron microscope.

RESULTS AND DISCUSSION

Metal supported films

Figure 2 shows an extensive coverage of about 1 μm thick crystals of the MFI-type with mainly the crystal c-direction perpendicular to the plane of the Al-support. The SEM photograph clearly shows a minimum intergrowth and thus as many crystal faces or zeolite pores as possible are exposed this way. Other metal supports such as Ni-, Ti-, and Cu-platelets gave similar results. The crystallization of MFI-type zeolite on a stainless steel gauze, on a cordierite module and a quartz support resulted in an abundant but randomly oriented crystal layer with elongated prismatic forms axially grown on the support surface. At higher concentration the crystals seem to adopt a more lateral orientation as observed on an Al-foil support. The supports used are supposed to be oxidized and form hydroxyl groups protruding into the synthesis mixture under the prevailing conditions. The zeolite growth on the support surface is then expected to start via a condensation mechanism thus resulting in firm chemical bonding of the crystals on the surface even after calcination and also after performing a reaction in a liquid phase using the composite as the catalyst.

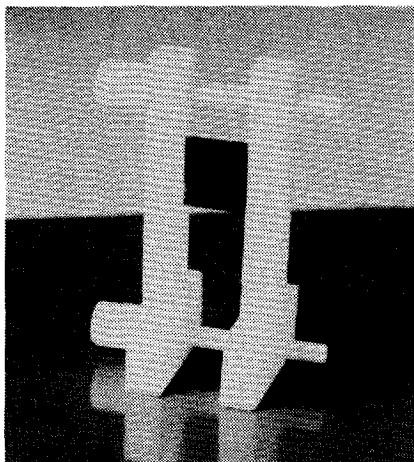


Figure 1. Teflon holder with silicon wafer. The holder was used in 35 ml stainless steel teflon lined autoclaves to adjust the silicon platelet vertically and close under the synthesis mixture level.

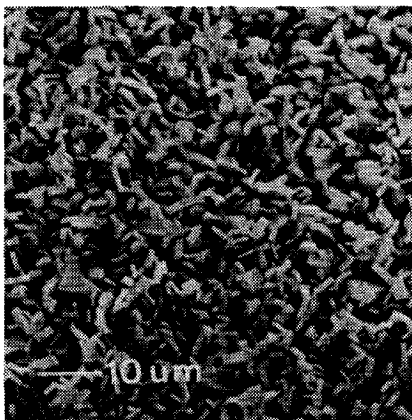


Figure 2. Axially oriented zeolite crystals of the MFI-type on a metal support, mean thickness of the crystals 1 μm .

Silicon supported films

The effect of the concentration of the components in the synthesis mixture on the final growth of a silicon supported zeolite film was studied. It was found that the crystallization time, using the largest observed crystals as a yardstick varies inversely with the concentration, see Figure 3, whereas the final crystal size is smaller at higher concentration, see Figure 4. In the final products the support is for more than 98% covered with a continuous monocrystal film with crystals having a lateral orientation as is shown in Figures 5c and 6b,c for experiments A and 4A, respectively.

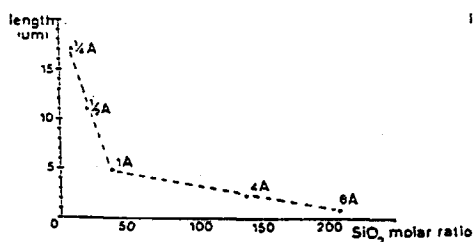


Figure 3. The maximum crystal dimension in c-direction versus the SiO₂ molar ratio of synthesis mixtures 1/4A, 1/2A, A, 4A, 6A.

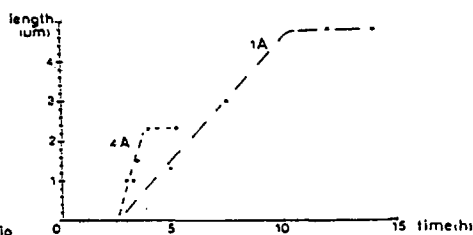


Figure 4. The crystal dimension in c-direction as a function of synthesis time, using synthesis mixtures A and 4A. In both cases a continuous monocrystal film was achieved.



Figure 5. Evolution of the crystal growth of MFI-type with synthesis mixture A, a) first observed crystals after two hours in gel phase, b) crystals apparently associated via surface tension forces after 3 1/4 hours, oriented with the ac plane parallel to the support surface, c) A 20° view angle on final crystallization of a monocrystal film of 500 nm in thickness, indicating a slight deviation of the crystals with respect to each other and the support surface.

The narrow crystal size distribution of both products indicates an equal growth time for each crystal although Figures 5a and 6a show that the homogeneous nucleation is not an explosive but rather a gradual progressive process. The unexpected homogeneous crystal size distribution which is observed might be due to a drastic change in nutrient concentration during crystallization. Initially small globular shaped fast growing crystals are formed, see Figure 6a, which are embedded in a gel layer of about 0.5 μm thickness which covers the silicon platelets. Accordingly initial growth occurs under conditions of extremely high supersaturations. The smooth rounded and/or cubic form of the initial crystallization, see Figures 5a and 6a, indicates a kinetic roughening of the crystals growing in the gel layer. An analogous observation has been

reported earlier for crystallization of zeolites in gel spheres and it was concluded that nucleation occurs at the gel/liquid interface.^[6] It is assumed that also in the present experiments nucleation occurs at the gel/liquid interface as shown by the initially observed 'loose' crystallites in the top layer of the gel.

The crystallization then proceeds into the gel (layer thickness about 0.5 μm) which is consistent with the typical crystal form obtained in very high supersaturations.^[6] As the gel density (1.6) is lower than the crystal density (2.0), a liquid phase is gradually formed between the growing crystal and the consumed gel. Nuclei started with different orientation on the gel/liquid interface will result in crystals with different orientations. The crystals developed in the direction of the Si-platelet and surrounded by liquid, are then probably affected in their orientation by the Si-platelet via surface tension- and v.d. Waals forces. The crystals are, based on the above, all more or less oriented parallel to the Si-platelet. Hereafter chemical bondings are formed apparently via condensation of hydroxyl groups of the crystals and surface hydroxyls of the Si-platelet which is assumed to possess an oxidized surface. Even after calcination the crystals are still firmly bonded to the platelets. The coverage and orientation of the crystals on the silicon platelets is shown in Figures 5c and 6c. The orientation of the crystals is almost completely parallel. A powder X-ray diffraction scan shows diffraction lines representing 0k0 planes only, see Figure 7, indicating a strong preference of the crystal orientation. Figure 7b gives the intensities of the 0100 plane at different ω -offset angles. It can be concluded that after 2° ω -offset, the intensity of the 0100 plane has been disappeared. The crystal monolayer is thus within 4° deviation flat and the absence of other diffraction lines shows that of the crystallites are mainly in a parallel orientation.

In the case of more diluted synthesis mixtures such as $\frac{1}{2}\text{A}$ and $\frac{1}{4}\text{A}$ almost no gel layer is formed and the crystals show the well known elongated prismatic shape. The crystals are larger but less abundantly present. Here the nucleation occurred, according to the SEM-photograph in Figure 8,

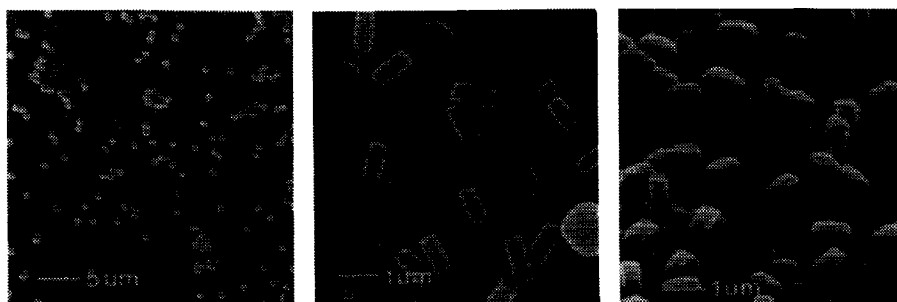


Figure 6. Evolution of the crystal growth of MFI-type with synthesis mixture 4A, a) smallest observed crystals after two hours, b) A 90° view angle on final crystallization showing a continuous monocrystal film and more than 10% additional film, c) A 20° view angle on final crystallization indicating the rather parallel orientation of the monocrystal film of 400 nm in thickness.

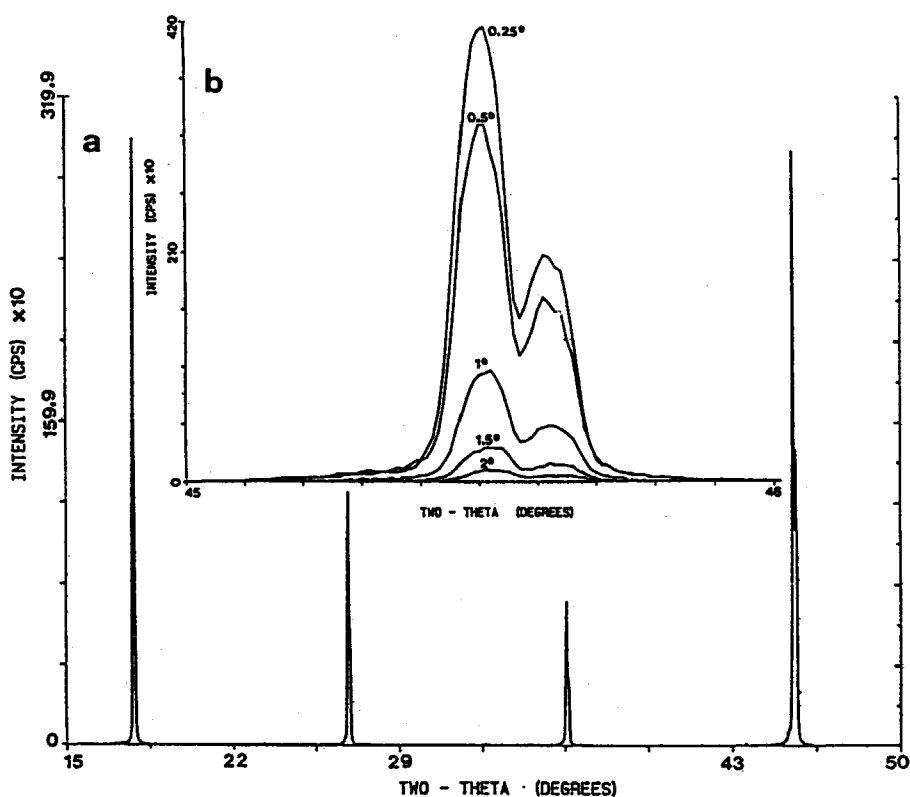


Figure 7. XRD powder pattern of zeolite MFI crystals in lateral orientation, see Figure 6c, a) Only 0k0 diffraction lines with relative intensities of MFI-lattice are observed here, b) 0100 intensities at different ω -offset angles clearly show the unique orientation of the crystals within 4°.

on the surface of the Si-platelet and axial growth with a random orientation of the crystals is clearly obtained. The addition of sodium ions to the synthesis mixture, code NA, resulted in a heterogeneous coverage of the Si-platelet with gel. Crystals were grown partly from the gel/liquid interface and partly from the Si-platelet surface. For this reason a mixture of crystal orientations was observed.



Figure 8. Surface nucleation on the Si-support using 1/4A synthesis mixture, resulted in axially grown crystals.

Experiments without template TPA^+ but with NaOH and without and with an aluminum source, mixtures NA and NAAL respectively, gave so far no results under the prevailing synthesis conditions.

CONCLUSION

It can be concluded that crystals of zeolite MFI can be grown on a proper support which appear to be firmly bonded even after calcination. The orientation is mainly axial when low concentrations and temperatures are used with the support on the bottom of the autoclave. The crystal orientation is parallel to the support surface when, *i*) a relatively low temperature, *ii*) support vertical in the upper part of the synthesis mixture and, *iii*) refined synthesis conditions, thus without Na^+ , are used.

REFERENCES

1. Sano,T., Kawamura,M., Mizukami,F., Takaya,H., Mouri,T., Inaoka,W., Toida,Y., Watanabe,M., Toyoda,K., Zeolites 11 (1991) 842.
2. Davis,S.P., Borgstedt,E.V.R. and Suib,S.L., Chem. Mater. 2 (1990) 712.
3. Lachman,I.M., Patil,M.D., US Patent 4,800,187 (1989).
4. Runyan W.R. and Bean K.E., Semiconductor Integrated Circuit Processing Technology, Addison-Wesley Publishing Company, Inc., (1980) 26-31.
5. Kern,W., Puotinen,D.A., RCA Review 31 (1970) 187-206.
6. Jansen,J.C., Engelen,C.W.R. and van Bakkum,H., ACS Symp. Ser. 398 (1989) 257.

SUMMARY

Although the main application of synthetic zeolites lies in the field of ion-exchange numerous studies have been carried out on the preparation, modification and application of zeolite as a catalyst.

The refinement of a zeolite catalyst for a specific reaction requires probably much effort compared to a zeolite ion-exchanger.

In this thesis a contribution is given to the preparation, modification and guest-host interactions of the MFI-type zeolite.

After an introduction in which the present-day consumption of the molecular sieves and the history of the MFI-type sieve are presented, Chapter 1, some general considerations are given in Chapter 2, which molecular sieve type is most tailored for a certain catalyst application, and how it can be selected from the various types, modifications and framework flexibilities. It is concluded from scanning tunnelling microscopy (STM) and scanning electron microscopy (SEM) that the unrequested external surface of the MFI-type crystals can be about 20 times larger than the calculated surface based on crystal dimensions. Modification of the crystal form might result into much smaller external/internal surface ratios. For this reason general crystal growth principles regulating the crystal forms and morphologies of zeolites were applied. In particular the forms of the MFI-type crystals could be understood and influenced.

In the last part of Chapter 2, it is shown that (de)hydration and guest molecule accomodation, can induce changes in phase transformations and framework flexibility. In this connection various interactions between p-xylene and the internal surface of the MFI-framework could be understood as well as some migration phenomena.

Chapter 3, reviews the synthesis and direct modifications of zeolites and silica analogues as developed in our laboratory and as given in literature. The present work led amongst others to the synthesis of large single crystals of tetrapropylammonium (TPA)- ZSM-5 and p-xylene-ZSM-5. The structure analysis of TPA-ZSM-5 is reported in Chapter 4 , and that of p-xylene-ZSM-5

summarized in chapter 2.

A conclusion drawn from the TPA-ZSM-5 structure is the rather folded form in which the TPA⁻ ion is forced in the voids of the zeolite.

The large single crystals were also used in the first experiments with scanning tunnelling microscopy (STM). For this work the crystals were cleaved in order to observe the internal/ pore surface. The results are given in Chapter 5. The conditions for STM imaging of the rather poorly conducting silica material are supposed to be achieved by a proton hopping mechanism mainly via the external crystal surface. The ion conduction via the internal surface is not excluded as the material is slightly hydrophilic.

In a study, Chapter 6, on the crystal growth history of MFI-type zeolite the crystal formation was monitored. Two new crystal forms of zeolites of the MFI-type were reported. Pyramidal single crystals were found to grow at the surface of gel spheres, the formation of which is thought to be induced by the decomposition of tetrapropylammonium ions during the zeolite synthesis and by the presence of trivalent metal ions. The pyramidal crystals are shown to be precursors of the cube-shaped ZSM-5 single crystals described earlier. The homogeneous Al³⁺ distribution in the cube-formed single crystals is probably due to the homogeneous Al³⁺ distribution in a synthesis intermediate, being the dense gel sphere. Another morphology known for MFI-type single crystals, the elongated prismatic habit, is shown to transform into a lath-shape morphology when increasing amounts of boric acid were added to the synthesis mixture. A sometimes occurring enrichment in morphology was correlated to different equilibria between T- atoms involved in building-in and the different growing crystal faces.

Single crystals of [B]-, [Al]-, [Ga]- and [Be]-ZSM-5 have been synthesised from aqueous silicate gels using TPA⁺ as a template. Long shaped- and cube-shaped crystals were observed. The cubes were invariably accompanied by side products (depending upon the substituting T-atom used; quartz, beryllosilicate single crystals were of analcime and natrolite).

A series of experiments on B-ZSM-5 showed a linear relationship between the unit cell volume reduction up to 4B/uc in the crystal. A maximum of about 5 B/uc in the ZSM-5 framework is found, Chapter 7.

In a study on the growth of layers, films and coatings on various supports a continuous film of monocrystals of ZSM-5 zeolite of 200 nm thickness was achieved on a silicon support indicating the possibilities to obtain even coatings of a few hundred angstrom, Chapter 8.

SAMENVATTING

Zeolieten, microporeuze alumino-silicaten, vormen een subgroep binnen de moleculaire zeven.

Hoewel de belangrijkste toepassing van zeolieten -qua volume- ligt op het gebied van de ionwisseling zijn er toch vele studies verricht op het gebied van synthese en modificatie van zeolieten en het gebruik als katalysator. Voor de verfijning van een zeoliet katalysator voor een specifieke reactie kan thans beschikt worden over een groot aantal modificatie technieken.

Zeoliet katalysatoren vinden op ruime schaal toepassing in de petro chemische industrie. Ook voor het gebruik in de fijn chemische industrie is momenteel veel aandacht. In toenemende mate gaat zeoliet katalyse bijdragen aan z.g. schone technologie. In dit proefschrift is een bijdrage geleverd aan de synthese, modificatie en gast-gastheer interacties van de MFI-type moleculaire zeef, ook wel ZSM-5 zeoliet genoemd.

Na een inleiding waarin het huidige gebruik van moleculaire zeven en de historische ontwikkeling van de MFI-type zeoliet is gegeven, hoofdstuk 1, worden algemene overwegingen, hoofdstuk 2, met betrekking tot de keuze van de beste zeoliet voor een bepaalde katalytische reactie, gegeven op grond van de verschillende typen, de modificatie mogelijkheden en de flexibiliteit van het rooster. In dit hoofdstuk wordt met z.g. scanning tunneling microscopy (STM) en scanning electron microscopy (SEM) vastgesteld dat het buitenoppervlak van een hoog silica MFI-type monster ongeveer twintig maal groter is dan op grond van de kristalafmetingen verwacht mag worden. Wijzigingen in de kristal-vorm en -morfologie kunnen tot gunstiger verhoudingen leiden. Om deze reden werden algemene kristal groei principes die de groei en vorm van kristallen kunnen beïnvloeden toegepast. In het bijzonder konden de vormen en morfologie van de MFI-type kristallen gecontroleerd worden. In het laatste gedeelte van hoofdstuk 2 wordt de invloed van water op fase overgangen en de flexibiliteit van het rooster besproken evenals de invloed van organische gast moleculen hierop.

Hoofdstuk 3, geeft een overzicht van de synthese en modificaties van zeolieten

en analoge silicamaterialen zoals die ontwikkeld zijn op dit laboratorium en voorkomen in de literatuur. Dit werk heeft o.a. geleid tot de synthese van grote kubisch gevormde eenkristallen van tetrapropylammonium (TPA)-MFI. Deze eenkristallen zijn na activering (verwijdering van TPA) maximaal beladen met p-xyleen (8 moleculen per eenheidscel). De structuur analyse van TPA-MFI is gerapporteerd in hoofdstuk 4 en de positie van p-xyleen in MFI in hoofdstuk 2. Een van de conclusies die getrokken is uit de TPA-MFI structuur opheldering is de ingedrukte vorm van de propylgroepen van TPA in de ZSM-5 structuur t.a.v b.v. de propyl groepen in de TPABr structuur. Kennelijk wordt dit veroorzaakt door het silikaat rooster waarin TPA^+ is opgesloten in TPA-ZSM-5.

Grote eenkristallen werden ook gebruikt in de eerste experimenten met STM. Behalve reeds vermeld werk aan het buitenoppervlak kon ook het binnenoppervlak worden geobserveerd. Daartoe werd een groot eenkristal gekleefd evenwijdig aan het ab-vlak van het kristal. De resultaten van dit onderzoek zijn vermeld in hoofdstuk 5. De geleidingscondities welke noodzakelijk zijn om een STM beeld te kunnen verkrijgen worden verondersteld tot stand te komen door geadsorbeerd water. Een film van watermoleculen op en in het, vooraf gecalcineerde kristal, wordt voldoende geacht ook in geval van silicaliet voor een protongeleiding. In hoofdstuk 6, is een studie opgenomen over de kristalgroei historie van een MFI-type zeoliet waarbij, *in situ*, observaties zijn verricht. Twee nieuwe kristalvormen worden gerapporteerd. Een pyramidaal gevormd eenkristal werd gevonden in de buitenste lagen van grote gellichamen zich ontwikkelen als functie van de afbraak van TPA^+ en de aanwezigheid van enige honderden ppm overgangsmetaalionen. De pyramidale kristallen blijken een voorloper en ook een onderdeel te vormen van de daarna ontwikkelde eerder genoemde meer kubische eenkristallen. De homogene Al^{3+} distributie in de kubische kristallen die eveneens groeien in de gellichamen is vermoedelijk een gevolg van de homogene verdeling van Al in de gellichamen. Een tweede morfologie van de MFI-type is de orthorhombische vorm die ontstaat uit synthese mengsels waaraan een boriumbron is toegevoegd.

Een onderzoek naar de inbouw van B^{3+} , Al^{3+} , Ga^{3+} Be^{2+} in MFI-type roosters vormt het onderwerp van hoofdstuk 7. Zowel langwerpig prismatische als kubische kristalvormen werden, respectievelijk als unieke en als met bijproduct gemengde fase, gesynthetiseerd. De bijproducten bleken afhankelijk van het type metaalion- kwarts, analciem, natroliet of beryllsilikaat te zijn. Een maximale inbouw van ongeveer 4 B/uc werd vastgesteld.

De groei van dunne lagen van kleine eenkristallen van de MFI-type zeoliet op

verschillende dragermaterialen bleek mogelijk, hoofdstuk 8. Laterale kristalgroei met een unieke monolaag- bedekking van kleine kristallen werd ontwikkeld op 1 cm² siliciumwafer materiaal terwijl meer axiale groei verkregen kon worden op metaal plaat en - gaas. Een aantal factoren die de groei beïnvloeden is onderzocht. Een van de conclusies van dit hoofdstuk is dat de laterale kristallaag alleen gesynthetiseerd kan worden op de silicium wafer indien hier een gellaag aan vooraf gaat waarin de kristallen kunnen groeien.

DANKWOORD

Voor de totstandkoming van dit proefschrift dank ik mijn promotor Prof. Herman van Bakkum voor zijn enthousiasme en zijn brede aandacht en grote toewijding. Prof. Gerda van Rosmalen dank ik voor de vele denkbeelden die zij mij heeft geschetst op het gebied van kristallisatie.

Dr. Henk van Koningsveld ben ik veel dank verschuldigd voor de wetenschappelijke discussies die stimulerend gewerkt hebben.

Ook dank ik hiervoor Prof. G.W. van Oosterhout, Prof. Jan Reedijk en Dr. Herman Kouwenhoven.

Ik dank Ir. D. Schalkoord, Ing. Nico van der Pers en Joop Padmos voor de snelle en korrekte wijze waarop zij analyses van preparaten voor dit proefschrift uitvoerden.

In het bijzonder dank ik Mevr. Mieke van der Kooij voor de vele spoedoperaties t.a.v. het realiseren van getypte versies van hoofdstukken.

De Hr. Ernst Wurtz is voor mij onmisbaar geweest in vele opzichten. Hij leverde apparatuur en technische bijstand en toonde altijd veel belangstelling voor het werk.

Ik dank de Hr. Wim Jongeleen en Fred Hammers voor hun steun bij het teken- en fotowerk.

Tenslotte dank ik iedereen van het Laboratorium voor Organische Chemie en Katalyse die op welke wijze dan ook heeft bijgedragen aan de samenstelling van dit proefschrift.